Characterization and Evaluation of Non-Line-of-Sight Paths for Fixed Broadband Wireless Communications

Timothy M. Gallagher

Dissertation submitted to the faculty of the Virginia Polytechnic Institute and State University in partial fulfillment of the requirements for the degree of

Doctor of Philosophy
In
Electrical Engineering

Dr. Charles Bostian, Committee Chair
Dr. Scott Midkiff
Dr. Dennis Sweeney
Dr. L. William Carstensen
Dr. Gary Brown
Dr. Brian Woerner

June 17, 2004
Blacksburg, Virginia

Keywords: LMDS, non-line-of-sight, diffuse scattering, channel sounding, cognitive radio

Characterization and Evaluation of Non-Line-of-Sight Paths for Fixed Broadband Wireless Communications

Timothy M. Gallagher

Abstract

Channel impulse responses collected on the Virginia Tech campus show combinations of specular multipath and diffuse scattering at LMDS frequencies. An algorithm is presented that estimates link performance based on the channel impulse response. Presented and analyzed are representative impulse responses (one is primarily specular in nature and one shows significant diffuse scattering) to show that the proposed algorithm is appropriate for analyzing channels exhibiting either of these characteristics. Monte Carlo simulations logged the sequence number of each bit error to gain an understanding of the distribution of errors over time. The results show that for these static channels the errors occur randomly rather than in bursts, leading to the conclusion that average bit-error rate statistics are appropriate for channel characterization. Zero-Forcing (Z-F) and Minimum Mean Square Error (MMSE) equalizers employed on these channels had a significant impact on the link quality. In many cases, the performance of the MMSE equalizer performed only slightly better than the Z-F equalizer. However, when deep nulls were present in the channel response, the MMSE equalizer performed significantly better. Algorithms for determining the number of taps necessary to approach an optimum equalization are presented for both types of equalizers and a '98%' rule of thumb is presented. The algorithm's role in adaptive and cognitive radio systems is discussed and two applications are presented to illustrate its utility.

Grant Information

The author would like to thank the National Science Foundation for its support of this work through NSF award #9983463, Digital Government: Testbed for High-Speed 'End-to-End' Communications in Support of Comprehensive Emergency Management.

Acknowledgements

I'm fond of saying that the only things people truly have that can be called their own are their mistakes. Well, there is a corollary that I believe is also true. No one accomplishes lofty goals without help. I've certainly had help.

Dr. Charles Bostian has been more than an advisor to me. He has been a mentor in the truest sense of the word. His character and integrity are unparalleled and I feel being associated with him has been one of the most enriching things I have ever done in my life. His legacy will live on.

The hardware for this project was built by Dr. Dennis Sweeney so the data collection for this entire project would not have been possible without his hard work and perseverance. He also acted as a sounding board for most of my crazy ideas and left his door open even though he knew I was only across the hall and he was only ever minutes from another, 'Dr. Sweeney, I have a problem.'

I had the pleasure of working closely with Dr. Scott Midkiff and Dr. Bill Carstensen on the NSF project. Dr. Midkiff was always the voice of reason and quick with a smile. We should all be so lucky. To gain a measure of Dr. Carstensen, one has only to ask his students what they think of him. I got to work with a few of them and could tell how much they enjoyed themselves and respected him. I'm glad I got to work with him as well.

Dr. Gary Brown and Dr. Brian Woerner not only helped me gain insight into some of the nuances of ultrawideband measurements and communication theory, but they are also two of the nicest people I have met anywhere. Of course, I'm writing this before I have my final defense!

Other professors have contributed to my growth here at Virginia Tech whether they realized it or not. Dr. Tim Pratt has shown me 'it's OK to be an engineer' and that there are always more questions to be answered. Dr. Ira Jacobs may not have always had answers to my questions, but he always had better questions. Dr. George Morgan has a way of asking questions that can turn a problem on its head. We can all do with a change of perspective occasionally.

Where would I be without Shelley Johnson, Judy Hood, Christie Thompson, and Kathy McCloud? I'd be lost, uninformed, unpaid, and unhappy. They've made coming to work everyday fun. I'm very lucky that way. Not everyone can say that.

I've worked with too many students to count who have made a positive impact on me. Students like Shital, Cindy, Mary, Nathan, Jason, Paige, Tianmin, Suem Ping, Bin, Tim, Preethi, and Shyamal are what make working at a university worthwhile and challenging. They're all good people and I wish nothing but the best for all of them.

The two students I have worked most closely with are Christian Rieser and Tom Rondeau. Christian has spent many afternoons listening to me rant that I'm right until he's beaten me into submission and I change my approach. His patience is almost limitless and for his generosity, I will always be grateful.

I Love Tom.

Both my parents and Donna's parents have always been behind our decisions and have supported us emotionally (and financially). We can never pay back all of the things our parents do for us. We can only hope to pay it forward to our children and live our lives so they can be proud.

I could never have done this without the love and support of Donna. She has trusted me from the beginning and together we've gone back and forth across the country living our adventure. Some days have been more adventurous than others, but she's never wavered in her support of me. She's my best friend and I will love her forever.

For Morganne and Madison.

Your dreams are mine. May they all come true.

Table of Contents

List of Figures

1 Introduction

1.1 Motivation

In 2000, the Center for Wireless Telecommunications (CWT) at Virginia Tech received a National Science Foundation grant to develop prototype hardware and software for a rapidly deployable broadband wireless telecommunication system. The aim was to develop a system architecture that could provide an end-to-end wireless communications solution for use by emergency response personnel in disaster and emergency situations. The prototype consists of geographic information systems (GIS) propagation estimation software, an integrated broadband channel sounder, and adaptive network protocols. CWT built the system and, with our partner SAIC, demonstrated two prototype radios for numerous federal, state, and local entities with a vested interest in emergency response. The functionality and innovations of the system are described in detail in [1].

At the project's inception, inexpensive, off-the-shelf, broadband radios were not available. CWT decided to build prototype hardware to operate in the Local Multipoint Distribution Services (LMDS) band for a combination of historical and practical reasons. For one, Virginia Tech owns the LMDS licenses in a major portion of Virginia including the basic trading area (BTA) surrounding the university. The LMDS band consists of an 850 MHz contiguous block of frequencies around 28 GHz which was enough spectrum to accommodate the broadband requirements of the system. Plus, CWT had relationships with manufacturers of LMDS hardware. The innovative aspects of the system are, however, frequency independent. In fact, work is in progress at Virginia Tech to move the operation to unlicensed 5 GHz spectrum where less expensive off-the-shelf hardware is now currently available.

The development of the system at 28 GHz raised interesting questions regarding the nature of signal propagation in this band. Commercial radios operating at these high frequencies are almost universally considered line-of-sight (LOS) technologies. In a disaster, however, when time is critical, detailed site planning impractical, and LOS links not possible, non-line-of-sight (NLOS) links may be the only alternative. In commercial applications, these paths will be avoided where possible, but in a disaster, they may be

'paths of opportunity,' not ideal, but the difference between a degraded communication link and none at all.

Little has been published regarding the characteristics of these paths and their ability to sustain broadband communications. It is expected that NLOS paths at these frequencies would exhibit rough surface, also called diffuse, scattering. The particulars of this type of reflection mechanism will be discussed in Section 2.1, but it is quite different than the traditional reflection according to Snell's Law in which the angle of incidence equals the angle of reflection. In diffuse scattering, a continuum of energy is reflected to the receiver from many points along the surface. It is unclear what effect this has on the link quality and what might be an appropriate technique to decrease the degradation. The purpose of this study is to investigate the nature of NLOS paths at these frequencies and consider their usefulness in sustaining broadband communication links with reasonable fidelity.

1.2 Contributions of the Research

Two questions regarding NLOS millimeter-wave communications have received little attention in the literature. One concerns the estimation of performance of NLOS paths in broadband communication links in frequency bands routinely used only for LOS communications. The other is the utility of degradation mitigation techniques for the particular types of distortion that occur in these bands. This dissertation addresses both of these questions by presenting an algorithm that can be used to estimate performance quickly based on the channel impulse response and a technique to implement appropriately sized equalizers to increase performance. The algorithm and equalizer implementation were developed specifically to address problems unique to NLOS millimeter-wave channels, but were found to be effective for more traditional channels as well.

Preliminary work at Virginia Tech has shown that NLOS paths at 28 GHz can be quite different from their lower frequency counterparts. Dillard [2] documents the diffuse scattering possible in these links and Miniuk [3] presents Monte Carlo simulation results that suggest traditional performance metrics may not be appropriate for these channels. This dissertation extends their work in three important ways.

1) Two measured channels on the Virginia Tech campus illustrate that knowledge of the surface is not adequate to determine the channel response.
2) A channel impulse response based performance estimation algorithm is developed that does not require Monte Carlo simulations.
3) Equalizer performance is assessed and implementation techniques are presented for these channels.

Dillard [2] presents data that show significant diffuse scattering from limestone walls. The same type of surface is investigated here and shows significant specular multipath rather than diffuse scattering. A second surface investigated appears smooth, but produces a significant amount of diffuse scattering. This illustrates that simple knowledge of the surface characteristics may not be enough to make reasonable assumptions about the impulse response.

An important part of this work is to develop an algorithm, based on the channel impulse response, to estimate the performance that can be expected from these links. Monte Carlo techniques, such as those used in [3], for performance estimation are the standard, but cannot be reasonably implemented in a deployed system because the time it takes to complete even a single run is excessive. The algorithm presented here is an alternative to traditional Monte Carlo techniques that can generate performance estimates without resorting to very long simulations. The advantage is that this algorithm is easily implemented in systems with the ability to change configuration based on the environment, such as adaptive and cognitive radios. The information derived by this algorithm can be used at the front end of these systems to estimate performance and provide a tool or platform for system configuration trade-offs.

Numerous techniques to increase performance in wireless links have been proposed over the years, but none that specifically address channels with diffuse scattering. The final sections of this dissertation consider the effectiveness of equalizers in these channels along with procedures for practical implementation.

1.3 Measured Channels for Analysis

Countless channel responses have been collected over the years since the broadband channel sounder described in [1] was built. These results have been published in refereed journals [1] [2] and presented at technical conferences [3] [4]. The collected responses

show a broad range of characteristics from reflections off a broad range of surfaces and illustrate how diverse these responses can be. One goal of this particular study is to add to that body of experimental data and at the same time establish a method for estimating wireless communication link performance based on that data. Therefore, the investigation must cover the range of channel characteristics in order to fully exercise the algorithm.

Most wireless communication links suffer from distortion due to multipath. Multiple versions of the transmitted signal may arrive at the receiver via reflections caused by objects in the environment. These signals arrive at the receiver with different time delays and are collectively referred to as multipath. In most systems, each reflected path consists of a single reflection (specular multipath) and can be represented as an impulse in the channel impulse response. This assumption is valid as long as the carrier wavelength is large compared to the surface irregularities.

At higher frequencies, this assumption may no longer be valid, and the surface may reflect a continuum of energy. This type of reflection is referred to as diffuse scattering. Diffuse scattering has received little attention in regards to its effect on link performance and it is unclear what can reasonably be done to mitigate the distortion it causes. The performance estimation algorithm described here was specifically designed with diffuse scattering in mind, but is shown to be general enough to work in specular multipath channels as well.

The broadband channel sounder collected numerous channel pulse responses, but one primarily specular multipath channel and one primarily diffuse scattering channel were subsequently chosen to validate the performance estimation algorithm. These two responses represent the two extremes of NLOS LMDS channels and therefore are a reasonable set to observe the algorithm's performance in different circumstances. To further exercise the algorithm, different bandwidth signals were placed in different frequency bands in each channel. Throughout the analysis, the algorithm performed reasonably in every radio configuration and for every channel.

A quick preview of the algorithm highlights its independence of most radio configurations and environments. The algorithm begins with the response of a channel to the sounder pulse. A copy of the sounder pulse is known to the algorithm, so it is a

straightforward mathematical process to extract the channel impulse response using Fourier transforms and linear-time invariant (LTI) system analysis regardless of the sounder pulse shape. The channel impulse response is then convolved with a mathematical representation of each different transmitted pulse used in data transmission. The convolution process is valid as long as the system is LTI, regardless of pulse shape or modulation. This signal is sampled at the optimum time and correct rate to determine the mean signal level and contributions to intersymbol interference (ISI). When equalizers are available, they are modeled as filters and convolved with the results of the pulse and channel convolution, either before or after sampling. The performance is then estimated based on the ISI and whatever receiver noise is present.

All of this is independent of sounder pulse shape, transmitted pulse shape, channel characteristics, equalizer presence, modulation, data rate, and even receiver noise power spectral density. The algorithm is based on mathematical concepts and is appropriate as long as the system is LTI and the channel impulse response is static.

1.4 Procedure

Our team used the broadband channel sounder described in [1] to collect channel responses by reflecting 28 GHz RF pulses off numerous surfaces on the Virginia Tech campus. MATLAB® programs post-processed the collected responses to obtain their baseband equivalents. Modeling these channels as filters allowed for their inclusion in the software package Signal Processing WorkSystem (SPW). SPW simulations are traditional Monte Carlo simulations run to determine bit error rate (BER) as a function of carrier-to-noise ratio (C/N). The MATLAB® based performance estimation algorithm results and SPW simulation results were compared to determine the algorithm's suitability for estimating performance.

The SPW simulations included equalizers when appropriate and the results compared to the algorithm's results to determine the algorithm's effectiveness in estimating performance in the presence of equalization. The algorithm and SPW simulations results compared favorably and the equalizer effectiveness in mitigating channel distortion was studied.

1.5 Summary of Results and Conclusions

The channel impulse response measurements show significant diffuse scattering may occur in channels at LMDS frequencies. Presented and analyzed are representative impulse responses (one is primarily specular in nature and one shows significant diffuse scattering) to show that the proposed algorithm is appropriate for analyzing channels exhibiting either of these characteristics.

The SPW simulations logged the sequence number of each bit error to gain an understanding of the distribution of errors over time. The results show that for these static channels the errors occur randomly rather than in bursts.

Zero-Forcing (Z-F) and Minimum Mean Square Error (MMSE) equalizers employed on these channels had a significant impact on the link quality. In many cases, the performance of the MMSE equalizer was only slightly better than the Z-F equalizer. However, when deep nulls were present in the channel response, the MMSE equalizer performed significantly better. Algorithms for determining the number of taps necessary to approach an optimum equalization are presented for both types of equalizers and a '98%' rule of thumb is presented.

1.6 Dissertation Organization

Chapter 2 provides background including basic information on link performance in NLOS channels as well as previous work done in this area, traditional strategies for estimating performance in wireless channels, and techniques for improving link quality. Chapter 3 presents the channel impulse response measurements as well as a description of the procedure used to obtain them and how they were used. Chapter 4 presents the effects of non-ideal channel responses on link performance and compares the performance estimates of the proposed method to those of traditional techniques. Chapter 5 is an investigation of the effectiveness of Z-F and MMSE equalizers. Chapter 6 contains comments on the differences between specular multipath and diffuse scattering. Chapter 7 is a step-by-step guide to implementing the performance estimation algorithm. Chapter 8 discusses the use of the algorithm in adaptive and cognitive radios and is followed in Chapter 9 with some concluding remarks on the results.

2 Background

2.1 Link Performance in NLOS Channels

Much has been published regarding the nature and effects of non-ideal channels on wireless link performance, but the vast majority is concerned with low data rate mobile applications. For mobile applications, the amplitude of the signal is assumed to undergo Rayleigh fading and the phase is a random variable with a uniform distribution between 0 and 2π. The distortion introduced by the channel is a result of either the radio moving around in the environment or the channel characteristics changing over time. Signal distortion can occur when multiple reflections reach the receiver with various time delays. The multiple received versions of the signal are collectively called multipath. These extra signal paths cause intersymbol interference (ISI) which can result in severe degradation to the link performance.

Two assumptions made for the analysis of low data rate mobile channels need to be reconsidered when the radios are fixed and the frequency is an order of magnitude higher than what is used for commercial cellular mobile devices: time-varying channel response and specular multipath.

For fixed broadband wireless communications, the radios can be portable, but are not expected to be mobile. That is, the radios can be quickly deployed at a location, but are not expected to operate while in motion. Fixing the radios in position greatly reduces the need to assume Rayleigh fading of the signal since the channel remains relatively static. For these fixed radios, treating the channel as a statistical model becomes unnecessary so the models can be replaced with deterministic characteristics.

Multipath components in the mobile radio bands are normally considered to be specular. Specular refers to reflections from surfaces that produce single reflections in which the angle of incidence equals the angle of reflection. See Figure 2-1.

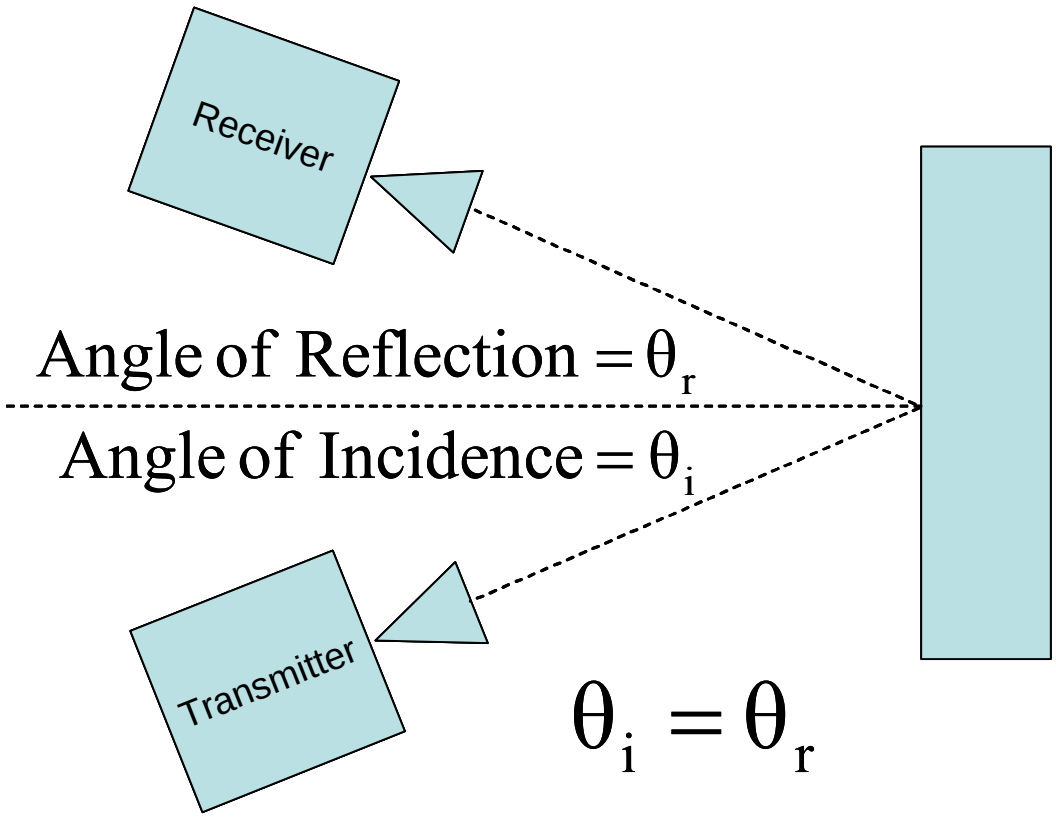

Figure 2-1: Example of specular reflection.

These reflections reach the receiver with different time delays as in Figure 2-2 and, with suitably precise detection, can be separated and removed or recombined to increase the receiver performance. The amplitude response of the channel for the reflections in Figure 2-2 is shown in Figure 2-3.

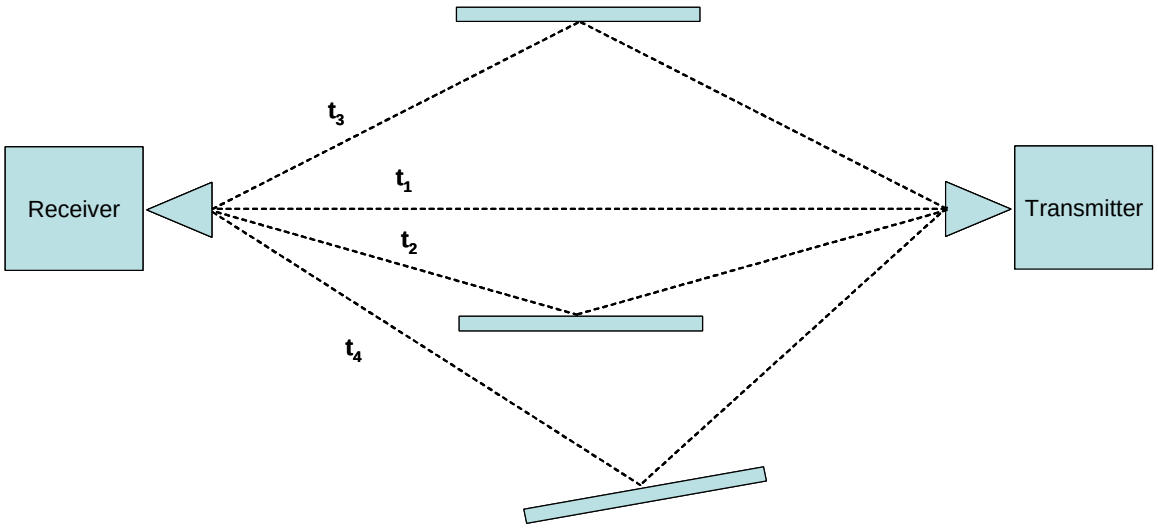

Figure 2-2: Multiple specular reflections arrive at the receiver with different time delays.

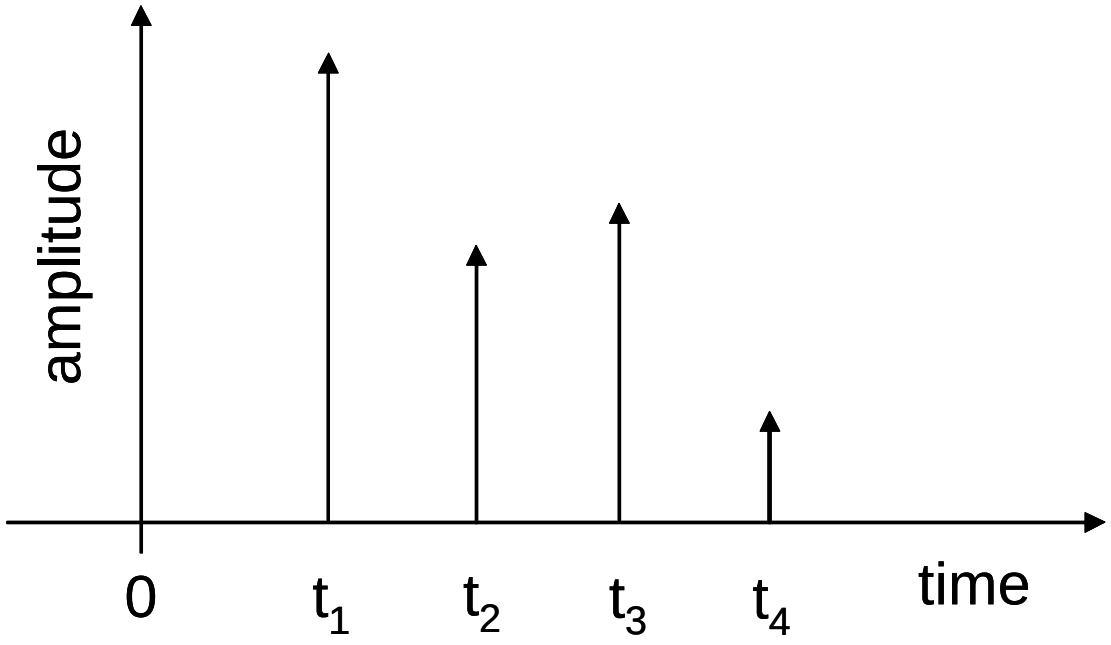

Figure 2-3: Amplitude response of the channel pictured in Figure 2-2.

Note how the reflections at the receiver are represented as impulses in Figure 2-3. This specular assumption becomes less accurate, however, as the wavelength of the carrier approaches the height of irregularities in the surface. When a signal with a carrier

wavelength close to the height of the surface irregularities bounces off the surface, energy is scattered from the surface in many directions as shown in Figure 2-4.

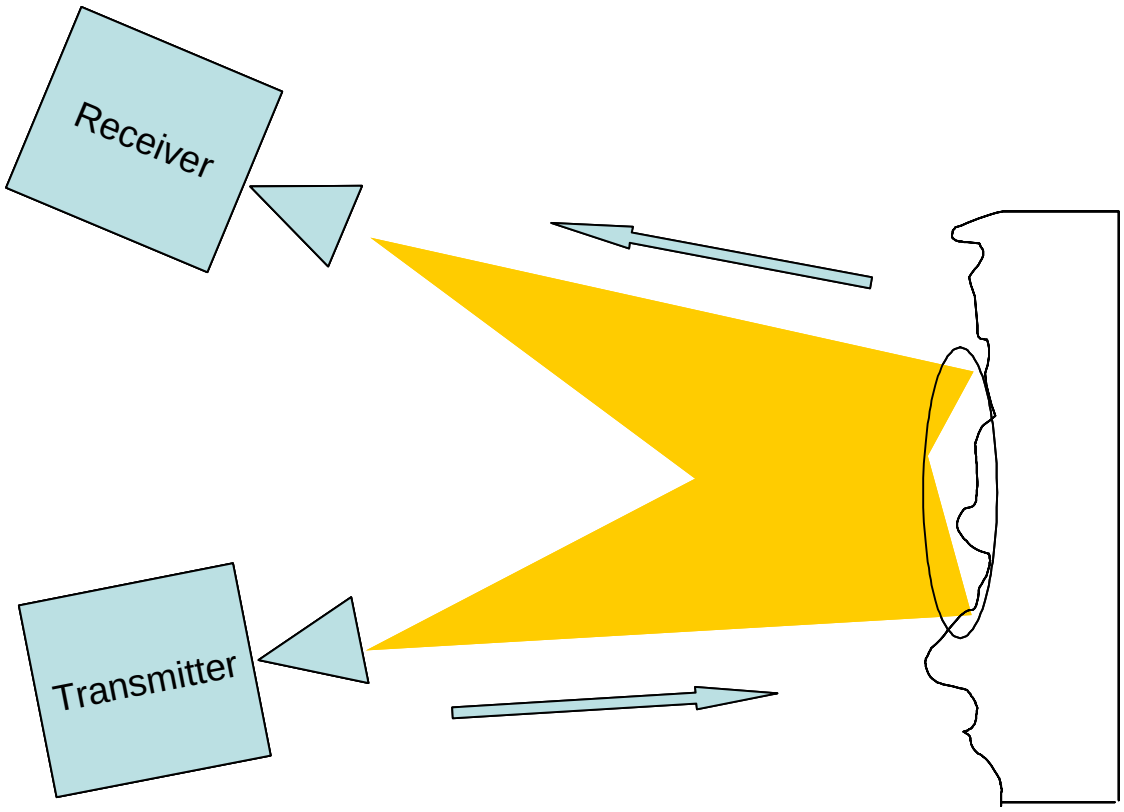

Figure 2-4: Example of diffuse scattering due to a rough surface.

The receiver in this case is more likely to see a continuum of energy rather than discernible bounce paths. This is referred to as diffuse scattering. Wavelengths used most often by mobile devices are on the order of tens of centimeters and thus, the surfaces look smooth. A signal with a 28 GHz carrier frequency has a wavelength of approximately 1 centimeter. At this wavelength, surfaces are more likely to look rough and therefore produce diffuse scattering rather than specular multipath. An example amplitude response of a channel with diffuse scattering is shown in Figure 2-5.

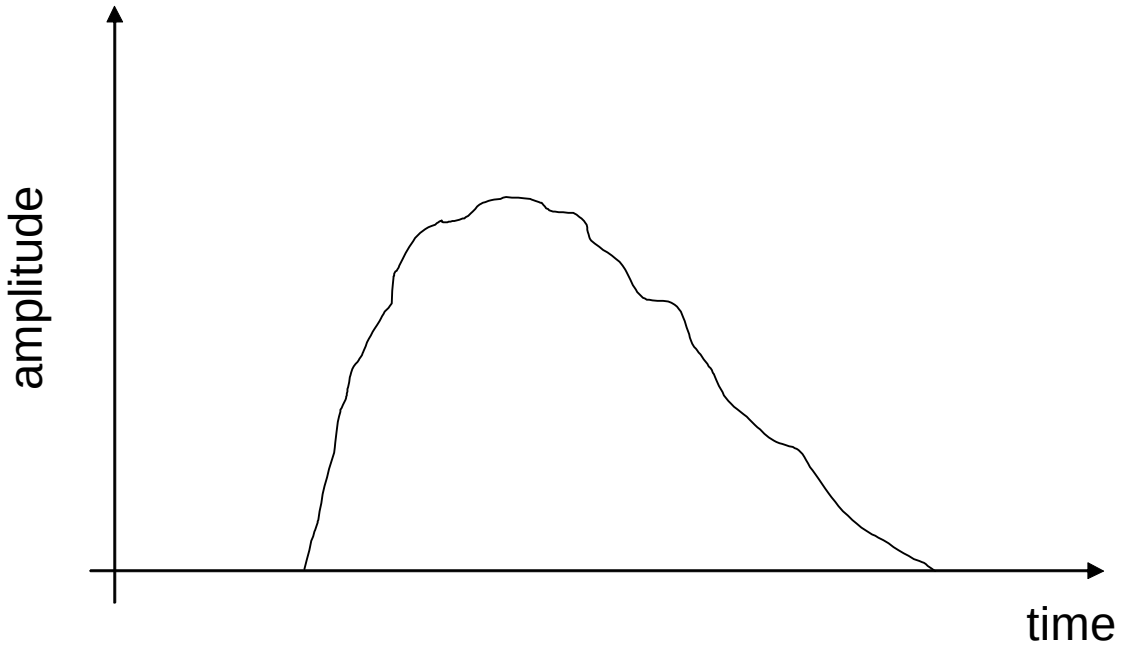

Figure 2-5: Example amplitude response of a channel with diffuse scattering.

Notice that there are no longer any discernible impulses in the channel response shown in Figure 2-5. The received signal is now a combination of reflections from a larger portion of the reflecting surface and it is unclear how this phenomenon affects link quality or what techniques can be used to decrease the degradation.

The literature offers almost no discussions of the effects of this combination of diffuse scattering and relatively time-invariant channels on link performance. The intent of this dissertation is to address that need.

2.2 Investigations of Wireless Channels at Millimeter Wave Frequencies

What little is published regarding the utility of NLOS broadband communications at millimeter-wave frequencies is mainly concerned with coverage area estimates and ways to increase that area for useful commercial communications.

Seidel and Arnold [5] in 1995 conducted 28 GHz propagation measurements in an urban setting to gain some practical knowledge of NLOS paths and their effect on signal strength. They concluded that while they did see signals from what appeared to be bounce paths, the signal strength was too low to be of any use for providing commercial

service. An NTIA study [6] also found severe attenuation in NLOS situations for signals at 28 GHz as well as noting signal variability through vegetation.

Maurer et al [7] recorded numerous frequency response measurements in many locations in Germany. They found differences in measurements that suggest polarization affects signal propagation from surfaces and suggested radio configurations that minimize the depolarization that occurs. In [8], Hayn et al suggest taking advantage of those paths by placing elliptical reflectors on buildings to help fill in coverage areas.

Each of these studies is concerned with either characterizing or maximizing the percent coverage area of LMDS systems. Ultimately, this dissertation is concerned with characterizing these channels to better understand the system performance one can expect when using these channels.

2.3 Strategies for Estimating Link Performance in Wireless Channels

Many methods are in use to obtain estimates of the channel impulse response and most rely on transmitting a known sequence to the receiver. The receiver can then estimate the channel response by comparing the received signal to the expected signal. Adaptive equalization techniques can also be employed to estimate the channel response. The tap weights are adaptively changed based on a known input sequence. The equalizer is designed to minimize the mean square error of the decision output by forcing the taps to values that compensate for the non-ideal characteristics of the channel. The inverse of the frequency response of the equalizer is the estimated frequency response of the channel.

Equalizers that do not have the benefit of a known transmitted sequence are called blind equalizers. These equalizers invariably converge more slowly on the channel impulse response, but do not require the overhead of bits that do not contain any data.

These techniques estimate the channel response, but as yet, nothing has been published regarding the estimation of link performance based on them. Papers such as Chuang [9] propose metrics such as irreducible bit error rate based on the power delay profile and assumptions about the time-varying nature of the channels, but the extension to lower carrier-to-noise ratios (C/N) is absent. This dissertation presents an efficient

algorithm that estimates bit error rate (BER) performance as a function of C/N for known, static channels.

2.4 Techniques for Increasing the Performance of a Wireless Link

Many methods are available to the system designer to increase the performance of a wireless communication system. The trade space is large and many of the variables can (and necessarily will) be traded against one another.

The simplest strategy is to increase the effective isotropic radiated power (EIRP) by either increasing the signal power delivered to the antenna or increasing the gain of the antenna. This will work as long as the link is limited by thermal noise. If, however, the link suffers from mulitpath that introduces intersymbol interference (ISI), no performance gain will be realized. ISI is a form of self-interference. As its name implies, ISI is energy from one symbol interfering with another. If a symbol's energy is increased, its effect on other symbols will be increased as well. Since the ISI follows the symbol energy, increasing a signal's power also increases the ISI.

Another method is to decrease the order of modulation. For example, to maintain the same BER, less C/N is required for a QPSK signal than is required for a 16-QAM signal. Improving the link quality here is accomplished by decreasing the data rate.

If the problem is not C/N but rather distortion in the channel, other methods such as equalization or coding may be employed to increase performance.

Adaptive equalizers are filters that adjust their characteristics based on a known transmitted sequence of symbols. Equalizers attempt to compensate for the non-ideal nature of the channel by either eliminating ISI or balancing the effects of ISI and the thermal noise present in the receiver bandwidth. The disadvantage here is that the known sequence carries no usable data to the end-user thus resulting in decreased throughput. Blind equalization techniques do not require a known transmitted sequence and therefore do not decrease throughput. However, the equalizer may be slow to converge and may not fully compensate for the channel distortion.

Many forms of error detection and error correction can be employed to increase the probability that blocks of data will be correctly decoded by the receiver. Different

types of coding work better in different circumstances, but all suffer from the disadvantage that they too increase the overhead and may as a result decrease throughput.

3 Channel Impulse Response Measurements

3.1 Data Collection

3.1.1 Experimental Configuration

The channel sounder is a modified short RF pulse bistatic radar whose detailed operation is explained in [1]. The channel sounder characterized 250 MHz of spectrum centered around 28 GHz. The transmitter utilized a 14 dB gain 90^o sectoral horn antenna and the receiver a 30 dB dual reflector parabolic antenna. In all of the measurements but the calibration, the antennas were pointed at the specular reflection point, i.e. the point on the surface that determines the shortest distance from the transmitter to the wall to the receiver. The transmitter sends out a short RF pulse train at 28 GHz which the receiver downconverts to an 1850 MHz intermediate frequency (IF) before sampling and storing on the sounder data collection board.

The calibration measurement carried out in a field west of Whittemore Hall on the Virginia Tech campus produced the reference pulse. The radio configuration shown in Figure 3-1 limited the distortion to the received pulse and allowed for determination of the channel impulse responses from the succeeding measurements.

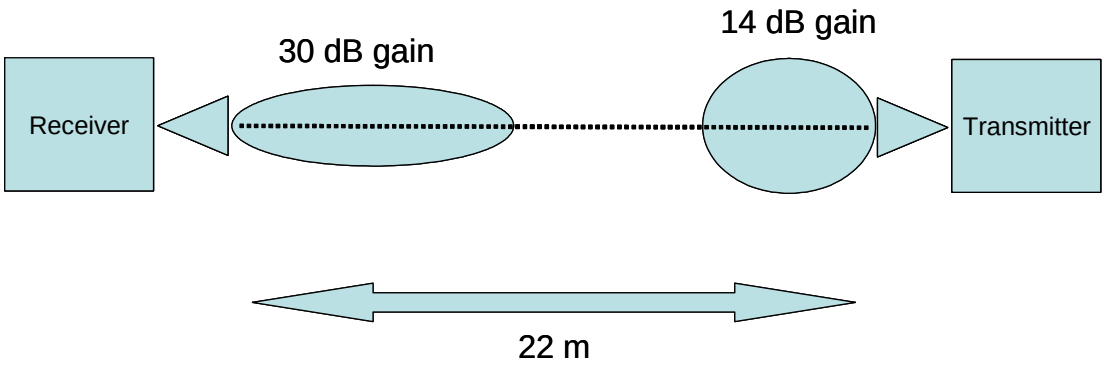

Figure 3-1: Calibration measurement geometry.

Many channel sounder measurements were collected during the course of this investigation. Two representative channel sounder measurements are described in the following sections and analyzed through the remainder of the dissertation. The first channel is composed of specular multipath and the second exhibits significant diffuse

scattering. The proposed algorithm's effectiveness in these two channels illustrates its ability to estimate performance based on the impulse response in either environment.

The path that contained primarily specular multipath was a bounce path off Hancock Hall on the Virginia Tech campus. The wall is shown in Figure 3-2 and the geometry of radio placement with distances is shown in Figure 3-3.

Figure 3-2: Photograph of Hancock Hall measurement location.

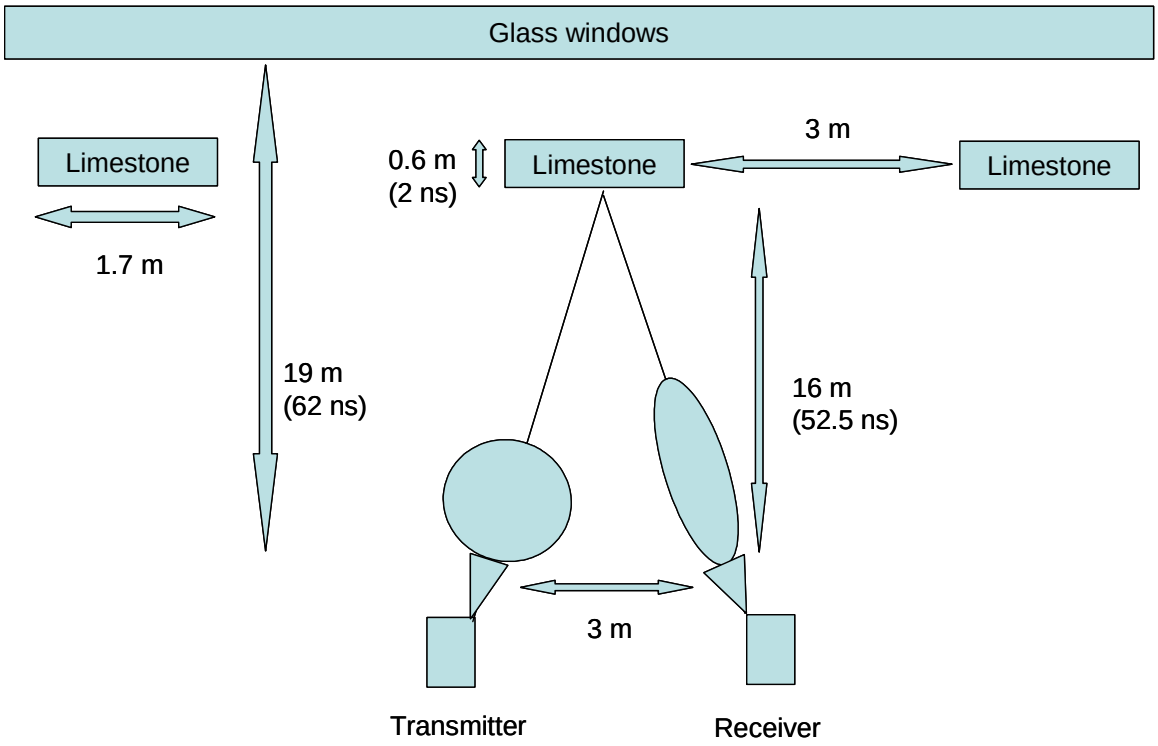

Figure 3-3: Hancock Hall measurement geometry with relevant signal propagation delays shown in parentheses.

The path that contained diffuse scattering was a measurement taken of a bounce path from Cowgill Hall, also on the Virginia Tech campus. That wall is shown in Figure 3-4 with its geometry depicted in Figure 3-5.

Figure 3-4: Photograph of Cowgill Hall measurement location.

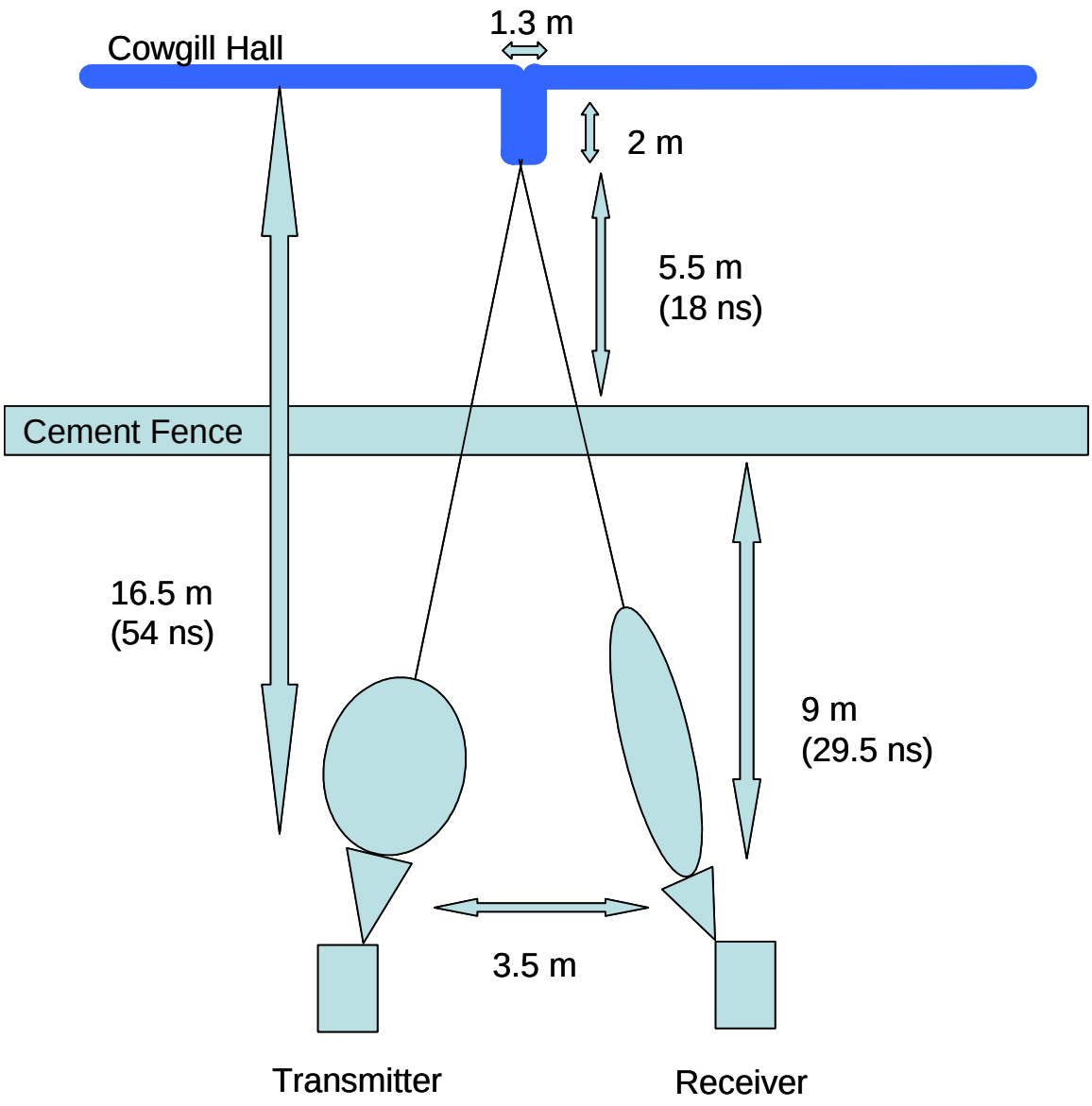

Figure 3-5: Cowgill Hall measurement geometry with relevant signal propagation delays shown in parentheses.

3.1.2 Channel Pulse Responses

One of the raw calibration pulse measurements is shown in Figure 3-6. Several responses were captured in succession and their baseband equivalents are shown in Figure 3-7. As expected, the responses are relatively constant, so an averaging operation was carried out to determine the reference pulse and is shown in Figure 3-8.

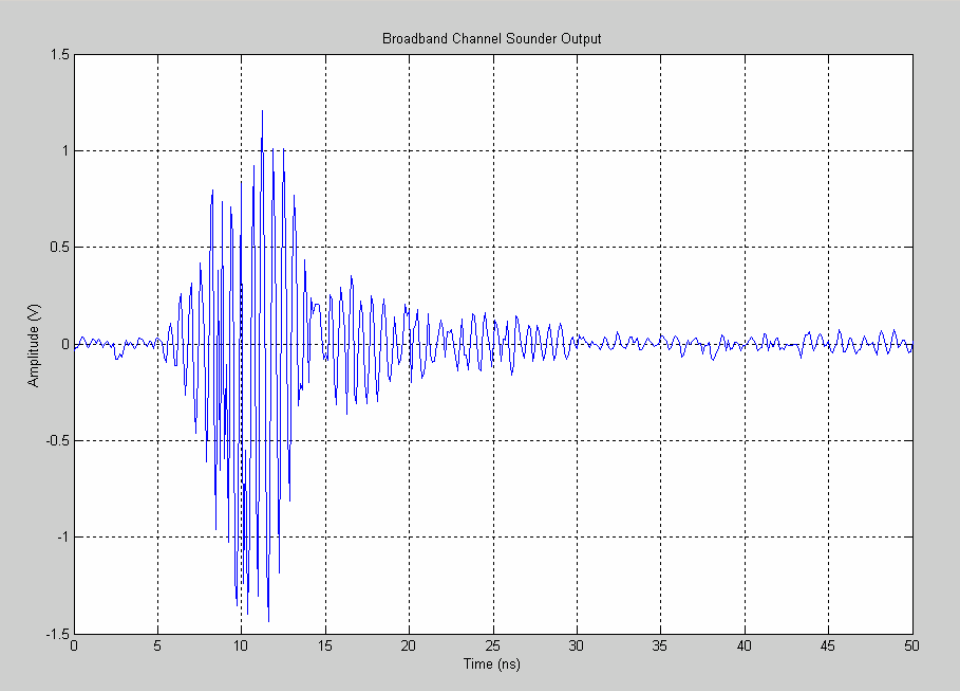

Figure 3-6: Sample broadband channel sounder output used in calibration.

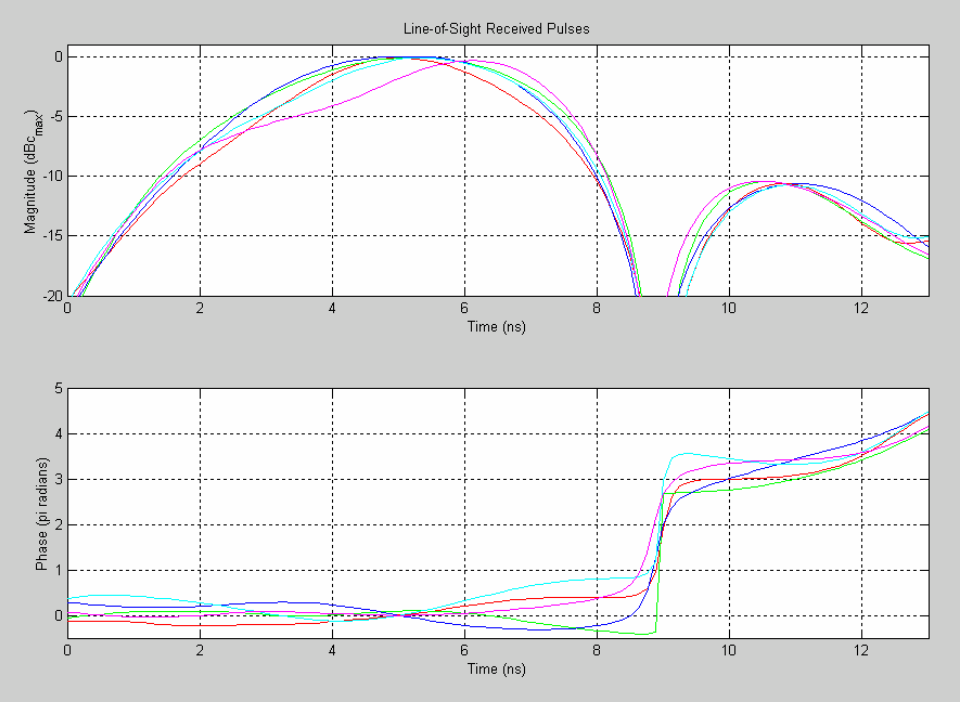

Figure 3-7: Baseband equivalent calibration measurements.

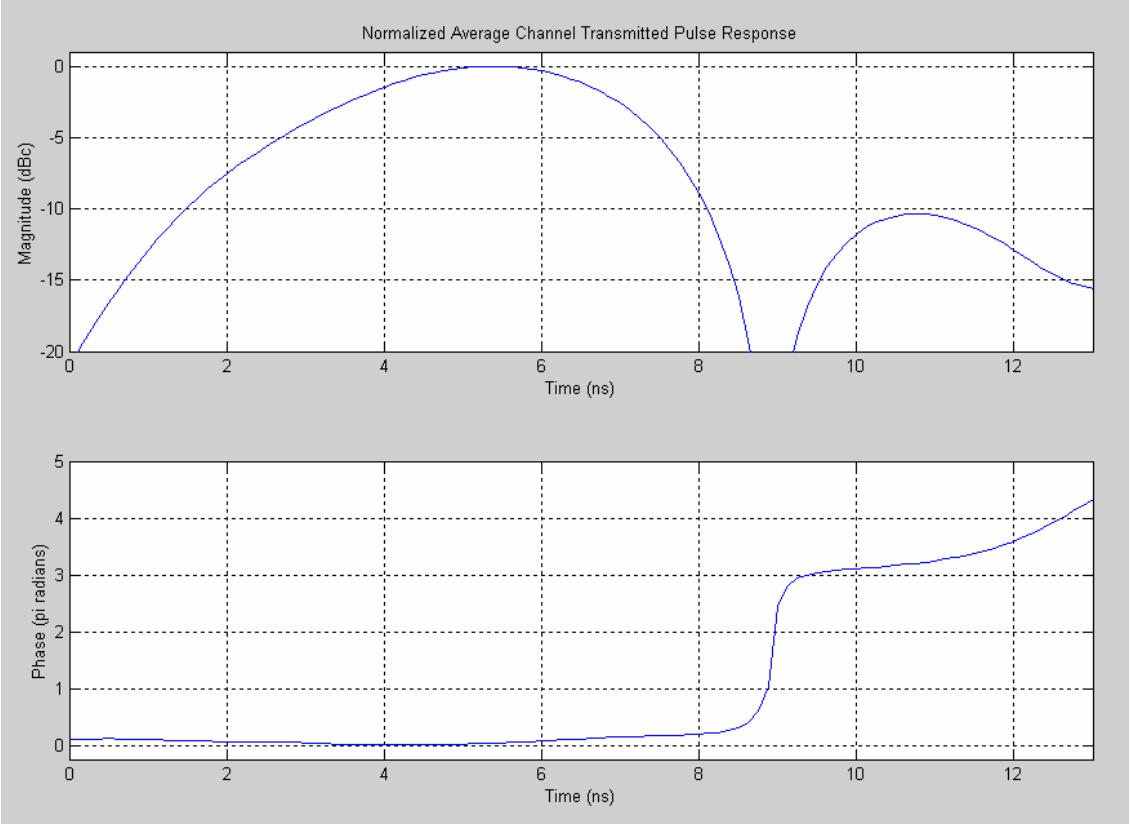

Figure 3-8: Average baseband equivalent calibration measurement.

Raw channel sounder measurements for the Hancock Hall and Cowgill Hall channels under investigation are shown respectively in Figure 3-9 and Figure 3-10.

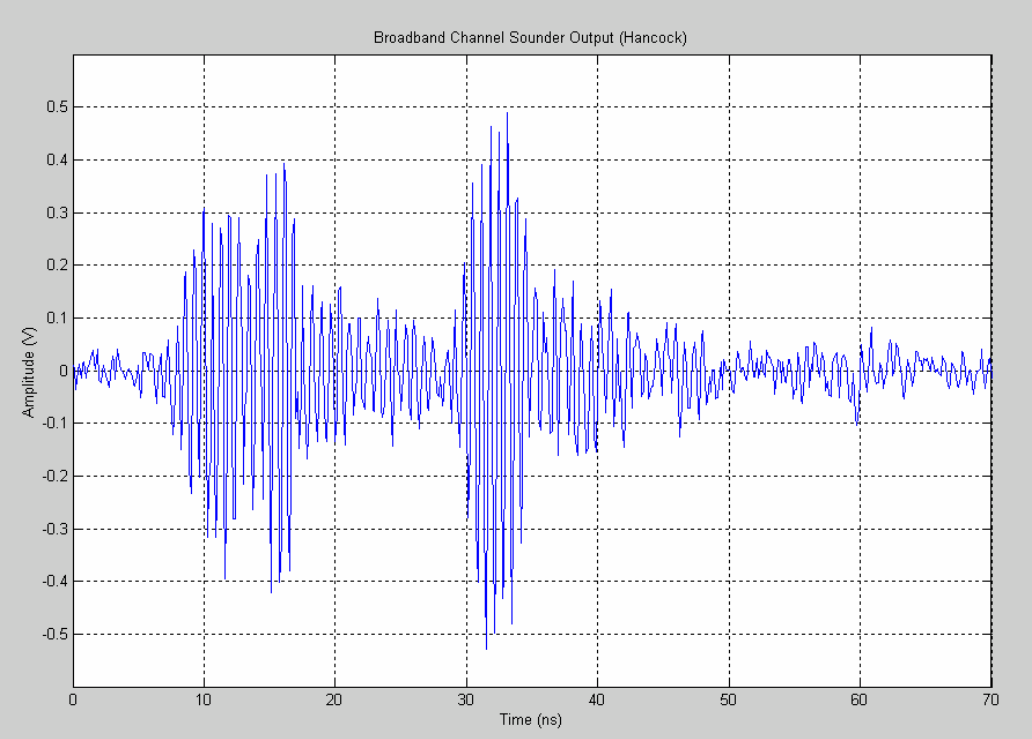

Figure 3-9: Sample broadband channel sounder output from Hancock Hall.

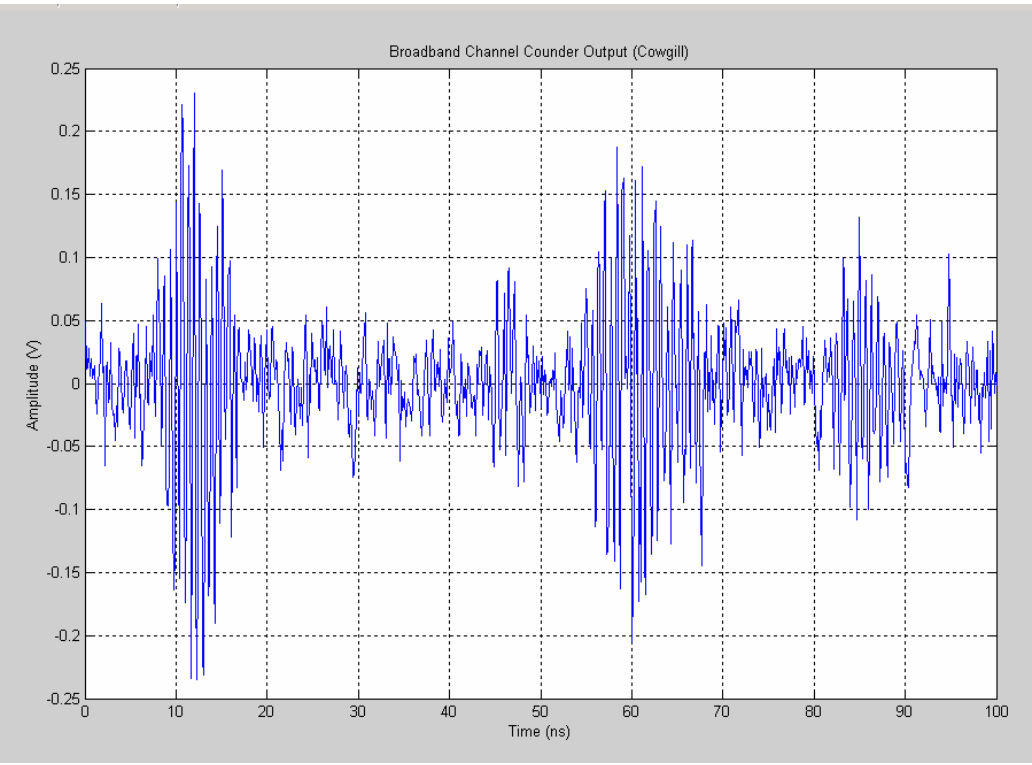

Figure 3-10: Sample broadband channel sounder output from Cowgill Hall.

Similar to the calibration measurement, both channels were sounded multiple times, found to be relatively constant over time, and averaged to determine a suitable channel pulse response. The baseband equivalent pulse responses and average response for Hancock Hall are shown in Figure 3-11 and for Cowgill Hall in Figure 3-12.

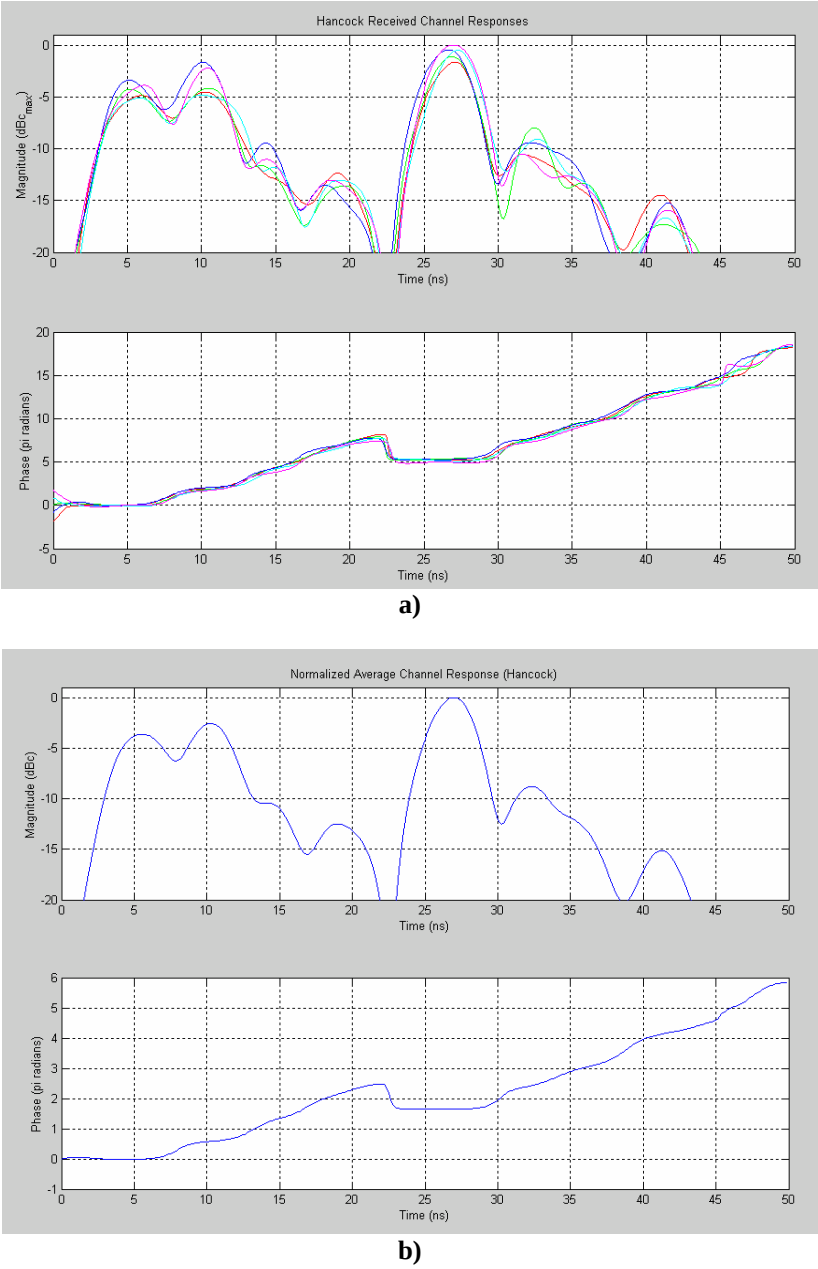

Figure 3-11: a) Baseband equivalent pulse response measurements and b) average pulse response for Hancock Hall.

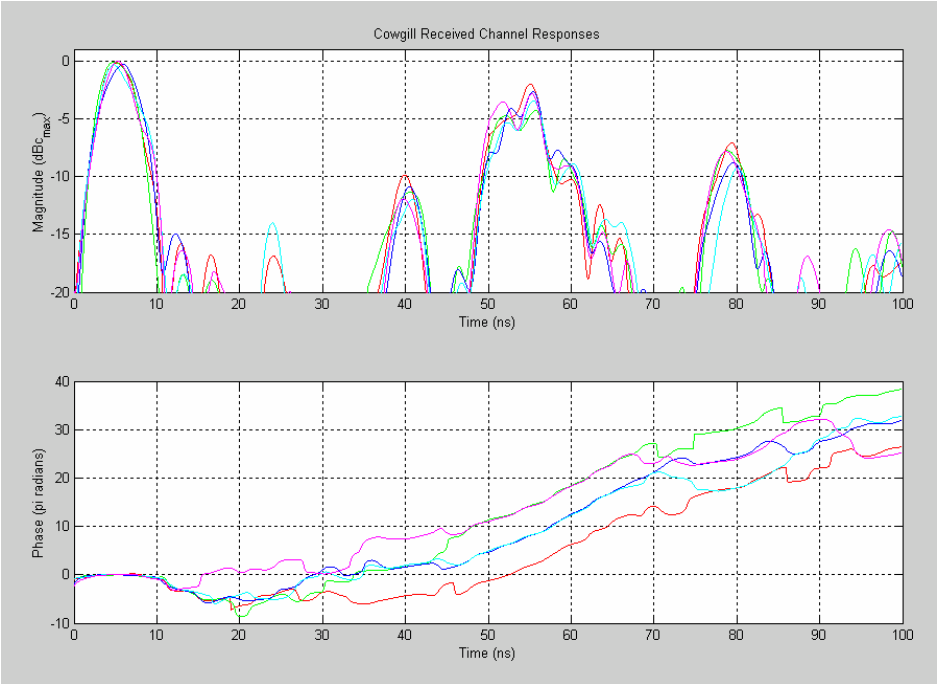

a)

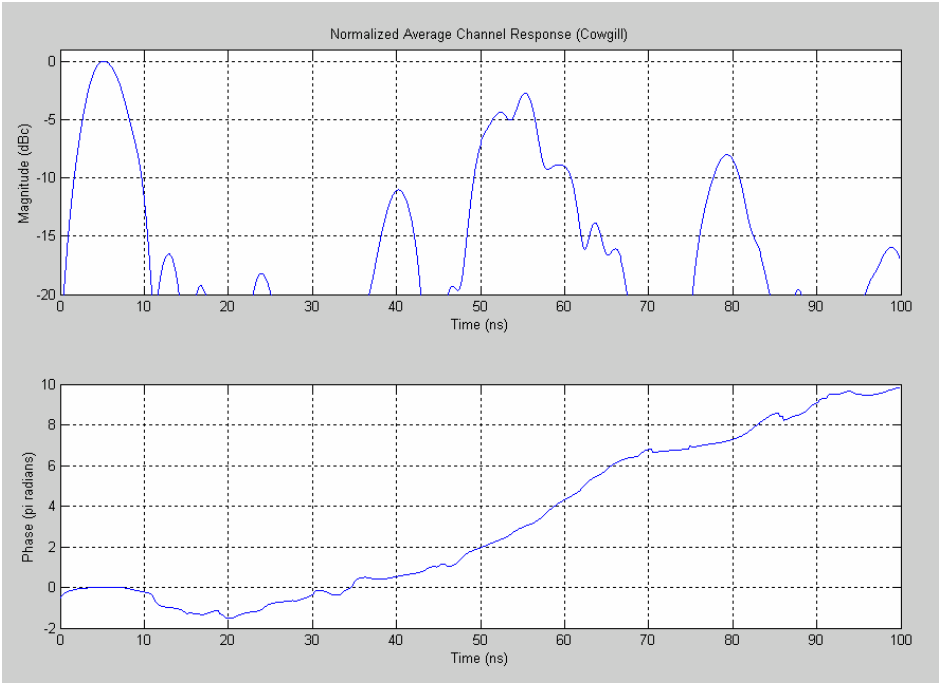

b)

Figure 3-12: a) Baseband equivalent pulse response and b) average pulse response for Cowgill Hall.

3.2 Channel Modeling for Simulation

3.2.1 Finding the Channel Impulse Response

3.2.1.1 Linear, Time-Invariant Systems

For linear, time-invariant (LTI) systems, the output, y(t), of the system is the convolution of the input signal, x(t), and the impulse response of the system, h(t). The block diagram is shown in Figure 3-13. The corresponding mathematical equation is (3.1), where $*$ denotes the convolution operator.

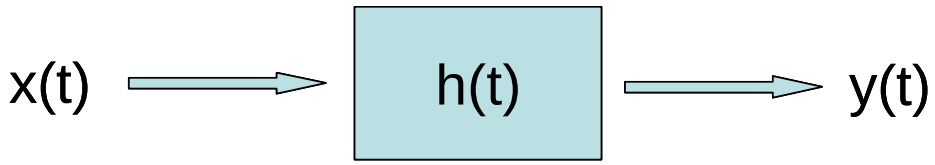

Figure 3-13: Basic block diagram of system input/output.

$$y(t) = x(t) * h(t) \tag{3.1}$$

A system is linear, as shown in Figure 3-14, if scaling the input by a constant, a, scales the output by the same constant.

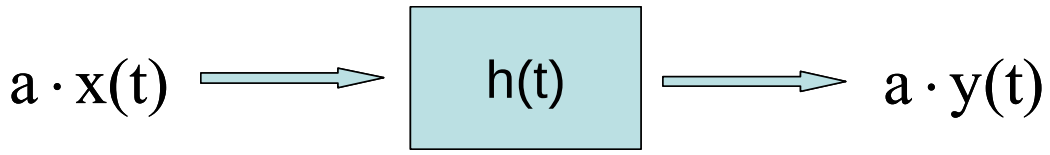

Figure 3-14: Block diagram of linear system.

$$a \cdot y(t) = a \cdot x(t) * h(t) \tag{3.2}$$

A system is time-invariant if delaying the input does nothing more than delay the output by the same amount. A block diagram of an LTI system is shown in Figure 3-15.

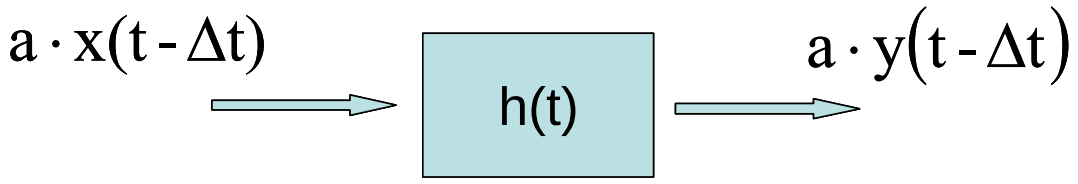

Figure 3-15: Block diagram of a linear, time-invariant system.

$$a \cdot y(t - \Delta t) = a \cdot x(t - \Delta t) * h(t) \tag{3.3}$$

3.2.1.2 Hancock Hall Impulse Response

The responses shown in Figure 3-11 and Figure 3-12 are a result of the convolution of the transmitted pulse and the impulse responses of the respective channels. In order to isolate the impulse response of each channel, it is necessary to deconvolve out the transmitted pulse. This can be done simply in the frequency domain by noting that for LTI systems, convolution in the time domain is equivalent to multiplication in the frequency domain.

$$Y(f) = X(f) \cdot H(f) \tag{3.4}$$

, where Y(f), X(f), and H(f) are the Fourier transforms of y(t), x(t), and h(t), respectively. To find the impulse response, h(t), divide Y(f) by X(f) and take the inverse Fourier transform of the result. This is shown in (3.5) where $F^{-1}\{Z\}$ is the inverse Fourier transform of Z.

$$h(t) = F^{-1}\left\{\frac{Y(f)}{X(f)}\right\} \tag{3.5}$$

The Hancock Hall impulse response is shown in Figure 3-16. It is interesting to note that discernible peaks appear in the time response. More importantly, the phase during these peaks is relatively constant. This indicates that these peaks are caused by discrete reflections.

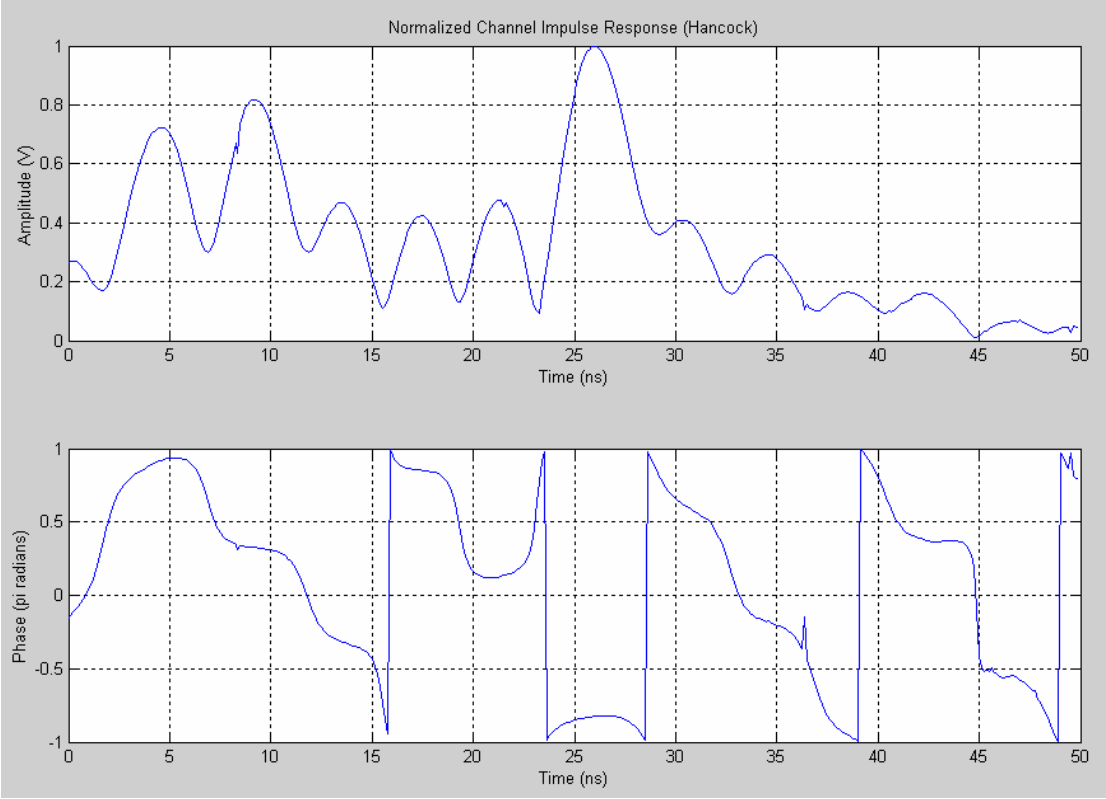

Figure 3-16: Hancock Hall impulse response.

Figure 3-17 is the result of replacing the local maxima with discrete impulses. Passing the reference pulse through this specular version of the impulse response resulted in an output comparable to the original received pulse. Since no significant difference was found between the two, the succeeding analyses for the channel utilized the specular version of the impulse response.

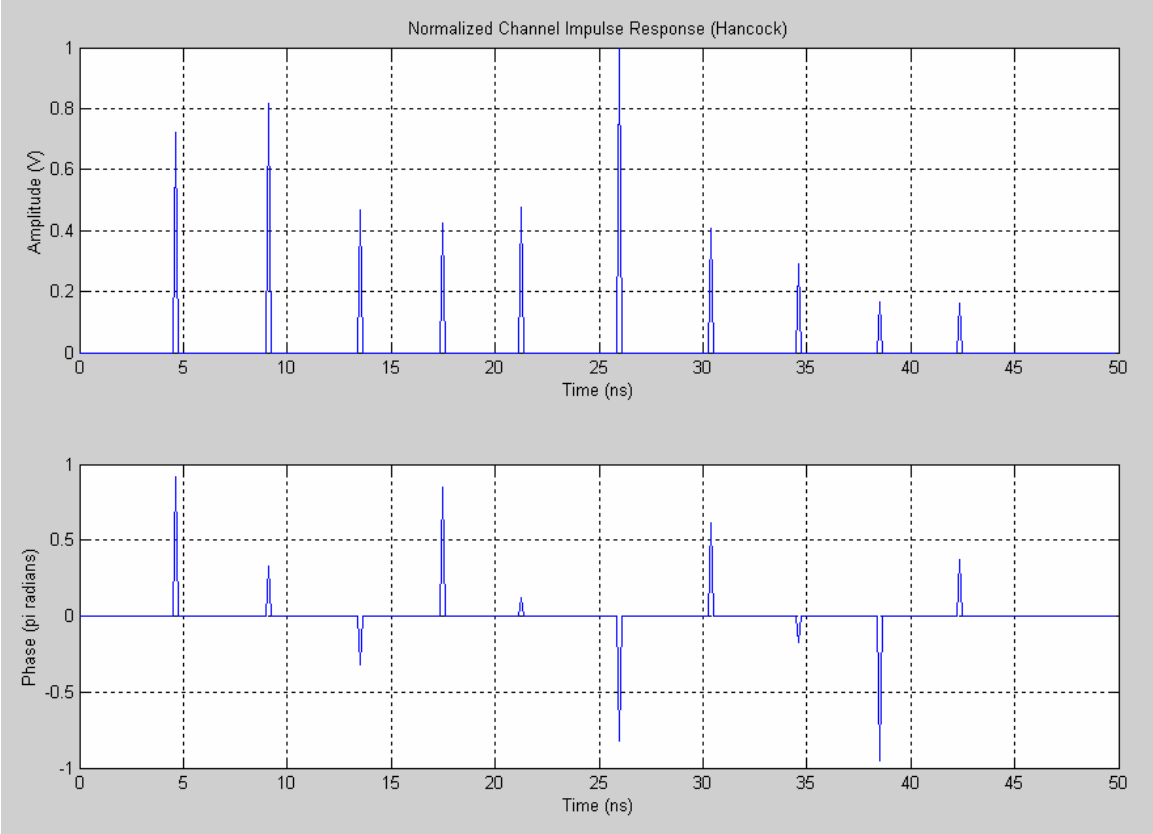

Figure 3-17: Specular representation of Hancock Hall impulse response.

This impulse response has some interesting characteristics. By comparing the time separation of the impulses in Figure 3-17 with the physical geometry of the channel in Figure 3-3 it may be possible to understand the mechanism causing each of the impulses in the response. The first assumption made is that the first pulse that arrives at the receiver is a reflection from the specular point on the limestone wall. This is reasonable since it is the shortest distance in the geometry. The pulse that occurs at 26 ns is probably a reflection from the glass windows behind the limestone structure. This also happens to be the only pulse that slightly deviates from the very regular, decreasing amplitude, pulse train that follows the initial pulse.

Starting at about 4 ns, successive pulses reach the receiver 4 ns apart and $0.7\,\pi$ different in phase. The pattern is only broken by the pulse at 26 ns attributed to the glass reflection which may be masking a smaller pulse occurring near that same time. The only distance in the geometry that could account for this separation is the depth of the limestone wall at about 0.6 m. The wall is not entirely limestone, but rather has a

limestone face with a concrete core. If the core of the limestone wall has some metallic support, it may be possible that the periodic pulses are caused by reflections from inside the wall.

The photograph of Hancock Hall in Figure 3-2 shows a surface that looks very rough. However, rather than a having a significant amount of diffuse scattering in the channel, the multipath is specular. This illustrates the dangers of drawing conclusions about the suitability of a NLOS path for a communications link. It also points out the utility of having a means for characterizing the impulse response of a channel.

3.2.1.3 Cowgill Hall Impulse Response

The Cowgill Hall impulse response is shown in Figure 3-18. In contrast to the Hancock Hall impulse response, this response contains a significant amount of diffuse scattering around 50 ns. Replacing the local maxima with discrete pulses produced a significantly different pulse response from the original. Since the discrete model did not produce a similar output, the succeeding analyses for this channel utilized the original response.

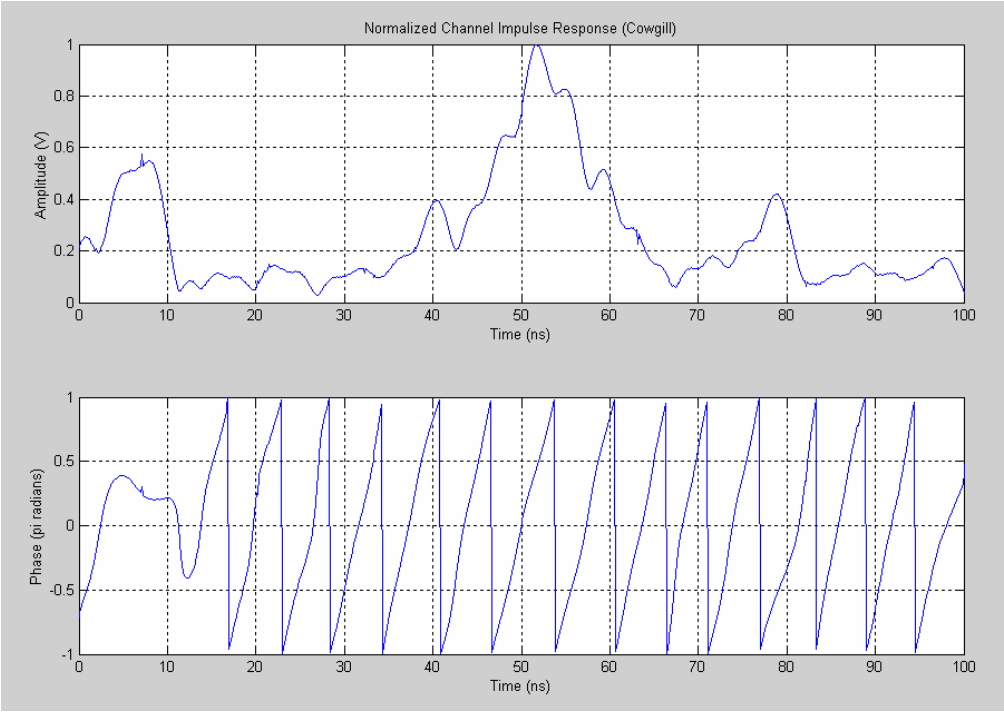

Figure 3-18: Cowgill Hall impulse response.

A comparison similar to the Hancock Hall analysis can be made by examining the physical channel in Figure 3-5 and deducing the mechanisms that caused the scattering and reflections seen in Figure 3-18.

The two closely spaced reflections near 5 ns in Figure 3-18 are probably due to the upper and lower portions of the fence that lines the front of Cowgill Hall. The difference in height could account for the difference in time delay. The geometry also suggests that the pulse that arrives around 40 ns is most likely due to the cement support that runs up the side of the building and protrudes about 2m from the building wall. This is very smooth cement, with a relatively small width that could account for the small amplitude of the reflection.

The continuum of energy that stretches from about 45 ns to 60 ns begins at approximately a time that corresponds to a reflection from the building wall. The significant scattering could be caused by a combination of multiple bounces between the glass wall and the cement support as well as from objects just inside the windows that may be good reflectors. The final reflection occurs at approximately 78 ns. This last pulse may be a result of multiple bounces from objects in the channel. The time corresponds to a bounce from the glass window to the cement fence and back to the window before reaching the receiver.

The Cowgill Hall photograph in Figure 3-4 shows a very smooth surface with a single relatively thin protrusion from the building. It might be assumed that this surface would produce very little diffuse scattering, but this is certainly not the case. This again shows that simple observations of surfaces may not be adequate to form reasonable estimates as to their suitability for NLOS communications.

3.2.2 Model Implementation in SPW

Modeling the impulse responses as filters allowed for their simple inclusion in Monte Carlo simulations. The signal processing software package SPW readily accepts filter based responses and is an excellent environment for Monte Carlo analysis. The SPW simulations produced BER curves as a function of C/N for different radio configurations and the results compared to the results of the proposed performance estimation algorithm. The basic SPW system diagram is shown in Figure 3-19.

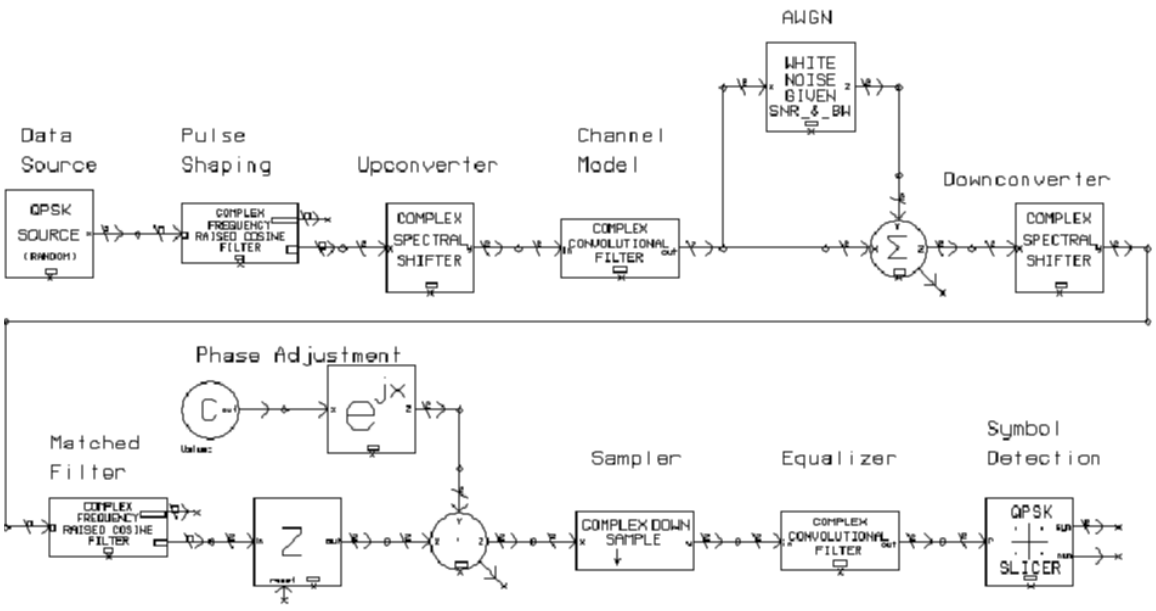

Figure 3-19: SPW system block diagram used in Monte Carlo simulations.

The data source block in the top left corner of Figure 3-19 is the start of the transmit chain. The data source block outputs a baseband QPSK data stream which is square-root raised cosine pulse-shaped. In some of the simulations, the signal is moved around in the channel by using a complex spectral shifter which works as an upconverter. The signal is then passed through the channel filter after which thermal noise is added. The signal is then returned to baseband by the downconverter block and match filtered. The delay and phase adjustment section is a manual operation that corrects the signal timing and phase so proper sampling can occur before symbol detection. When necessary, the equalizer is modeled as a filter and placed right before the symbol detection.

4 Estimating the Effects of Non-Ideal Channel Responses on Link Performance

4.1 Characterizing the Bit Error Distribution

Ways to characterize the performance of a communications link differ depending on the distribution of errors caused by the channel. If the errors appear to be uncorrelated, standard bit error probability curves as a function of C/N are adequate to characterize performance. If, on the other hand, the errors are correlated, other metrics must be included to describe the distribution of the errors. Characterizing this distribution is important since degradation mitigation techniques differ in applicability based on this distinction.

To determine the 'randomness' of the errors, autocorrelations were calculated on a number of different channel types, including those collected on the Virginia Tech campus. The autocorrelation of a discrete, real-valued, deterministic signal is defined as

$$R_s(\eta) = s(n) \cdot s(n - \eta) \tag{4.1}$$

, where $R_s(\eta)$, is the autocorrelation of the signal, s(n), at time delay η. s(n) is the discrete signal under investigation, n is an integer that represents a discrete time instant, and η is an integer time shift.

Autocorrelation is a measure of how similar a signal is with itself at different time delays, also called time lags. The maximum value of the autocorrelation sequence occurs at zero lag. That is the time at which the signal is perfectly aligned with itself. The autocorrelation produces a number at each time lag that corresponds to how alike a signal is with itself at that time difference. A signal whose autocorrelation goes to zero quickly as the time delay increases is considered to be very unlike itself over time. A signal whose autocorrelation decays slowly as the delay is increased is a signal that changes slowly with time. This implies that present values of the signal depend on previous ones.

SPW simulations utilized AWGN, Rayleigh fading, and the collected channel responses to find representative error sequences produced by each channel. SPW recorded error sequences for each of the channels investigated over a range of C/N and simple autocorrelation operations performed on the error sequences produced the results in the following figures. The autocorrelation result for one AWGN channel is shown in Figure 4-1.

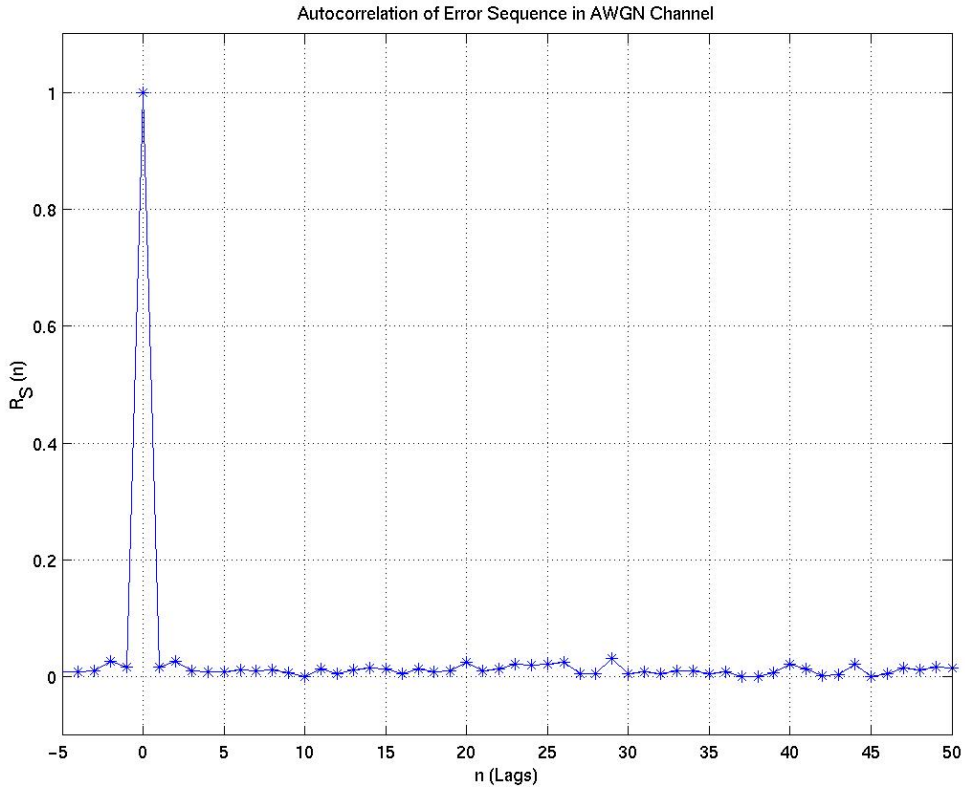

Figure 4-1: Autocorrelation for a sample error sequence derived from an AWGN channel.

Note that the peak occurs at zero lag and that the subsequent values are all approximately zero. This agrees with the common understanding that errors caused by AWGN are uncorrelated.

Figure 4-2 is a similar analysis done on a Rayleigh fading channel. In these channels, the signal amplitude changes over time causing errors to occur in bursts.

Again, we can see that the maximum occurs at the zero lag, but in contrast to the autocorrelation of the error sequence in the AWGN channel, the values decay very slowly as the time delay is increased. This is an indication that the errors in this channel are correlated.

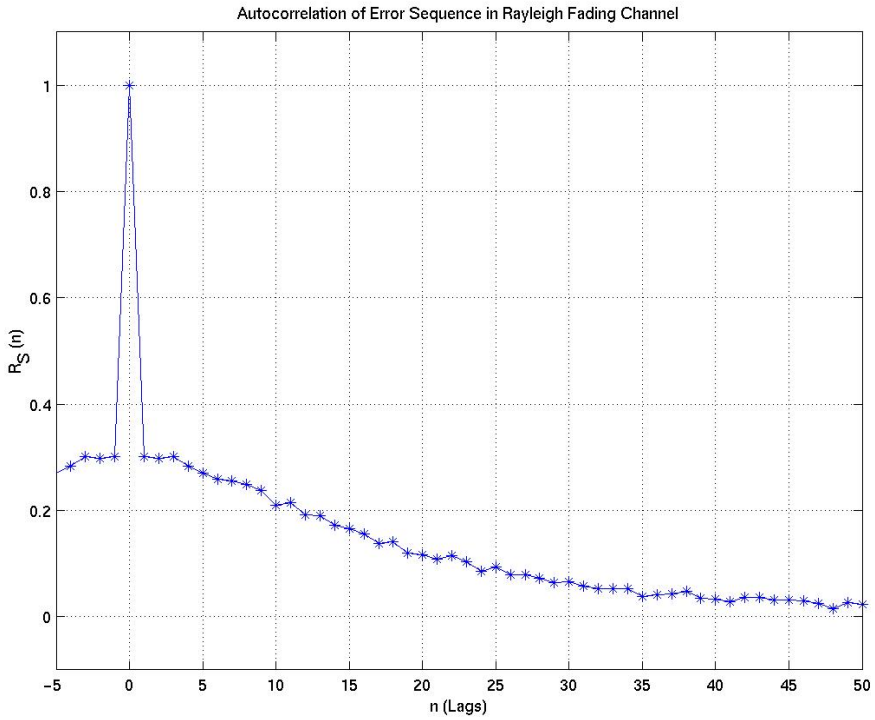

Figure 4-2: Autocorrelation for a sample error sequence derived from a Rayleigh fading channel.

Finally, the autocorrelations of the error sequences from several of the measured channels were calculated for comparison. Figure 4-3 is an example of the results for a Cowgill Hall channel and Figure 4-4is an example from the Hancock Hall channel.

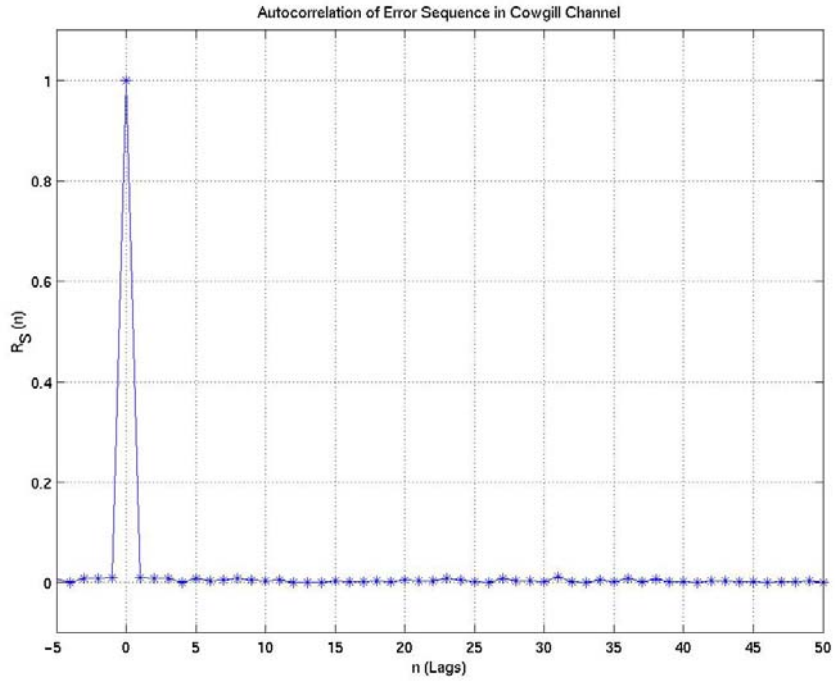

Figure 4-3: Autocorrelation for a sample error sequence derived from the Cowgill Hall channel.

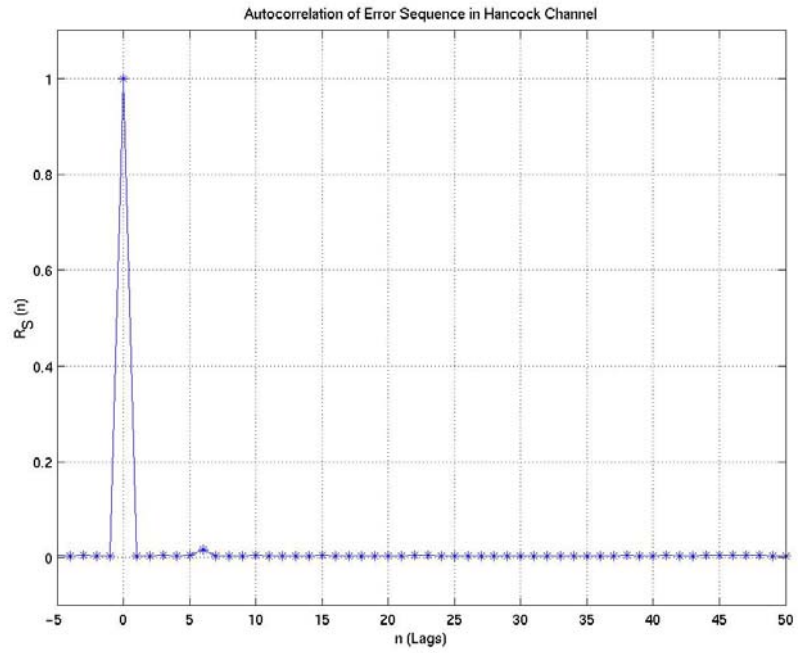

Figure 4-4: Autocorrelation for a sample error sequence derived from the Hancock Hall channel.

The almost imperceptible values of the autocorrelations at any lag other than zero show that the errors produced in these channel are also uncorrelated. Since the errors are uncorrelated, it is appropriate to consider average BER as a performance metric in these channels.

4.2 Determining the Irreducible BER

The irreducible BER is the BER of a link in the absence of thermal noise. This is the BER that the system can expect due solely to the channel induced ISI. The procedure to determine this from the channel impulse response will be illustrated with a specific example, but the procedure itself is independent of modulation and pulse shape. The following example is a QPSK signal with a raised cosine pulse shape and roll-off equal to 0.2. The transmitted pulse and channel impulse response used for this example are shown in Figure 4-5 and Figure 4-6.

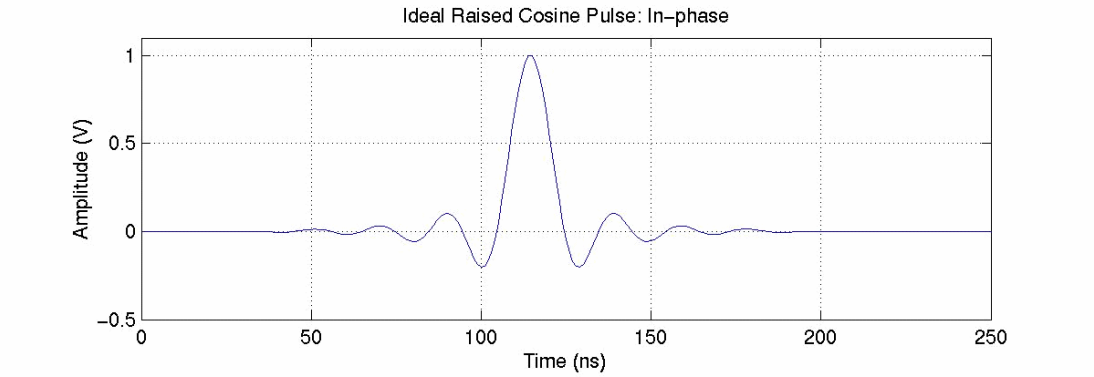

Figure 4-5: Ideal raised cosine pulse with roll-off equal to 0.2.

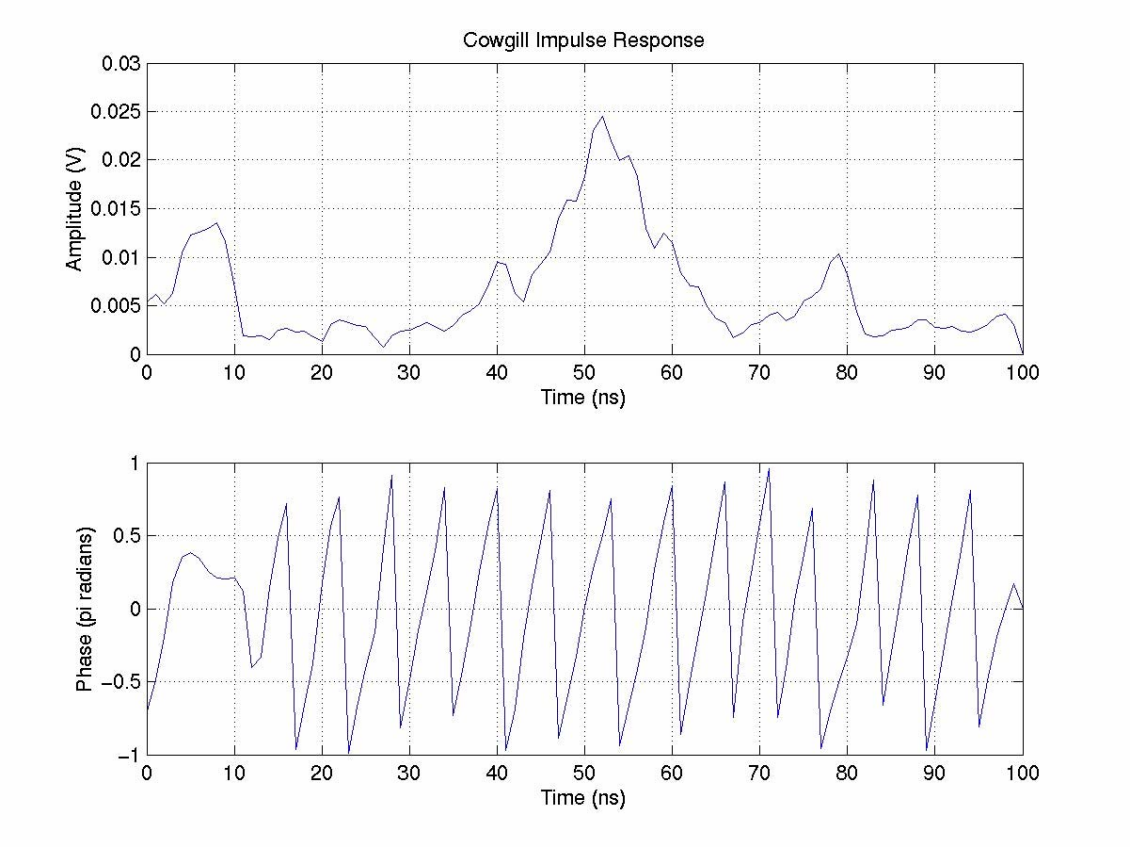

Figure 4-6: Channel impulse response used in irreducible BER example.

To find the received signal, convolve the pulse shape with the channel model and sample the resulting waveform at the symbol rate. To adjust for optimum sampling at the receiver, phase rotate the signal such that the maximum magnitude has zero phase before sampling. This output is shown in Figure 4-7.

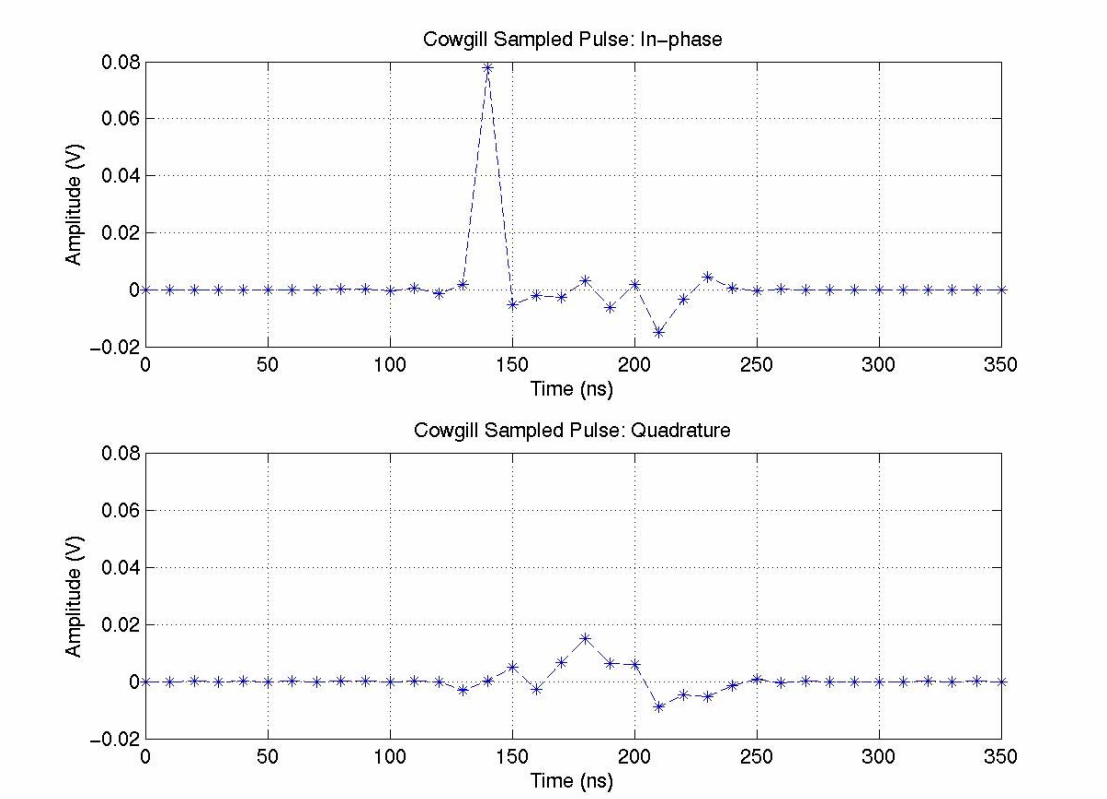

Figure 4-7: Sampled received signal as the convolution of the ideal pulse and channel model.

The maximum amplitude of the sampled waveform is the mean signal amplitude, μ_s, of a random data stream passed through the filter and sampled at the symbol rate. The rest of the samples contribute to the ISI. An illustration is helpful in understanding the arguments for the previous statement.

For simplicity, consider only the in-phase signal and look at a symbol transmitted across this channel, Figure 4-8.

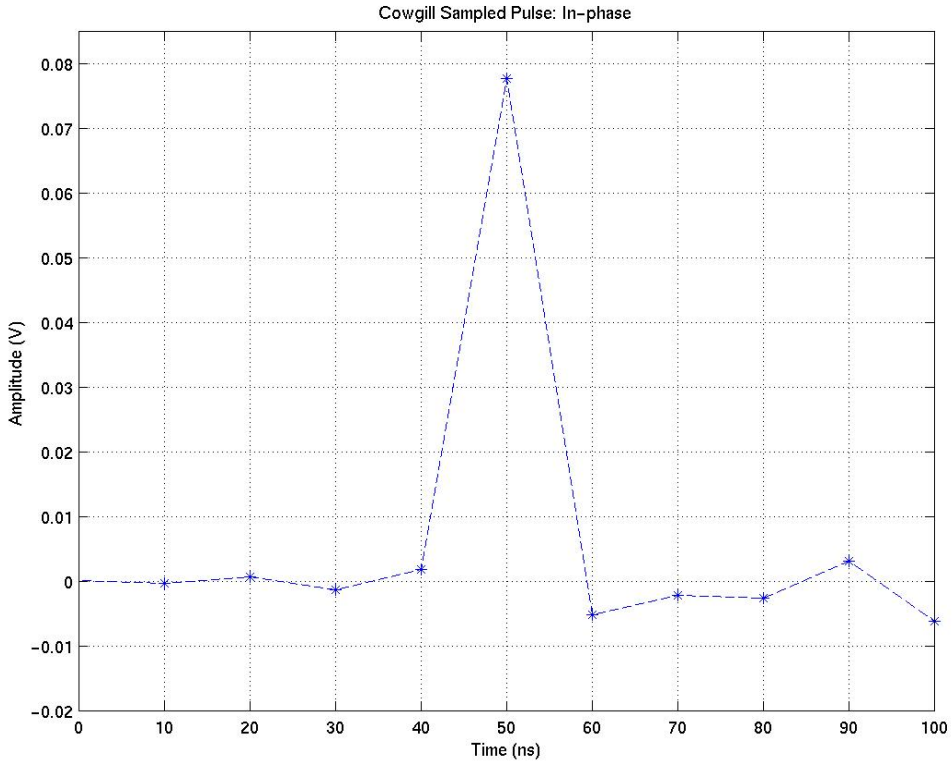

Figure 4-8: One channel distorted sampled received pulse.

The decision is made on this symbol at 50 ns. Suppose that the previous symbol sent has the same polarity, Figure 4-9, and is detected at 40 ns. Because of the non-ideal nature of the channel, the symbol at 40 ns contributes ISI to the symbol at 50 ns. This ISI has the same amplitude as the 50 ns symbol at time 60 ns.

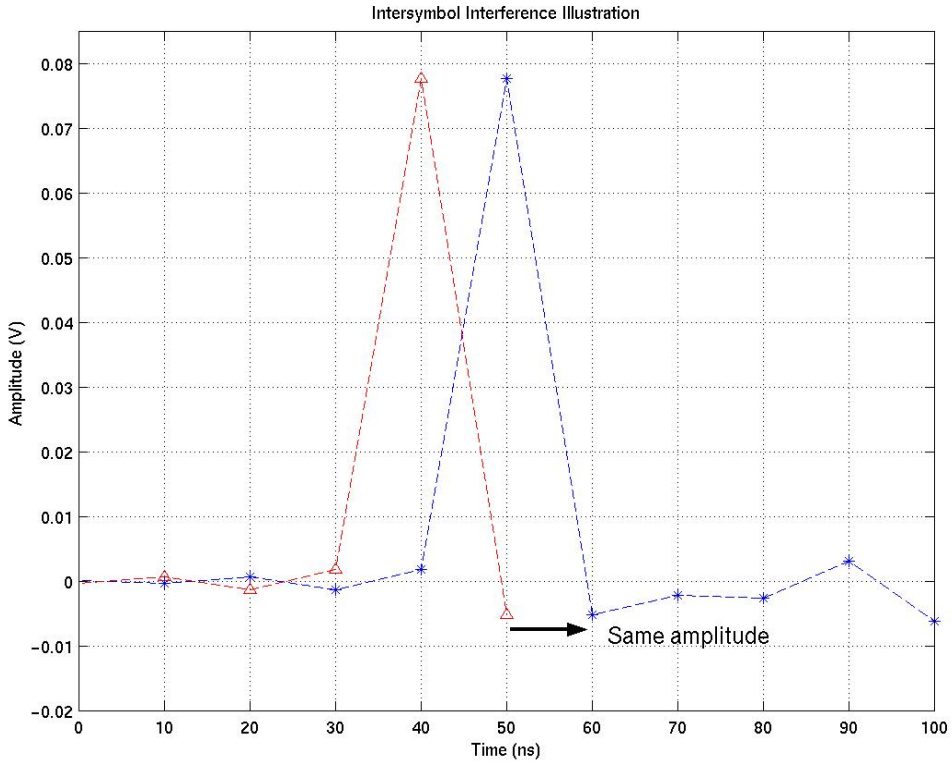

Figure 4-9: Intersymbol interference illustration with two successive pulses.

Now suppose that another symbol with the opposite polarity was sent immediately before the other two symbols and was sampled at 30 ns as in Figure 4-10. This symbol contributes ISI to the 50 ns symbol equal to the negative of the amplitude of the 50 ns symbol sampled at time 70 ns.

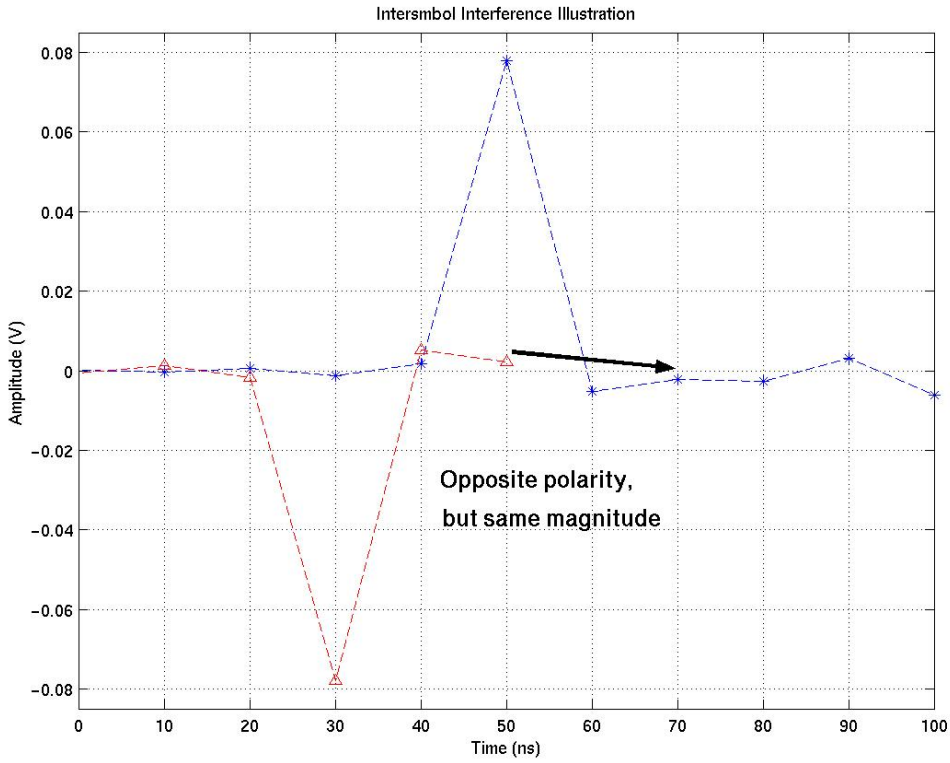

Figure 4-10: Intersymbol interference illustration with two symbols separated by two symbol periods.

One can imagine this process going on in either direction of the main pulse and see that the samples to either side of the main sample constitute the contributions to the total ISI possible from all other symbols. These ISI contributions can be positive or negative depending on the polarity of the interfering symbol. As long as it can be assumed that all symbols are equally likely and independent, a probability density function (PDF) can be formed from all possible combinations of the ISI samples.

Let A_i be a single ISI contributor found from the sampling process described above and let M equal the total number of ISI contributors used in the calculation. To find the largest possible value of ISI, sum the absolute values of A_i for i equals one to M.

$$I_N = \sum_{i=1}^{M} |A_i| \tag{4.2}$$

, where I_N is the largest possible ISI value and N is the total number of possible ISI values. The minimum ISI value, I_1, can be found by taking the negative of (4.2).

$$I_1 = -\sum_{i=1}^{M} |A_i| \tag{4.3}$$

To find the rest of the possible ISI values, calculate every possible combination of +/- the individual ISI contributors.

$$I_k = \sum_{i=1}^{M} (\pm)_k A_i \tag{4.4}$$

, where $(\pm)_k$ is a unique combination of + and -.

The PDF can be any shape, but the mean is zero since each combination of ISI contributors has a single exact negative that is also a possible total ISI value. That is, each ordered set $(\pm)_k$ has a counterpart $(\pm)_j$ where

$$(\pm)_k = -(\pm)_j \tag{4.5}$$

Since the mean of the ISI is zero, the maximum amplitude after sampling must be the mean amplitude, μ_s. A PDF is formed by constructing a histogram of the values in I and dividing the count in each bin of the histogram by the total number of possible ISI values, N. Mathematical bounds have been found for the PDF of these sums [10], but the bounds are too wide to be of much practical use. Instead, using the largest 20 ISI contributors to determine the PDF was a reasonable compromise between accuracy and computation time. The PDF of the ISI for this example is shown in Figure 4-11.

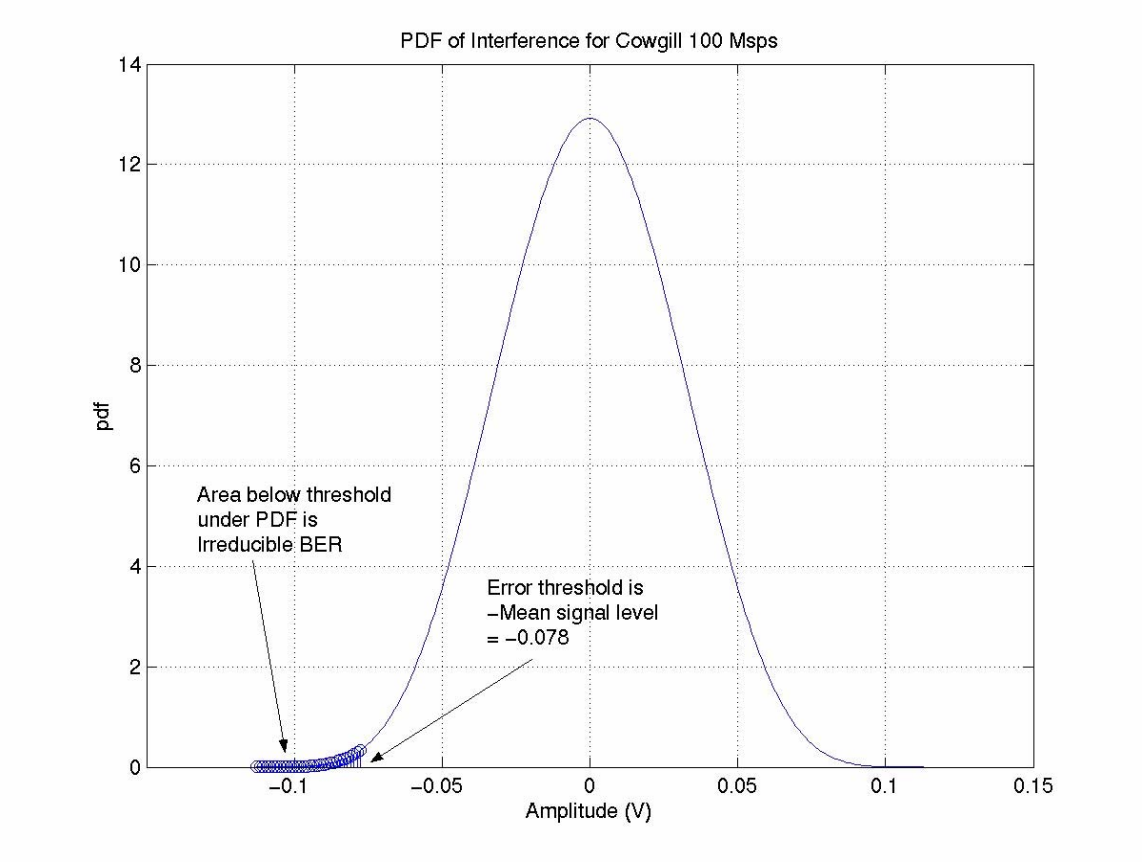

Figure 4-11: Example probability density function of intersymbol interference.

To find the irreducible BER, calculate the area under the PDF that crosses the decision threshold. In this example, it is the shaded area of the PDF in Figure 4-11, where the threshold is $-\mu_s$. This area is the probability that a bit error occurs in the absence of thermal noise and is the best possible BER for the channel.

Figure 4-12 is data from an SPW simulation that produced a BER curve as a function of C/N. The simulation shows that as C/N increases, the BER levels off at about 0.002 which is the level estimated by the algorithm.

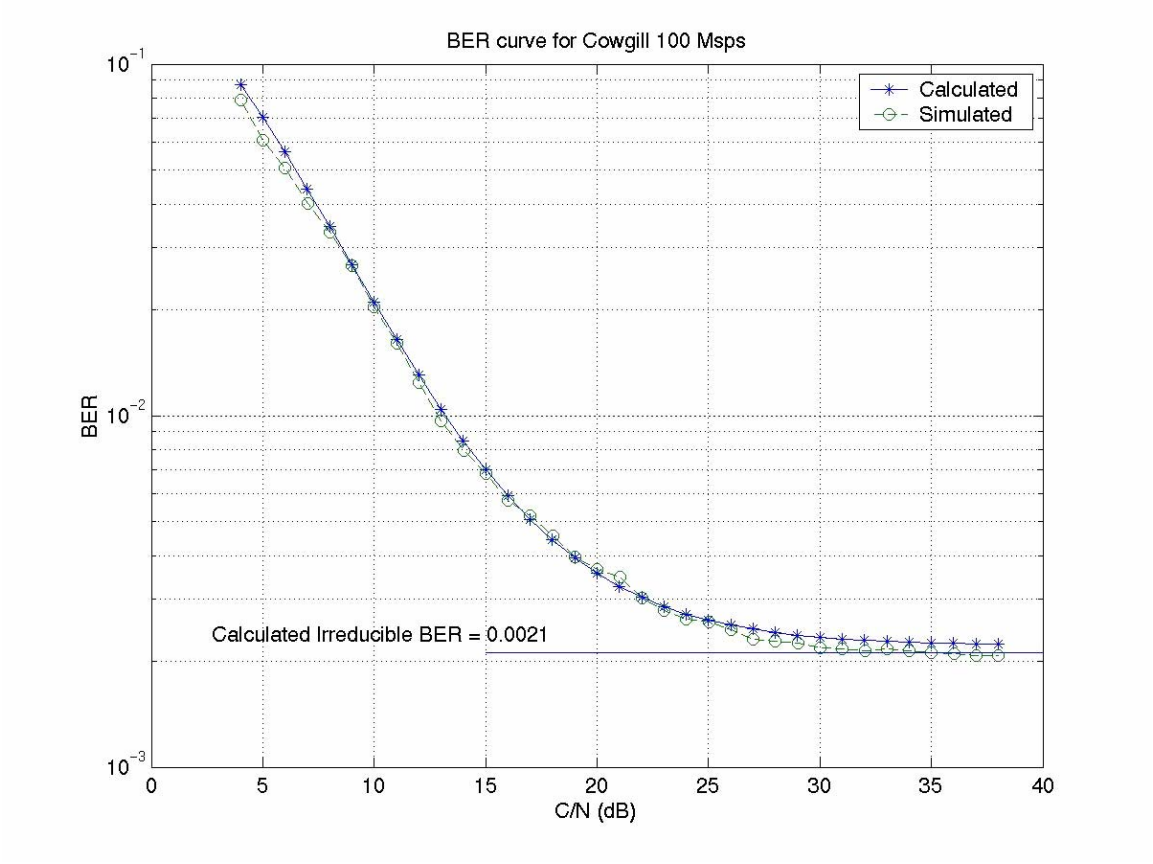

Figure 4-12: Irreducible BER calculation and Monte Carlo simulation results.

4.3 Average BER

From the analysis begun in Section 4.2, it is a quick step to estimate the average BER as a function of C/N. In Section 4.1, the PDF of the ISI was estimated. To find the average BER as a function of C/N, the PDF of the ISI must be combined with the PDF of the noise. By assuming that the noise and ISI are independent of one another, we can place them on orthogonal axes and easily combine them to form the conditional PDF of the received signal as shown in Figure 4-13. The conditional PDF is the combined PDFs of the ISI and noise given that a signal of a certain amplitude has been transmitted. In this analysis, the PDF of the ISI is shifted along the signal level axis and centered at the mean signal level, μ_s.

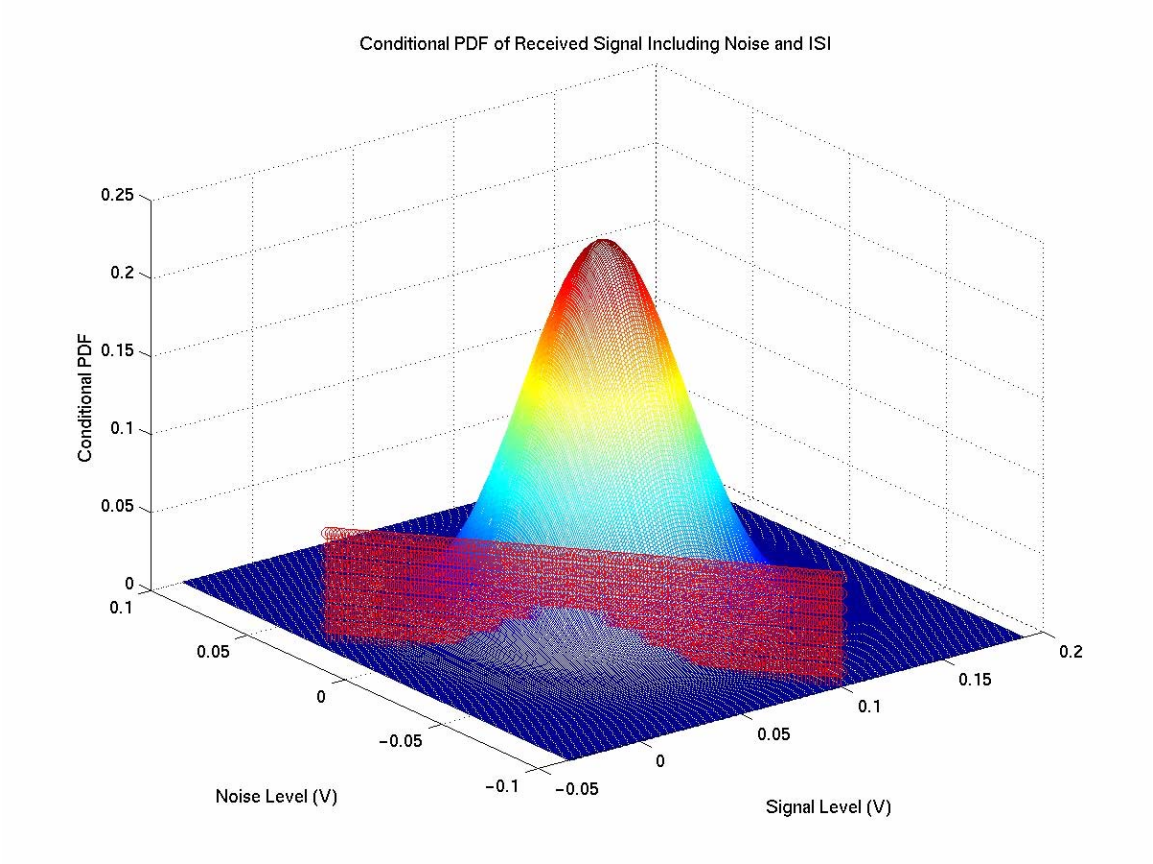

Figure 4-13: Conditional probability density function of received signal amplitude.

To find the average BER for a given ISI and noise distribution, first draw a plane normal to the signal-noise plane through the line N = -S. This is the threshold where the signal plus noise produce a zero voltage at the receiver output. It is shown in Figure 4-13 as the 'fence' cutting through the conditional PDF. The volume under the conditional PDF where the noise is large enough to change the sign of the signal is the probability of error.

The BER curves generated in Figure 4-14 and Figure 4-15 derived from SPW simulations and results calculated using the algorithm. Comparison of the simulated results to the calculated results should provide insight into the validity of the algorithm. Figure 4-14 is a comparison of the results for fixed data rate signals in several frequency bands within the Hancock Hall channel and Figure 4-15 is a comparison of results for different data rate signals with the same center frequency in the Cowgill Hall channel. The mix of channels and data rates demonstrates the performance of the algorithm for

different configurations. For all channels investigated, the algorithm results and SPW simulations agreed within 1 dB.

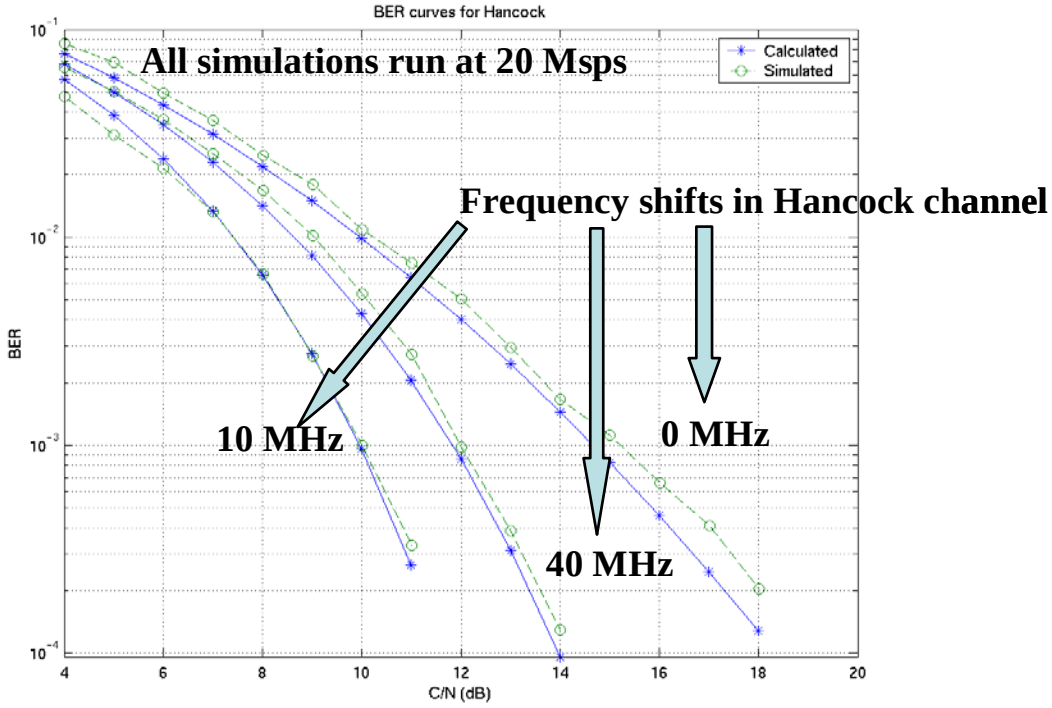

Figure 4-14: Comparison of SPW simulation and algorithm results for BER as a function of C/N for different bands in the Hancock Hall channel.

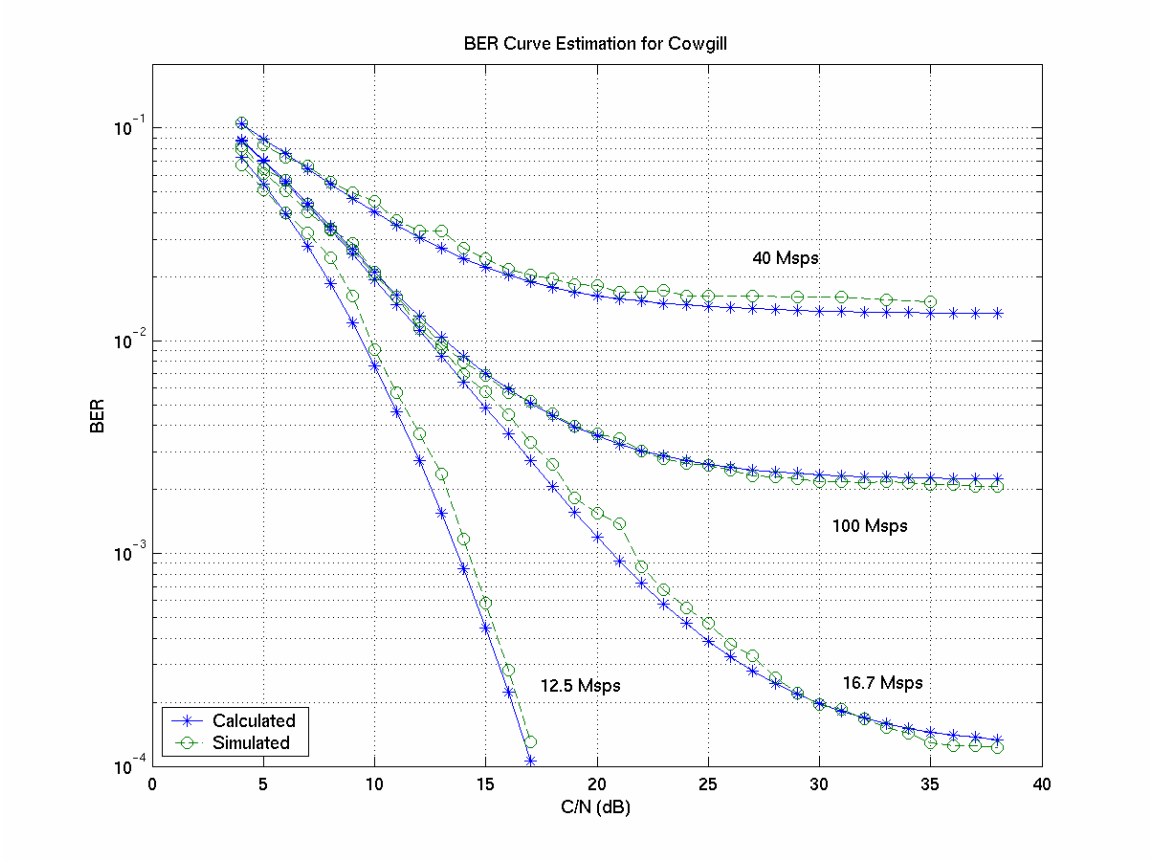

Figure 4-15: Comparison of SPW simulation and algorithm results for BER as a function of C/N for different bandwidth signals centered in the Cowgill Hall channel.

Figure 4-15 illustrates a peculiar phenomenon that occurs with static channels. Notice that the performance gets worse as the data rate is increased from 12.5 to 16.7 to 40 Msps before getting better when the data rate is further increased to 100 Msps. This increase in performance as data rate increases is counter-intuitive. Janssen et al in [11] make reference to similar results in their analysis of indoor channels.

Figure 4-16 and Figure 4-17 are the frequency responses of the Cowgill Hall 40 and 100 MHz channels. They both have the same center frequency, and include the largest frequency dropout in the band. This means that the peak-to-peak amplitude and group delay variation are the same in both channels. What is different is that the variance of the amplitude and group delay is markedly different for the two channels. The 100 MHz channel has an amplitude variance that is 2 dB better than the 40 MHz channel and a group delay variance that is better by almost 200 ns^2. This means that, relatively

speaking, the 100 MHz channel is flatter and has a phase response that is more linear than the 40 MHz channel and therefore can sustain better performance.

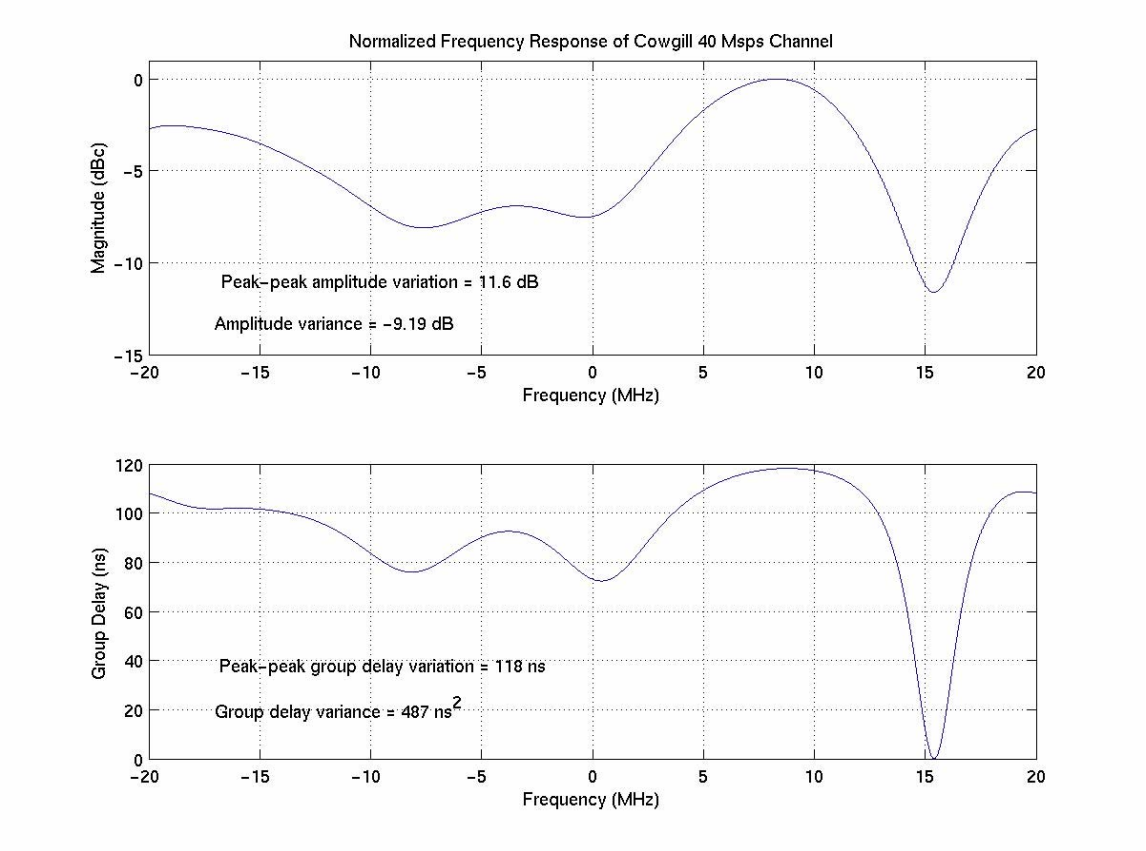

Figure 4-16: Frequency response of Cowgill Hall channel for 40 Msps signal.

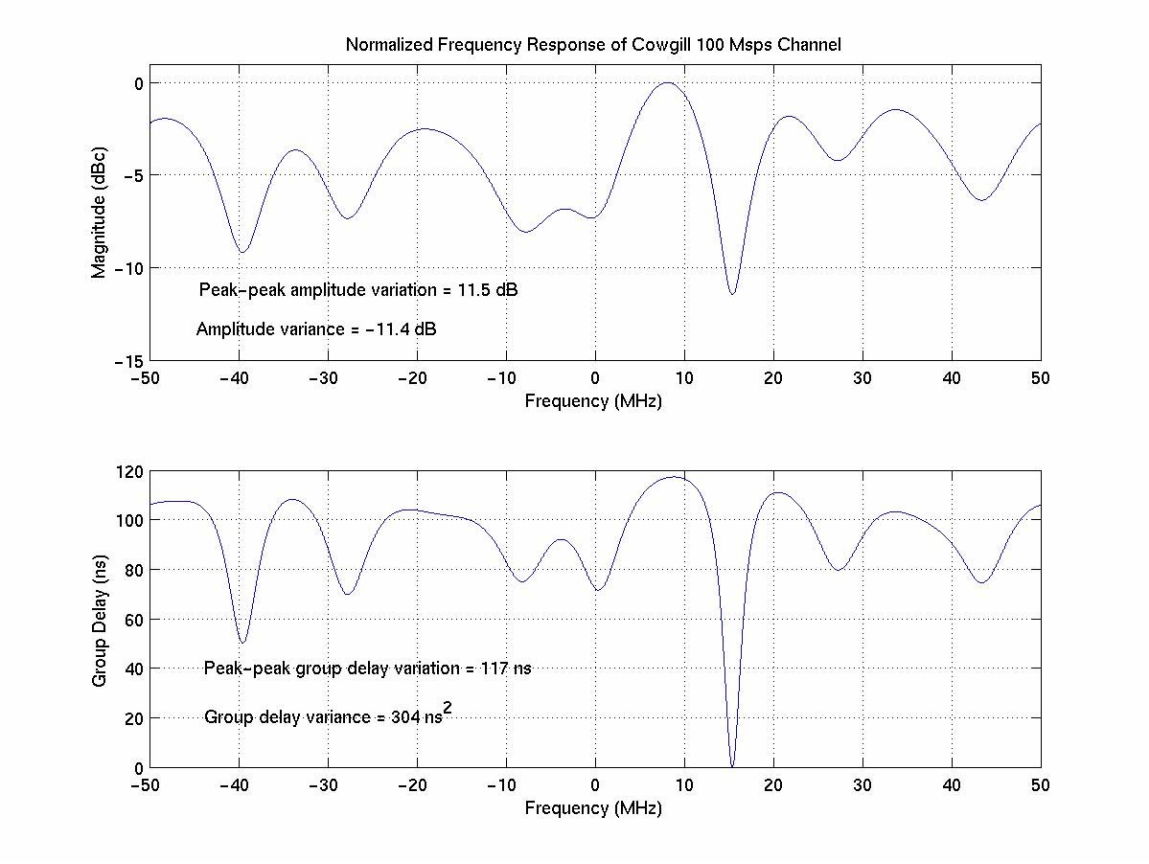

Figure 4-17: Frequency response of Cowgill Hall channel for 100 Msps signal.

5 Equalizer Performance

In an effort to minimize the system complexity and number of computations, the equalizers described in the following sections are symbol rate equalizers. That is, the taps are spaced at intervals equal to the symbol period, which is the minimum rate a receiver will sample a signal. If symbol rate equalizers work reasonably well, the complexity and time it takes to process the signal can be kept to a minimum.

5.1 Effective Channel Pulse Response

The effective channel pulse response differs from the effective channel impulse response in that it is the output of the channel and equalizer when excited by a representative transmitter pulse. The effective impulse response of the channel is the output of the channel and equalizer when excited by an impulse. In the time domain, the effective channel pulse response is the convolution of the transmitted pulse and the impulse responses of the channel and equalizer. The progression from pulse to effective pulse response is depicted in Figure 5-1.

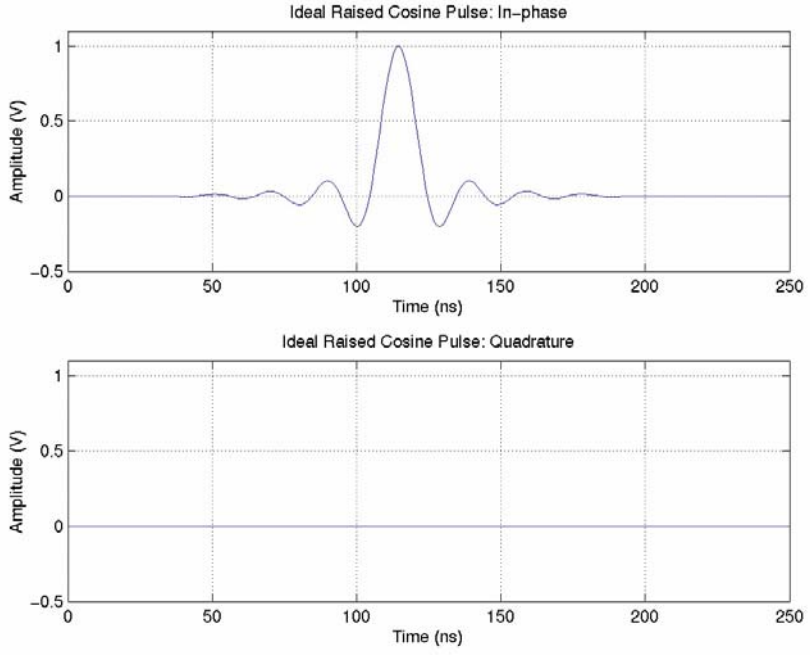

a)

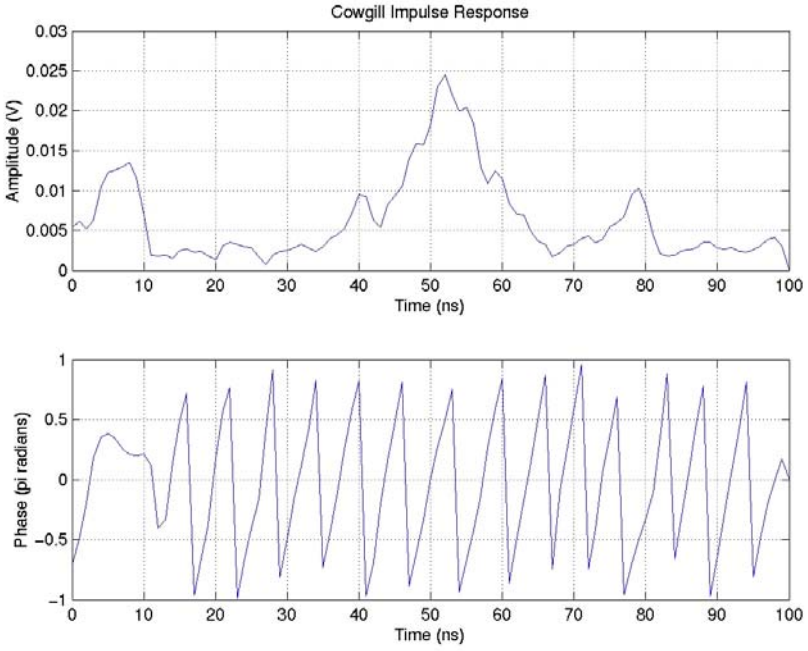
Cowgill Impulse Response
Amplitude (V)
Time (ns)
Phase (pi radians)
Time (ns)

b)

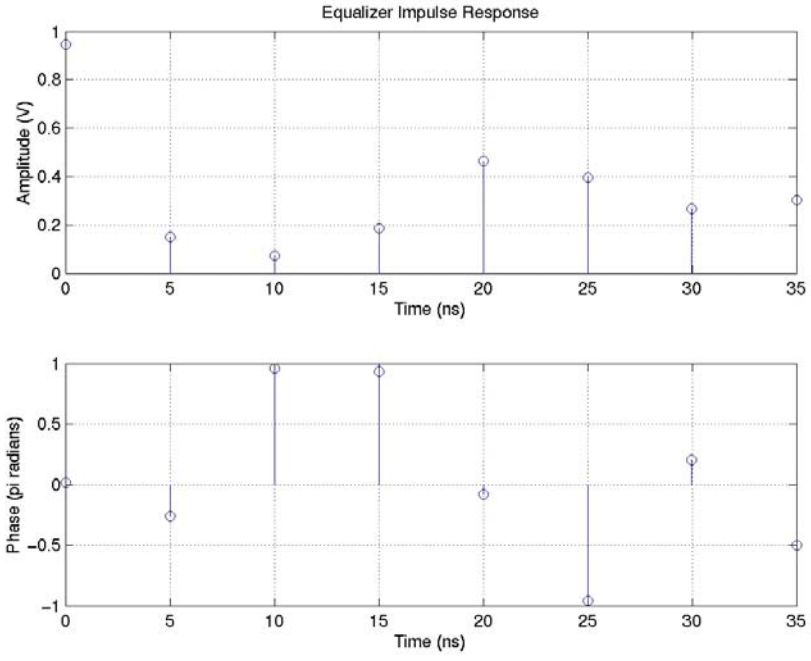
Equalizer Impulse Response
Amplitude (V)
Time (ns)
Phase (pi radians)
Time (ns)

c)

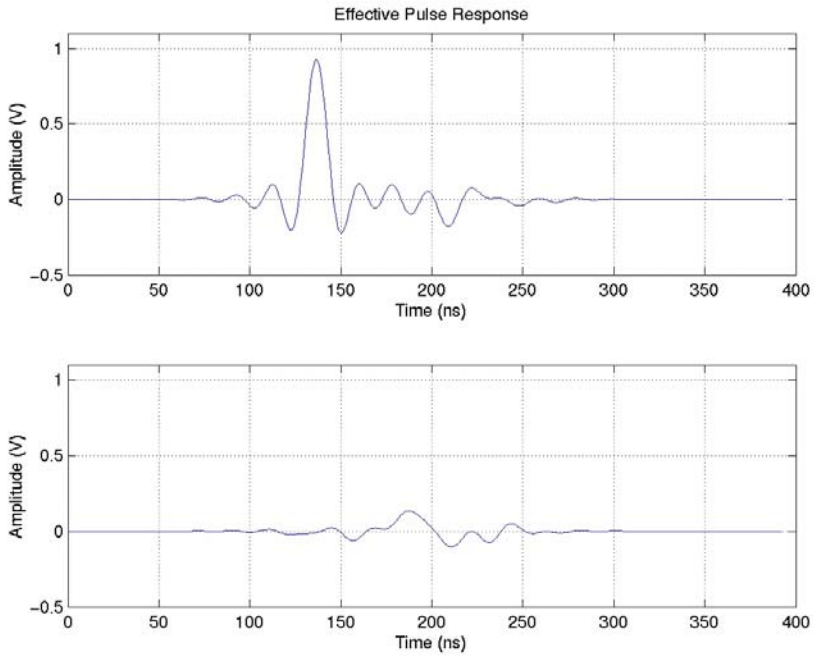

d)

Figure 5-1: Pulse to effective pulse response a) Ideal pulse b) Channel impulse response c) Equalizer impulse response d) Effective pulse response.

One example of the comparison between the SPW simulations and the algorithm results for equalized channels is shown in Figure 5-2, where it can be seen that the algorithm compares reasonably with the SPW simulations.

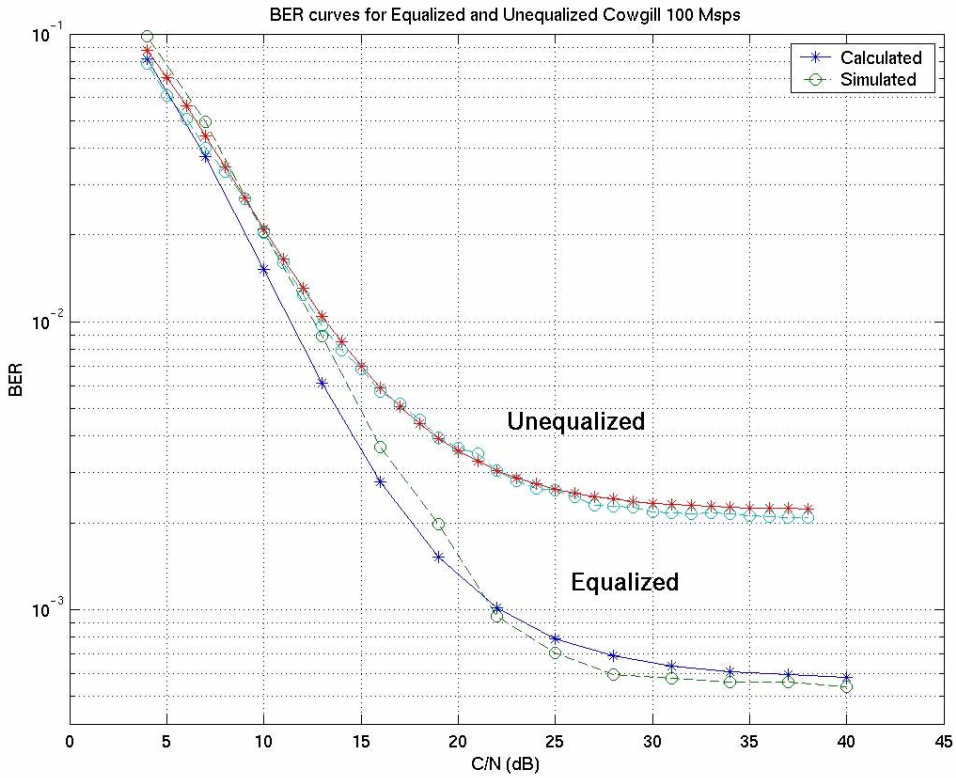

Figure 5-2: Comparison of Monte Carlo simulations and algorithm performance estimation for a Cowgill Hall equalized and unequalized channel.

The ability to run the algorithm on equalized channels does fit with intuition. The channel is modeled as a filter and the equalizer is merely a filter with a specific purpose. Convolving the two to obtain a new channel simply creates a new filter. Since the algorithm is indifferent to the filter model origin, the results should remain consistent.

5.2 Zero-Forcing Equalizer

Zero-Forcing (Z-F) equalizers are filters that attempt to force the channel induced ISI to zero. However, the equalizer also shapes the thermal noise present in the receiver and may also decrease the C/N. An example of a Z-F equalizer's effect on noise is shown in Figure 5-3.

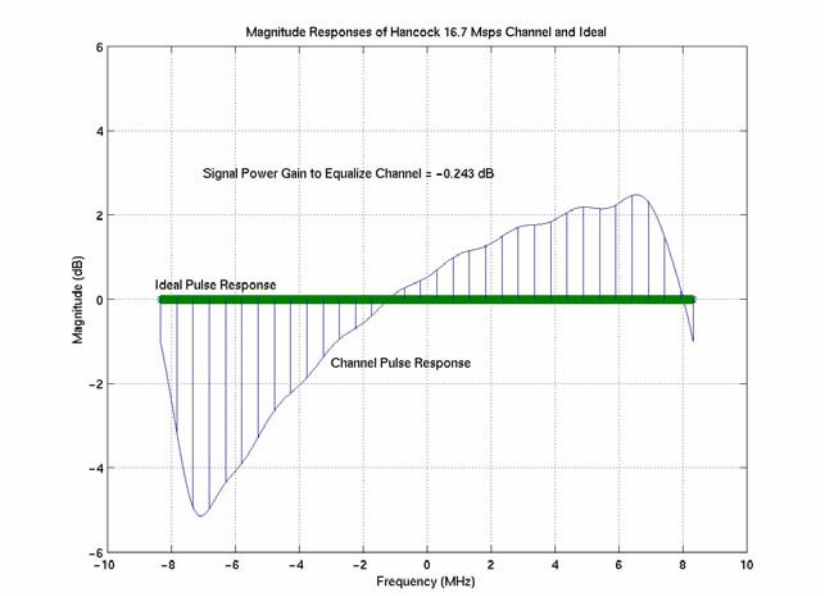

a)

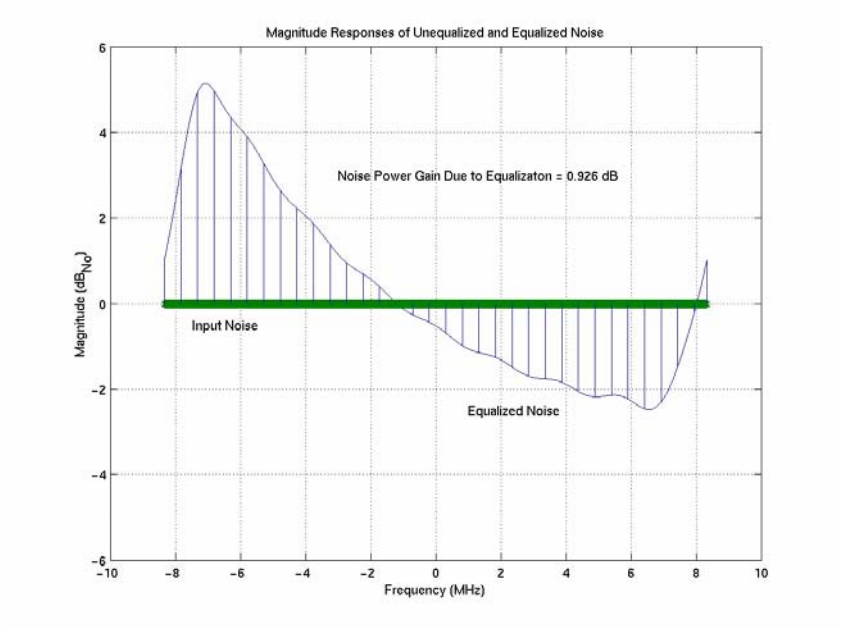

b)

Figure 5-3: Illustration of change in a) signal spectrum and b) noise spectrum due to a Zero-Forcing equalizer.

The flat line in Figure 5-3a represents the ideal signal amplitude response and the curved line is the actual signal amplitude response. In order to remove ISI, the Z-F equalizer flattens the amplitude spectrum by forming an equalizer frequency response that is the reciprocal of the channel frequency response. The shaded area in Figure 5-3a

is the change in signal power from the input of the equalizer to the output of the equalizer. Figure 5-3b shows what happens to the noise as it passes through the equalizer. The flat line in Figure 5-3b is the input noise power spectral density and the curved line is the frequency response of the equalizer. The shaded area is once again the change in signal power from the input to the output of the equalizer, only in this case, the signal is the thermal noise. To find the minimum degradation achievable in the channel, subtract the change in noise power from the change in signal power (in dB). In the case shown, this value is 1.2 dB.

To find the tap weights for the Z-F equalizer, first find the frequency response of that part of the channel in which the signal will reside. This can be done in practice by taking the fast Fourier transform (FFT) of the channel impulse response and keeping only those points in the chosen band. The FFT is an efficient algorithm for calculating the Fourier transform. The frequency spectrum spanned by the FFT is from $-f_s/2$ to $f_s/2$ where f_s is the sampling frequency of the original signal. The frequency steps are determined by the length of the FFT, so it is a straightforward calculation to find the points which correspond to the desired frequency band. These points are the channel frequency response, $H_c(f)$. The Z-F equalizer frequency response is (5.1).

$$H_{eq}(f) = \frac{1}{H_c(f)} \tag{5.1}$$

The tap weights, $h_{eq}(t)$, can then be found by taking the inverse FFT (IFFT) of $H_{eq}(f)$.

$$h_{eq}(t) = F^{-1}\{H_{eq}(f)\} \tag{5.2}$$

It is possible to use a windowing technique on the frequency response of the tap weights to further refine the time domain representation. In the interest of efficiency, this step was not performed so the computational load could be kept low.

Using all of the taps will effectively eliminate any ISI in the channel, but at a computational cost that might be excessive. A method should be devised that balances the desire to equalize the channel and also the need to keep processing time reasonable. Numerous cases were investigated for equalizer performance in both the Hancock and Cowgill channels. Figure 5-4 and Figure 5-5 show the frequency response and BER

performance for sub-channels within the Hancock and Cowgill channels. In all of the cases investigated, using about 98% of the energy in the tap weights gets performance to within 2 dB of the optimum Z-F equalizer performance.

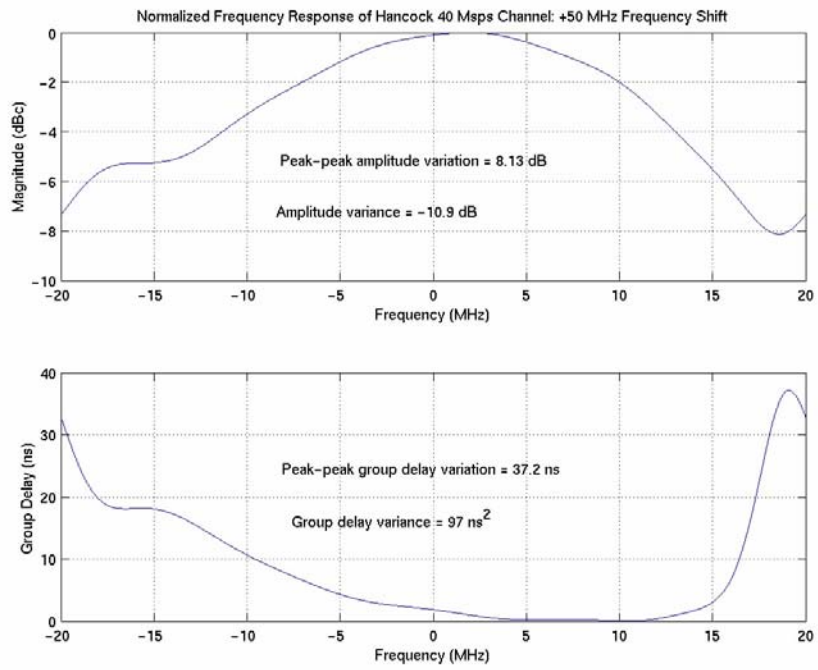

a)

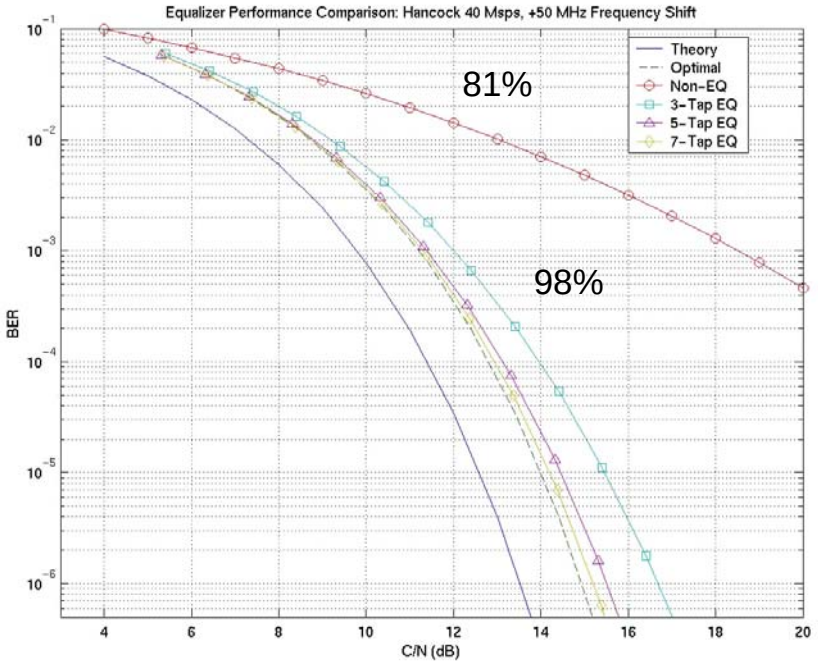

b)

Figure 5-4: Hancock Hall channel a) frequency response and b) BER performance for symbol rate equalizers with different numbers of taps and the total tap weight energy in percent.

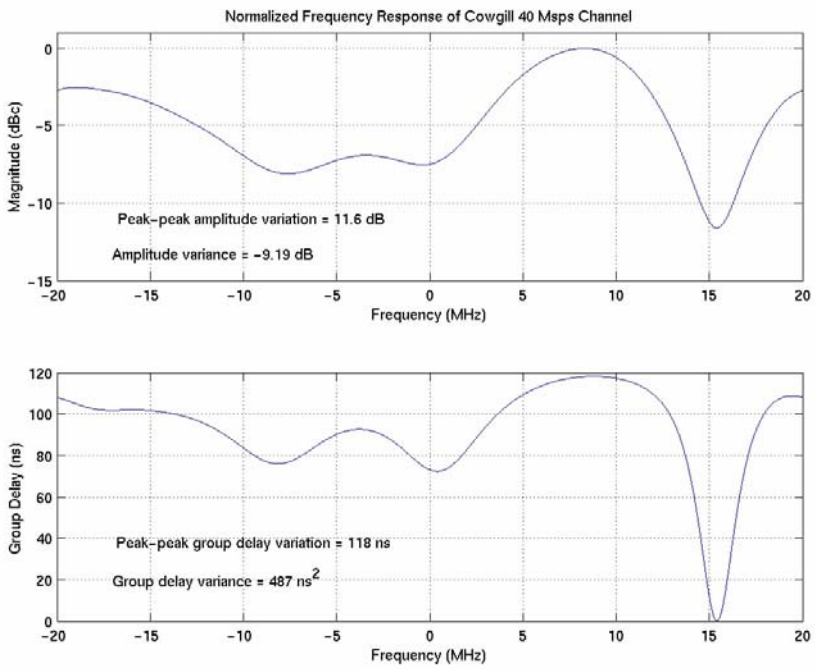

a)

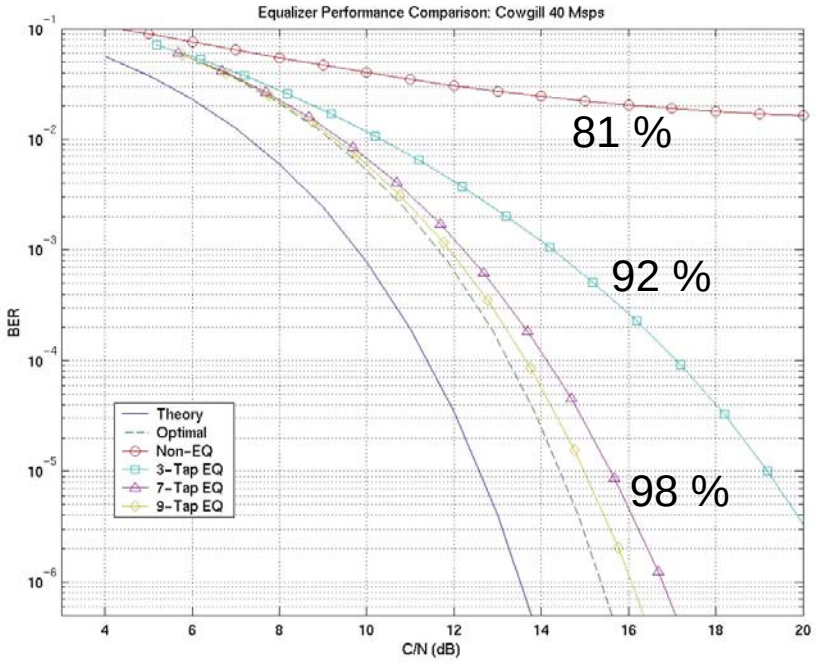

b)

Figure 5-5: Cowgill Hall channel a) frequency response and b) BER performance for symbol rate equalizers with different numbers of taps and the tap weight energy shown in percent.

5.3 Minimum Mean Square Error Equalizer

The Z-F equalizer, while simple to implement, suffers from the disadvantage that it does not take into account the effect it has on thermal noise in the receiver. The Minimum Mean Square Error (MMSE) equalizer attempts to balance the degradation caused by the ISI with the degradation caused by the thermal noise. This type of equalizer will, in general, work much better than a Z-F equalizer, but knowledge of the C/N is required as the tap weights are a function of C/N. A mathematical analysis of MMSE equalizers will not be presented here, but can be found in any number of texts on equalizers [12].

To find the tap weights of an MMSE equalizer, start with the sampled pulse, p(n), that has been passed through the channel and find the autocorrelation of it, $R_p(\eta)$.

$$R_p(\eta) = p(n) \cdot p(n - \eta) \tag{5.3}$$

Add to the value of the zero lag 1/(C/N) and call the result $R_{pmod}(\eta)$.

$$R_{pmod}(\eta) = R_p(\eta) \text{ for } \eta \neq 0$$

$$R_{pmod}(0) = R_p(0) + \frac{1}{C/N} \tag{5.4}$$

Calculate the FFT of both p(n) and $R_{pmod}(\eta)$ and call them P(f) and $S_{pmod}(f)$.

$$P(f) = F\{p(n)\} \tag{5.5}$$

$$S_{pmod}(f) = F\{R_{pmod}(\eta)\} \tag{5.6}$$

Divide P(f) by $S_{pmod}(f)$ and take the IFFT to find the tap weights, $h_{eq}(t)$.

$$h_{eq}(t) = F^{-1}\left\{\frac{P(f)}{S_{pmod}(f)}\right\} \tag{5.7}$$

The MMSE algorithm converges to the Z-F solution as C/N increases. This can be seen from the math above. If C/N approaches infinity, R_{pmod} in (5.4) approaches the autocorrelation of p(n). The Fourier transform of the autocorrelation of a signal is the power spectral density (PSD) which is the square of P(f). Dividing P(f) by the square of P(f) leaves 1/P(f) which is the frequency response of a Z-F equalizer.

Figure 5-6 is an example of MMSE equalization in a channel that has two large frequency dropouts. Using the MMSE equalizer improves the optimum performance by 6.5 dB over the Z-F equalizer.

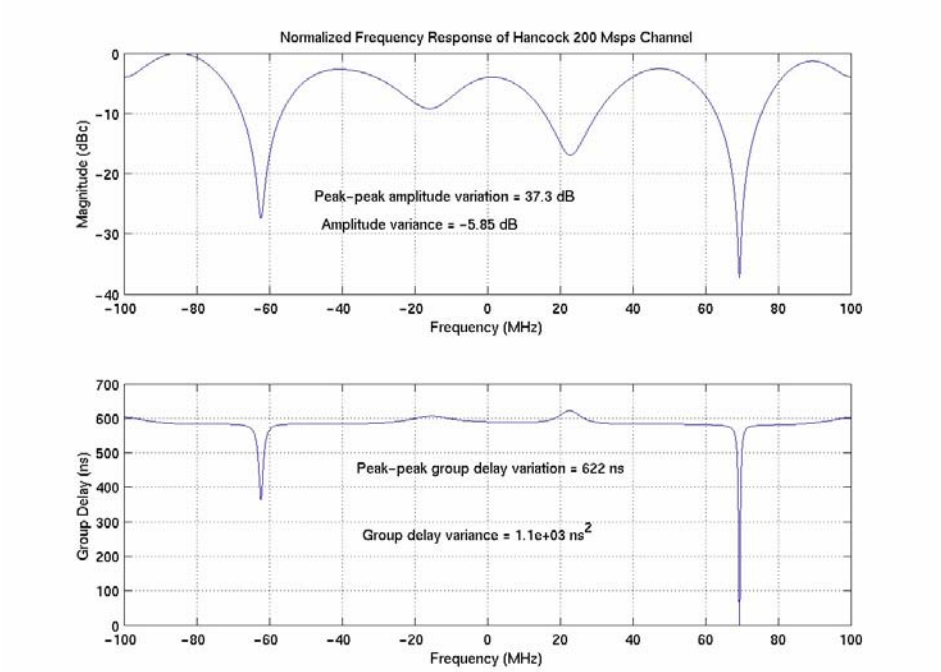

a)

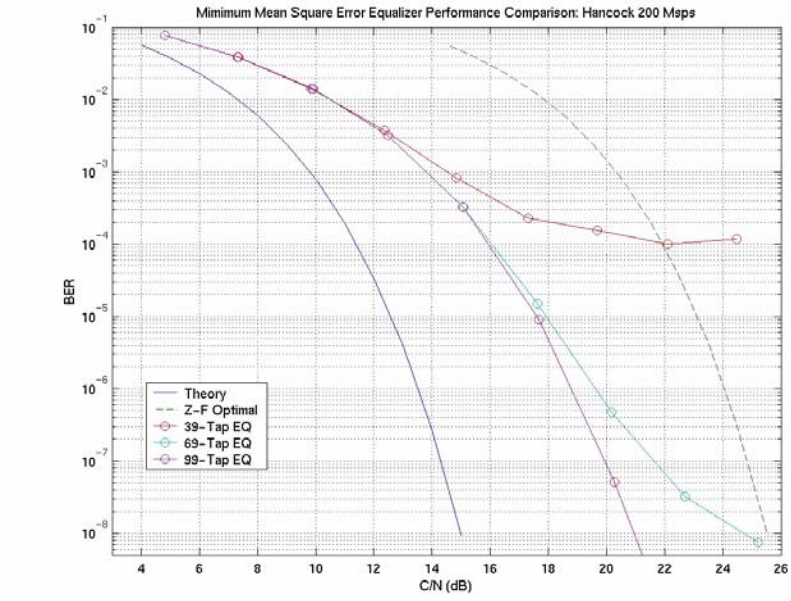

b)

Figure 5-6: Hancock Hall 200 MHz channel a) frequency response and b) comparison of minimum mean square error and optimum zero-forcing equalizer performance.

Since the tap weights change as a function of C/N for MMSE equalizers, the method used to choose the appropriate number of taps is slightly modified. Figure 5-7 shows BER performance curves for several different numbers of tap weights over C/N. As in the Z-F case, maintaining about 98% of the energy in the tap weights keeps the performance curves very close to the optimal. In the MMSE case, however, the number of taps and the values of the tap weights change with C/N.

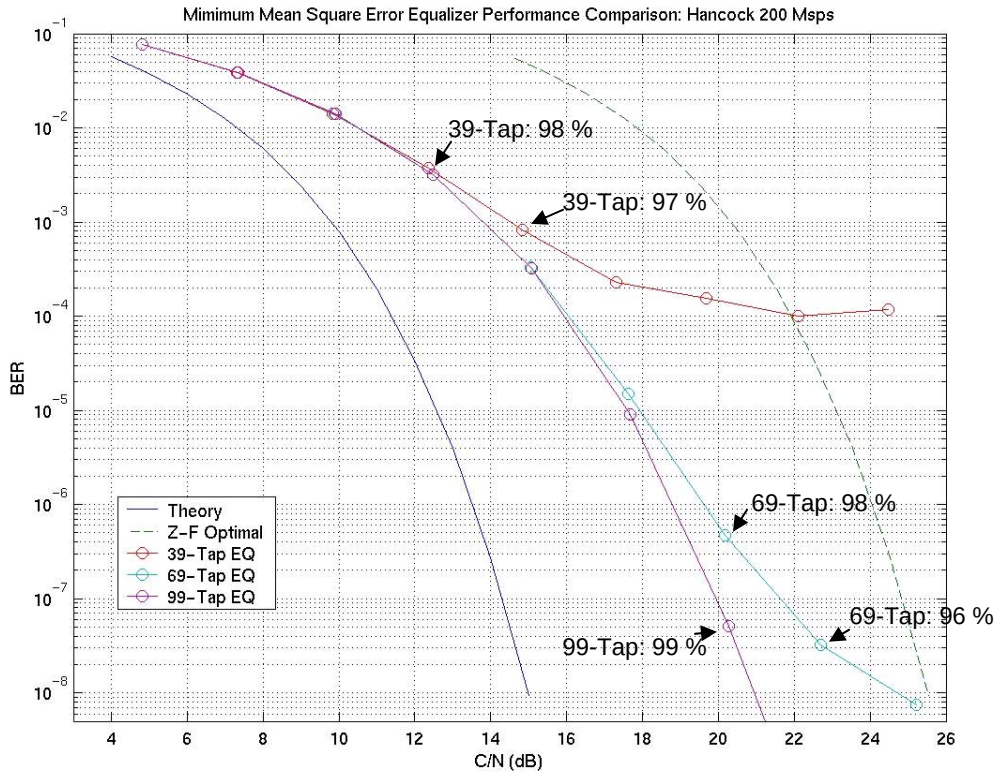

Figure 5-7: Minimum mean square error equalizer performance for different numbers of taps.

5.4 The Effectiveness of Equalization in Non-Ideal Channels

As can be seen from Figures 5-4, 5-5, and 5-7, significant improvement in performance can be gained with simple symbol rate equalizers. Whether this improvement is worthwhile depends upon the particular application and whether the processing power and time is available to run the necessary calculations.

As expected, the MMSE equalizer performs better than the Z-F equalizer, especially in channels with significant nulls in the frequency response. The Z-F equalizer is attractive because a simple calculation can be performed to determine the tap weights regardless of C/N. The disadvantage, however, is that in channels with deep nulls in the frequency response, a Z-F equalizer may significantly increase the thermal noise power in an attempt to eliminate ISI.

The MMSE equalizer balances the effects of noise and ISI, but knowledge of the C/N is required to calculate the tap weights. The procedure is slightly more complicated as the necessary number of taps and the tap weights themselves change as a function of C/N.

6 Comments on the Differences Between Specular Multipath and Diffuse Scattering

The two investigations here represent a channel with primarily specular multipath and a channel that is primarily composed of diffuse scattering. A channel with specular multipath is composed of discernible components that can be represented by discrete impulses. Channels with diffuse scattering contain no such discernible components, but rather are composed of a continuum of energy that cannot be represented as a series of discrete impulses. The appropriate use of degradation mitigation techniques must be considered carefully in light of this fundamental difference in the nature of these two types of channel distortion.

As shown above, equalizers may be used in both types of channels to increase performance. The procedure for defining the length of the equalizer as well as the tap weights is the same for a channel with specular multipath or diffuse scattering. The 98% rule of thumb was shown to be appropriate for either type of channel. The effectiveness of the equalizer is only limited by the number of taps used and the original distortion in the channel.

Another technique that was not investigated here is orthogonal frequency division multiplexing (OFDM). In OFDM, data is separated and transmitted on different subcarriers. Since the data is separated, the signal bandwidth associated with each subcarrier is much smaller than the original. The amplitude and group delay variation is then much smaller across each of the sub-bands than the entire band. Both diffuse scattering channels and specular multipath channels suffer from non-ideal frequency responses, so both channels should benefit from this technique.

Another technique that should work for both types of channels is Multiple Input-Multiple Output (MIMO) systems. In these systems, performance gain is achieved through a combination of transmission path diversity and signal combining. In its simplest form, the receiver simply chooses the best path. In specular multipath channels this is usually considered to be the channel with the best C/N, but Appendix 2 shows a

diffuse scattering example where this is not the case. Either way, a best path can be chosen based on the appropriate metrics for either type of channel.

In more complicated MIMO systems, the receiver combines the received signals at each input in a way that increases the performance. Two of these techniques are Maximal Ratio Combining (MRC) and Equal Gain Combining (EGC). The common trait is that each input to the receiver is phase shifted so all branches have the same phase. The branches are then summed to provide coherent voltage addition. MRC individually adjusts the gain for each path while the gains for all paths for EGC are the same. The problem is that most detectors for the adjustment of the branch phases assume the distortion in the channels is due to specular reflections. The performance of these detectors for diffuse scattering channels will need to be investigated to better understand their usefulness in these channels.

7 Summary of Algorithm Implementation

The following list is a guide to implementing the performance estimation algorithm described above. The algorithm assumes that the channel pulse response, $p_s(t)$, is available. This is the collected response from a short RF pulse channel sounder.

1. The sounder pulse response, $p_s(t)$, is the convolution of the transmitted pulse, $p_T(t)$ and the channel impulse response, $h_c(t)$.

$$p_s(t) = p_T(t) * h_c(t) \tag{7.1}$$

2. Convolve out the transmitted pulse from the sounder to isolate $h_c(t)$. This is simply done in the frequency domain by taking the Fourier transforms of $p_s(t)$ and $p_T(t)$. The ratio is the frequency response of the channel, $H_c(f)$. To find the time domain representation, take the inverse Fourier transform of $H_c(f)$.

$$P_s(f) = F\{p_s(t)\} \tag{7.2}$$

$$P_T(f) = F\{p_T(t)\} \tag{7.3}$$

$$H_c(f) = F\left\{\frac{P_s(f)}{P_T(f)}\right\} \tag{7.4}$$

$$h_c(t) = F^{-1}\{H_c(f)\} \tag{7.5}$$

3. Convolve a representative ideal pulse, $p_I(t)$, with the channel impulse response to get the received pulse, $p_R(t)$.

$$p_R(t) = p_I(t) * h_c(t) \tag{7.6}$$

4. If an equalizer is available, calculate the tap weights as described in Section 5.2 or 5.3 and convolve the received pulse, $p_R(t)$ with the equalizer, $h_{eq}(t)$. Otherwise, let $p_R(t) = p_{eq}(t)$ and continue.

$$p_{eq}(t) = p_R(t) * h_{eq}(t) \tag{7.7}$$

5. Represent the signal, $p_{eq}(t)$ in polar notation. The time at which the maximum magnitude occurs is the optimum sampling point. Multiply the entire signal by $e^{-j\varphi_{opt}}$, where φ_{opt} is the phase in radians at the optimum sampling point. This rotates the signal constellation so the pulse has the correct phase, as in Figure 7-1.

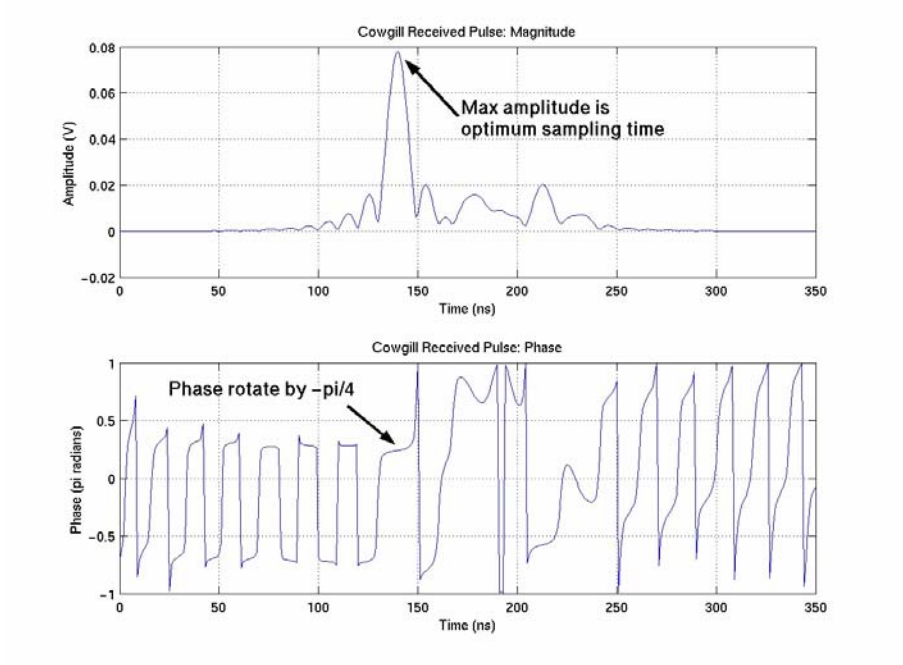

a)

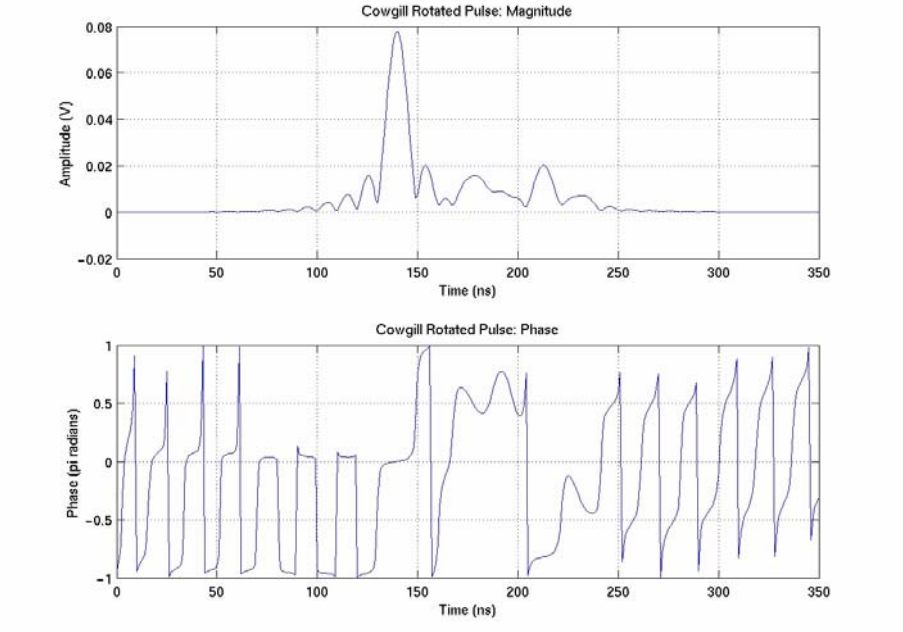

b)

Figure 7-1: Received pulse a) before and b) after phase rotation.

6. Return the rotated signal to real and imaginary parts and downsample at a rate equal to the symbol period. Be sure the optimum sampling point is included. The maximum amplitude of the downsampled signal is the mean amplitude.

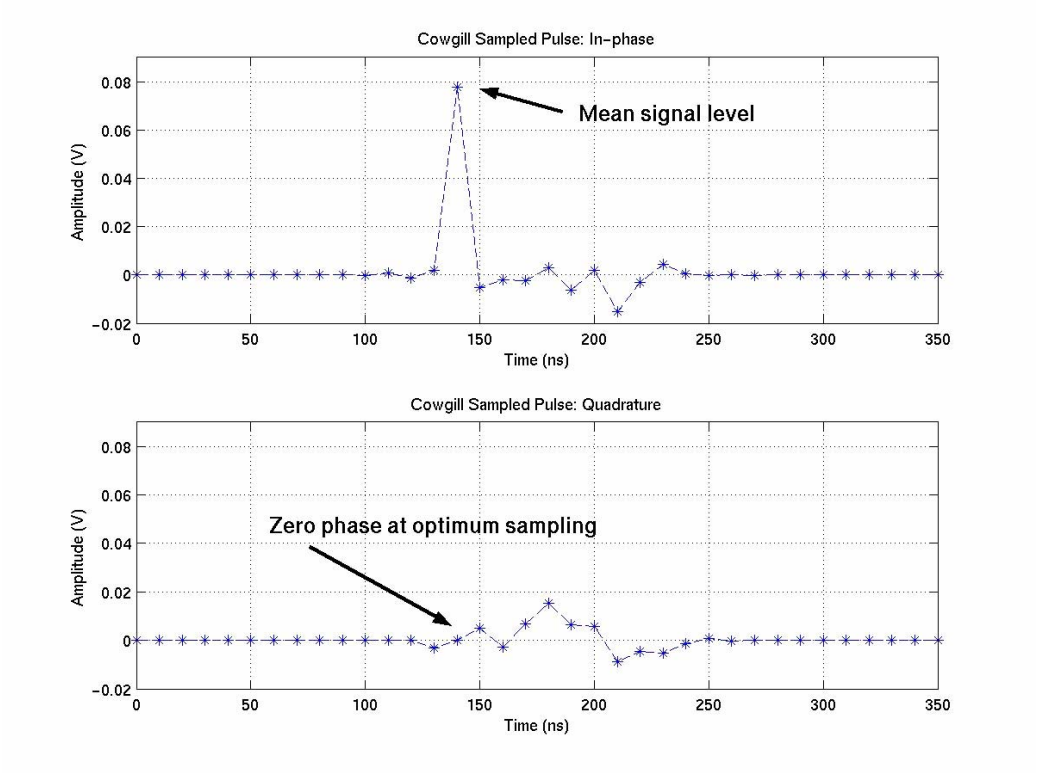

Figure 7-2: Properly sampled pulse showing the mean signal level.

7. The rest of the points contribute to ISI, so find the PDF of the ISI. To do this, find the twenty largest contributors and calculate every combination of +/- these values. Form a histogram with at least 100 bins from $-\sum_i |A_i|$ to $+\sum_i |A_i|$. Divide the bins by the number of combinations and the bin width to get the PDF of the ISI.

8. Combine the PDF of the ISI with the PDF of the receiver noise. Since these two can be considered independent, place them on orthogonal axes called S for signal and N for noise. Shift the PDF of the ISI to the mean signal level found in step 6 and run it along the S axis. The noise PDF is orthogonal in the N direction. Draw a plane through the S = -N line normal to the S-N plane. The volume where –N exceeds S is the probability of error.

9. To form a BER curve as a function of C/N, change the variance of the noise appropriately and run step 8 for each value of C/N.

8 The Algorithm in Adaptive and Cognitive Radios

The previous chapters have shown that the algorithm estimates the performance if a signal is transmitted over a known channel. The algorithm can estimate irreducible BERs, estimate average BERs over C/N, works well in the presence of equalizers, and can estimate the equalizers necessary to optimize the performance in the channel. Since it is also much more compact and efficient than traditional performance estimation techniques, it lends itself very well to adaptive and cognitive radio systems.

Adaptive radios are radios that have the ability to change their radio and network configurations in environments with anticipated characteristics. These radios tend to have a limited set of adjustable parameters and can adapt in preprogrammed ways. The algorithm presented here could be the basis for that adaptation. The algorithm can be run before deployment and its results put in memory. The radio can then compare its environment to those stored in the system memory. Adaptation can occur by simply matching the sensed channel with the set of stored channels. The performance estimation could also be run in real-time. Given information about the channel, the algorithm could perform trade-offs to determine the appropriate configuration and offer immediate feedback to the system.

Cognitive radios will be able to optimize their radio and network settings in environments with unanticipated characteristics. A learning process based on genetic algorithms (GA) has been developed at Virginia Tech that will control the system configuration and 'learn' how to best configure itself for unanticipated environments. This 'cognitive engine' can be operated in real-time and offers much promise for the FCC's goal of increasing spectrum efficiency.

Work continues at Virginia Tech on a hardware implementation of the GA-based approach to cognitive radio with off-the-shelf unlicensed 5 GHz radios. As described in [13], these radios obtain the impulse response of the channel using the same hardware as the measurements in this dissertation. The algorithm presented here is expected to play an important role in generating the error statistics and helping the GA weigh the possible system configurations. As the GA steps through its configurations, the algorithm can be used to provide a basic system evaluation based on the chosen parameters. The

applications described in the Appendices 1 and 2 are only two of the possible ways in which the algorithm can be utilized by the GA. The final implementation will be based on the ultimate needs of the GA and what information best helps the GA do its job.

The algorithm is capable of calculating the performance for every combination of radio and network configuration, but has no way of estimating beforehand what the best channels might be. Used in conjunction with a cognitive radio engine, the algorithm could quickly estimate performance for the configurations proposed by the GA, thus reducing the time to converge on a suitable system configuration.

A couple of limitations to the algorithm need to be addressed before practical implementation is reasonable. One is that the calculation of the PDF of the ISI is, by far, the most computationally intense step in the algorithm. Finding a way to put a reasonable bound on the PDF based on the ISI contributions would greatly reduce the performance estimation time. This is, however, a non-trivial mathematics problem as shown in [10]. It may be tractable, though, when considering reasonable transmit pulses and channel responses. More work can be done to investigate the sensitivity of the bounds in [10] to common combinations of transmit pulses and channels.

A second limitation is that the algorithm is currently designed for static channels. This implies that the estimation must be done at least as often as changes in the channel occur, or the algorithm must be adapted to handle time-varying channels. Although the work in this dissertation was based on an average impulse response, it would be wise to investigate the impact of the slight deviations in received responses on performance. While it may never be practical to implement the algorithm in mobile channels, it may be possible to characterize fixed channels based on a time-varying model that does not have to assume worst-case Rayleigh fading. The ISI can then be estimated based on this model and a less computationally intense analytic solution for performance arrived at.

9 Conclusion

The work presented here illustrates some interesting results concerning the nature of reflections in 28 GHz wireless communication links with performance that is at times counterintuitive. The algorithm reasonably estimates performance in these links in a fraction of the time it takes to run traditional Monte Carlo simulations. Equalizers are then shown to be an effective degradation mitigation technique in diffuse scattering channels as well as in specular multipath channels. Implementation procedures for the two equalizers discussed are presented where it is seen that using 98% of the energy in the taps results in near optimal performance.

Channel impulse response measurements collected on the Virginia Tech campus show various combinations of specular multipath and diffuse scattering. The impulse responses derived in Sections 3.2.1.2 and 3.2.1.3 illustrate that simple knowledge of the surface characteristics may not be sufficient to estimate the type of reflection mechanism. Surfaces that look smooth may produce diffuse scattering and surfaces that look rough may have predominantly specular multipath.

The distribution of symbol errors is investigated to determine the appropriate performance metrics for these channels,. Section 4.1 shows that the errors are uncorrelated suggesting that average bit error statistics are sufficient to characterize performance.

The channel impulse response based performance estimation algorithm presented is an accurate and efficient alternative to traditional Monte Carlo simulation analysis. This makes it especially suitable for adaptive and cognitive radio platforms. Two interesting observations are illustrated by the results. In Section 4.3 and Appendix A-2, results are presented that show higher data rates do not necessarily imply poorer performance. This is contrary to mobile system performance where upper limits on symbol rate are based on the assumption that performance degrades with increasing symbol rate. In Section 4.3 and Appendix A-1, results show that higher power does not necessarily imply better performance. A relationship between the relative flatness of the amplitude and group delay response and the resulting performance is suggested that

implies signal strength should not be the only consideration when determining the best channel.

The Z-F and MMSE equalizers significantly improved the link performance in both the specular multipath and diffuse scattering channels. The methods described in Chapter 5 to calculate the tap weights can be used to minimize the number of taps and therefore the time necessary to process the signal. It is shown that using 98% of the energy in the calculated taps approaches the maximum performance possible in each of the equalizer implementations.

Some limitations of the algorithm are presented in Chapter 8 that suggest further work to be done. The calculation of the ISI is the most time-consuming step in the performance estimation. At present, the distribution of the ISI is calculated based on an exhaustive computation of possible ISI values given the largest contributors. Developing a more compact ISI estimation step could significantly reduce the time necessary to estimate performance. The analysis also assumes the channel responses are static even though slight deviations were found in the collected responses. Several questions arise that deserve closer inspection for time-varying channels. What effect does this deviation have on performance and can this deviation be modeled? Does this deviation produce correlated errors and, if so, how should the performance metrics be modified? What effect does this imply for equalizer definition? These are reasonable questions that should be addressed as work continues towards the development of a fully functional cognitive radio.

Appendix 1: Case Study: Minimizing BER for a Fixed Symbol Rate QPSK Signal

The example that follows is one application of the proposed performance algorithm. The goal is to find the channel that has the best performance for a fixed data rate signal. The bandwidth is separated into three 30 MHz channels as shown in Figure A1- 1. The channels are then compared against one another in Figure A1- 2. The signal will transmit at 20 Msps and use QPSK modulation with a raised cosine pulse shape and roll-off = 0.2. The noise is assumed to be AWGN and the same in all three channels.

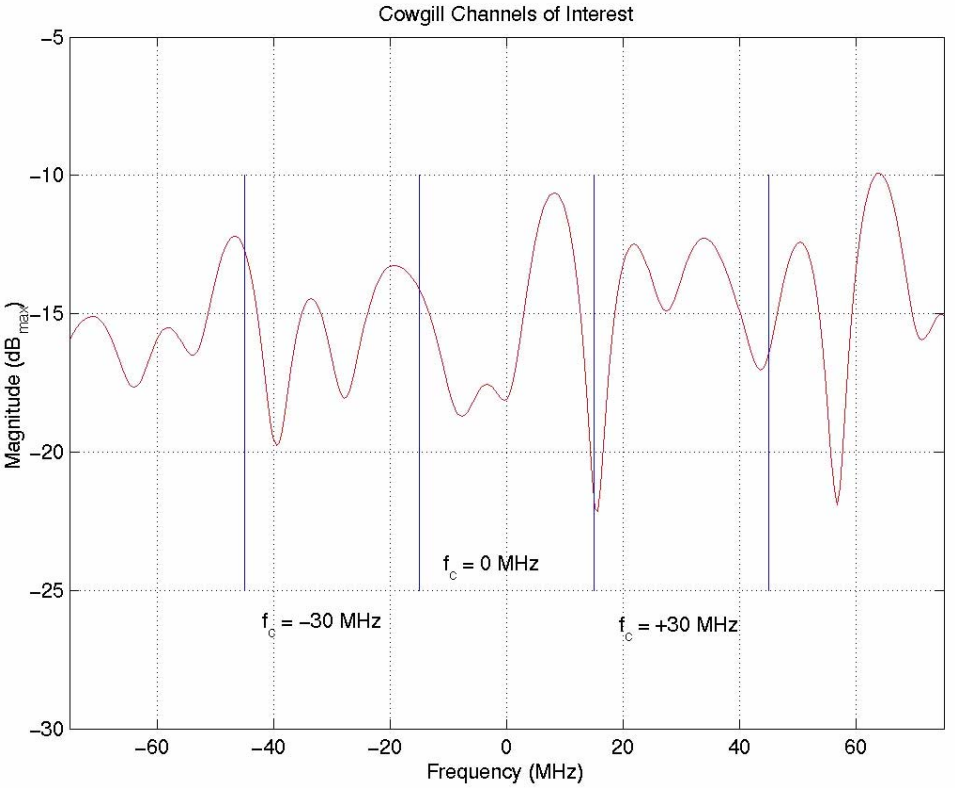

Figure A1- 1: Channelization of Cowgill Hall channel into three 30 MHz channels.

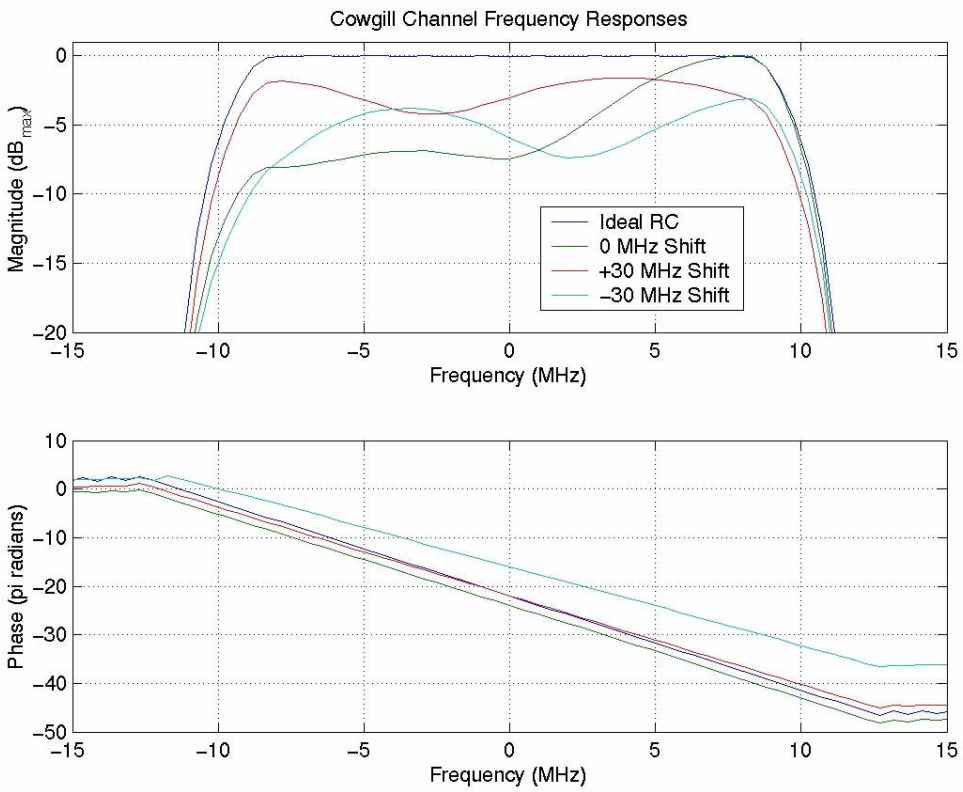

Figure A1- 2: Comparison of the frequency responses of the three channels used in the example.

The first step is to determine the distribution of the ISI. The frequency response and ISI distributions for all three channels are shown in Figures A1-3, 4, and 5. The algorithm is then run to find the BER curves as shown in Figure A1- 6.

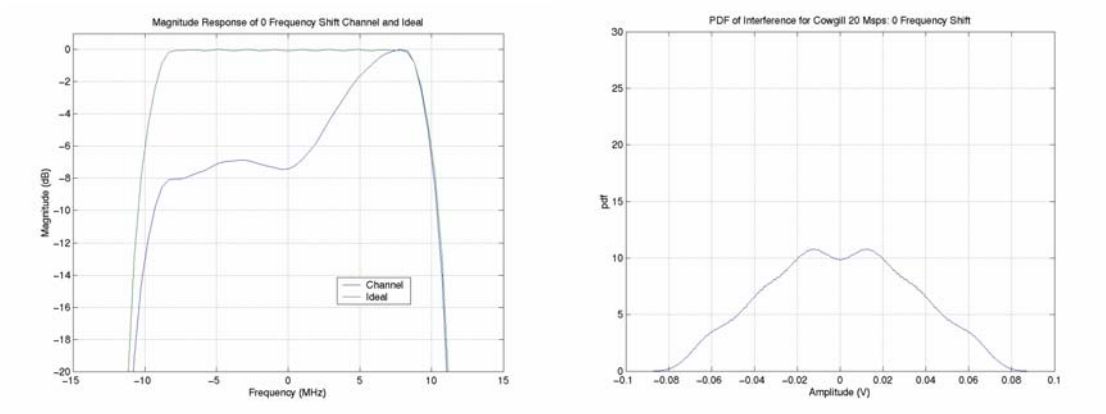

a) **b)**

Figure A1- 3: Center Cowgill Hall channel a) magnitude response and b) probability density function of the intersymbol interference.

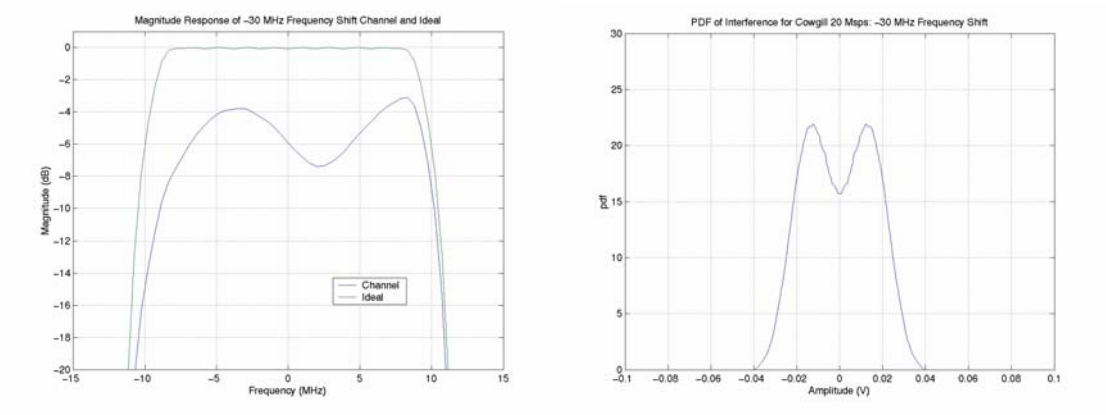

a) **b)**

Figure A1- 4: Lower Cowgill Hall channel a) magnitude response and b) probability density function of the intersymbol interference.

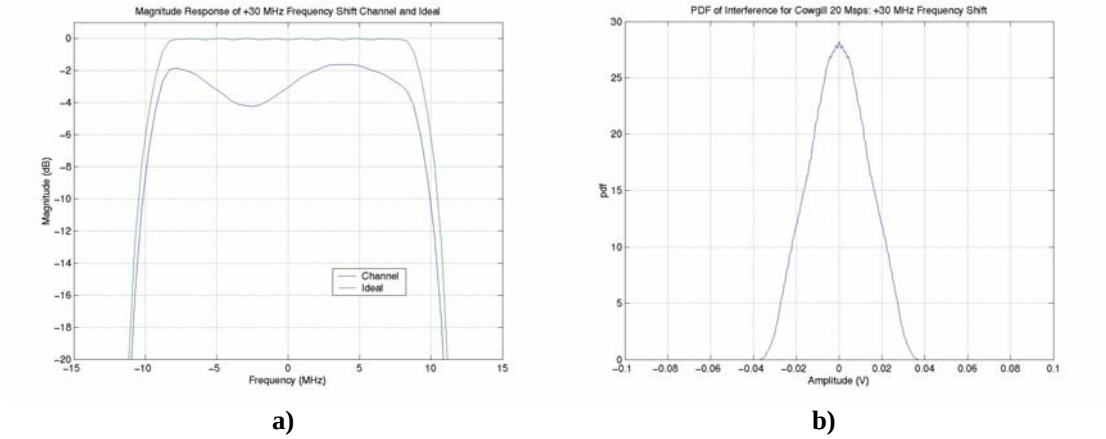

a) **b)**

Figure A1- 5: Upper Cowgill Hall channel a) magnitude response and b) probability density function of the intersymbol interference.

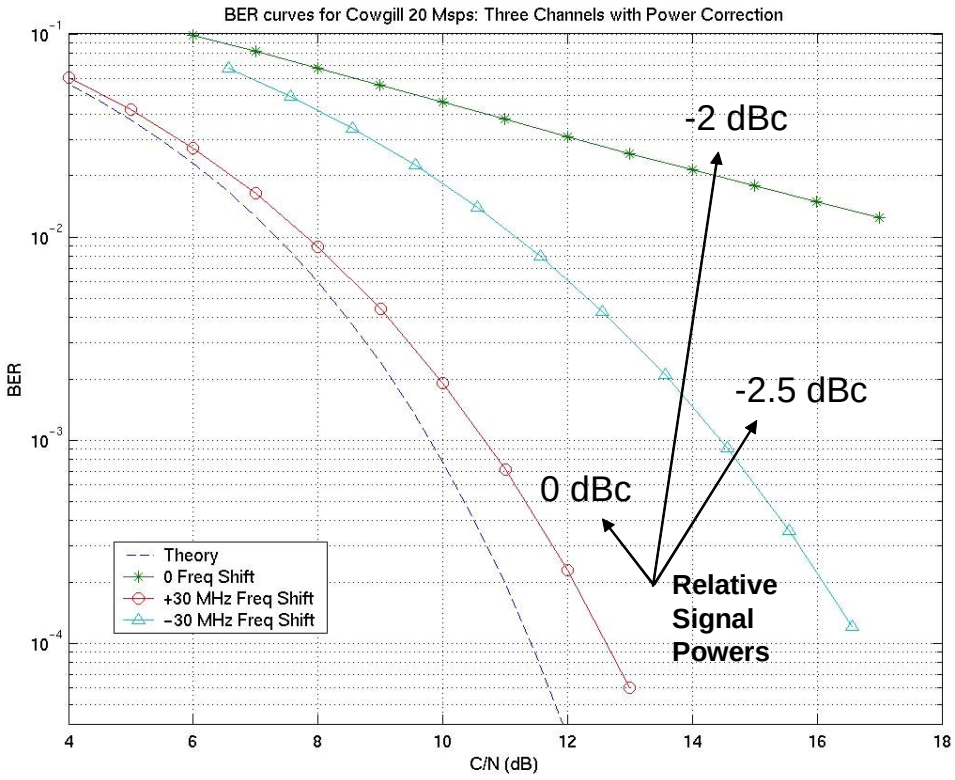

Figure A1- 6: Estimated BERs for the three Cowgill Hall channels and their relative received powers.

Note that in this case, the channel that would support the best performance is the upper frequency channel. This is also the channel that permits the highest received power. Using received power as a measure of signal quality, however, is not the proper metric for ranking as is illustrated with the other two channels. The lower channel has 0.5 dB more attenuation than the center channel, but supports better performance. In this case, ranking the channels on only the amount of signal attenuation would have been a mistake that could cost several dB of performance.

Appendix 2: Case Study: Maximizing QPSK Symbol Rate for a Specified BER

In this case, the specification is on a maximum BER and the goal is to maximize the symbol rate. The signal is QPSK modulated with a raised cosine pulse shape and 0.2 roll-off. Noise is assumed to be AWGN across the entire band and the center frequency is fixed. The received signal power is assumed to be the same for all data rates.

Figure A2- 1 shows the performance for 3 different data rates without equalization. Figure A2- 2 utilizes equalization using 98% of the tap weights for each channel. To choose the maximum data rate for a specified BER, simply find the highest data rate that can sustain the required BER given the operating C/N.

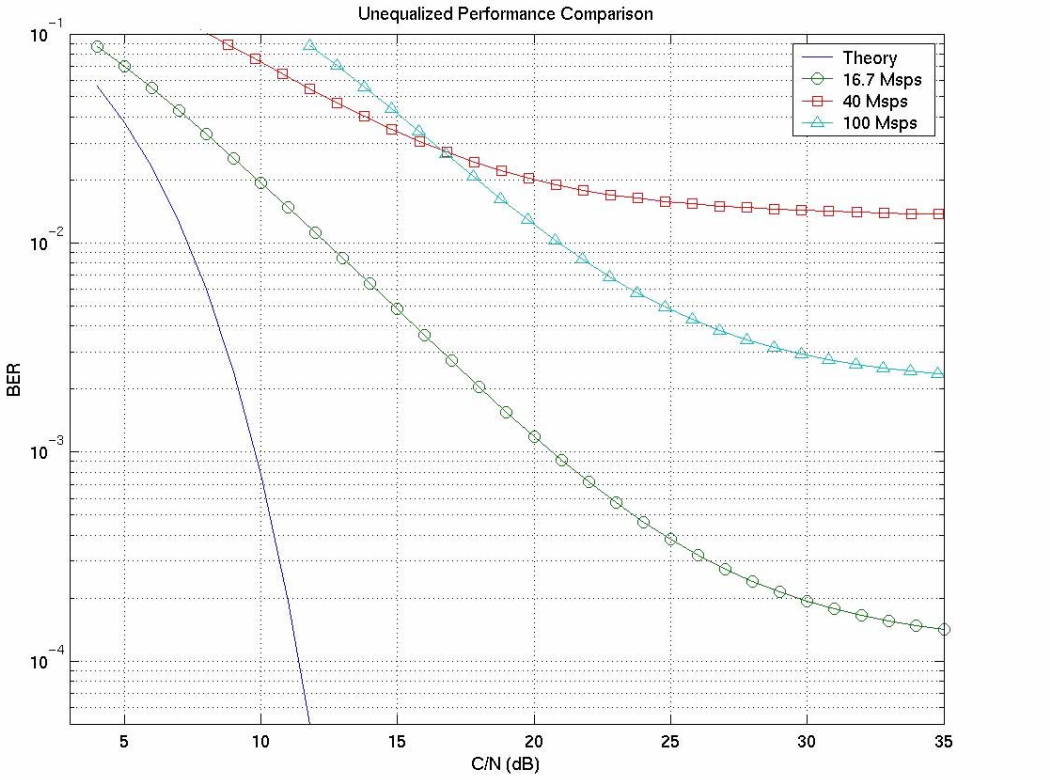

Figure A2- 1: Unequalized channel comparison for three different data rates.

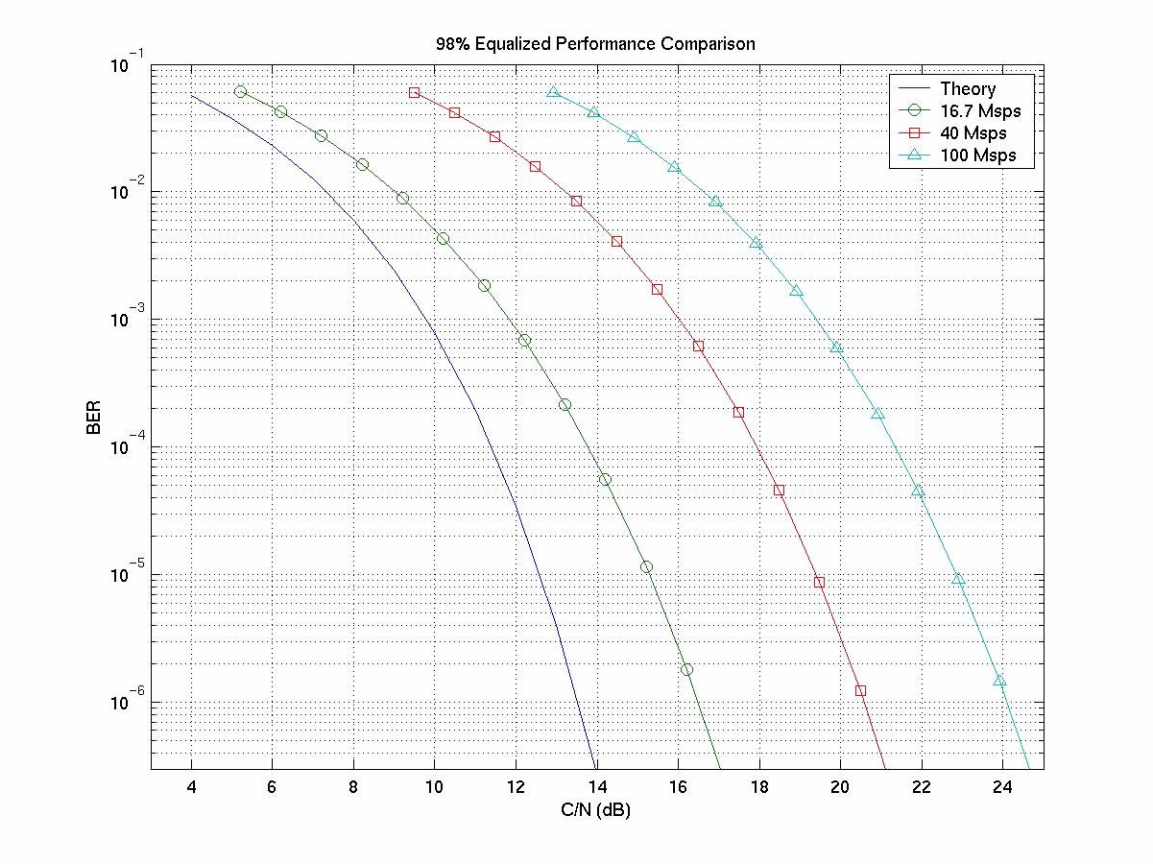

Figure A2- 2: Equalized channel comparison for three different data rates.

References

[1] Bostian, C.W., S.F. Midkiff, W.M. Kurgan, L.W. Carstensen, D.G. Sweeney, and T.M. Gallagher, "Broadband communications for disaster response," *Space Communications*, Vol. 18, no 3-4, pp. 167-177, 2002.

[2] Dillard, C.L., T.M. Gallagher, C.W. Bostian, and D.G. Sweeney, "Rough surface scattering from exterior walls." (Accepted, IEEE Transactions on Antennas and Propagation, February, 2005).

[3] Miniuk, M.T., T.M. Gallagher, and C.W. Bostian, "Transmission Characteristics of 28 GHz NLOS Paths," (To appear *2004 IEEE AP-S International Symposium and USNC /URSI National Radio Science Meeting, June 2004).*

[4] Gallagher, T.M., M.T. Miniuk, "Methodology and preliminary findings towards the characterization and evaluation of non-line-of-sight paths for fixed broadband wireless communications for emergency and disaster response," *National Conference on Digital Government Research*, May, 2003.

[5] Seidel, S.Y. and H.W. Arnold, "Propagation measurements at 28 GHz to investigate the performance of Local Multipoint Distribution Service (LMDS)," *Proc. IEEE Global Telecommunications Conference, GLOBECOM '95*, vol.1, pp 754-757, 1995.

[6] Papazian, P.B., et al, "Study of the Local Multipoint Distribution Service Radio Channel," *IEEE Trans. Broadcasting*, vol. 43, no. 2, pp 175-184, June 1997.

[7] Maurer, J. et al, "Wideband wave propagation measurements for Local Multipoint Distribution Services (LMDS) at 26 GHz," *IEEE Vehicular Technology Conference, IEEE VTS-Fall VTC 2000*, vol. 4, pp 1902-1908, September, 2000.

[8] Hayn, A., R. Bose, and R. Jakoby, "Multipath propagation and LOS interference studies for LMDS architecture," *Eleventh International Conference on Antennas and Propagation (IEE Conf. Publ. No. 480),* vol. 2, pp 17-20, April 2001.

[9] Chuang, J. C-I, "The Effects of Time Delay Spread on Portable Radio Communications with Digital Modulation," *IEEE J. Select. Areas Commun*. , Vol. SAC-5, NO. 5, pp. 879-889, June 1987.

[10] Montgomery-Smith, S.J., "The Disitribution of Rademacher Sums," *Proceedings of the American Mathematical Society*, vol. 109, no. 2, pp 517-522, June 1990.

[11] Janssen, G.J.M, P.A. Stigter, R. Prasad, "Wideband indoor channel measurements and BER analysis of frequency selective multipath channels at 2.4, 4.75, and 11.5 GHz," *IEEE Trans. Commun.* , Vol. 44, pp. 1272-1288, Oct 1996.

[12] Proakis, J., *Digital Communications 3rd ed.*, McGraw-Hill, New York, 1995.

[13] Rondeau, T.W., C.J. Rieser, T.M. Gallagher, and C.W. Bostian, "Online Modeling of Wireless Channels with Hidden Markov Models and Channel Impulse Responses for Cognitive Radios," *Microwave Symposium Digest, 2004 IEEE MTT-S International*, pp. 739-742, June 2004.

Vita

Timothy M. Gallagher

Contact Information

Work:
455 Whittemore Hall
Center for Wireless Telecommunications
24073 Virginia Polytechnic Institute and State University
Blacksburg, VA 24061
(540) 231-8037
tgallagh@vt.edu

Home:
655 Kamran Drive
Christiansburg, VA
(540) 381-1910
tdmmgal@netscape.net

- **EDUCATION**

  Ph.D., Electrical Engineering, August 2004
  Virginia Polytechnic Institute and State University (Virginia Tech), Blacksburg, VA
  Dissertation: Characterization and evaluation of non-line-of-sight paths for fixed broadband wireless communications
  Advisor: Charles W. Bostian

  M.S., Electrical Engineering, 1998
  University of Kansas, Lawrence, KS
  Thesis: A new methodology for the design of high-speed wireless communication systems based on experimental results
  Advisor: James A. Roberts

  B.S., Electrical Engineering; Minor: Applied Mathematics, 1996
  Lehigh University, Bethlehem, PA
  Senior Project: Wireless communications testbed
  Advisor: Rick S. Blum

- **RESEARCH/TEACHING INTERESTS**
  - Broadband wireless communications
  - Satellite communications
  - Ultrawideband
  - RF propagation
  - RF systems engineering issues

- **RELATED EXPERIENCE**

  Industry

  RF Systems Engineer, TRW, Redondo Beach, CA
  1998-2001
  - RF uplink channel lead for a complex satellite communication system
  - Prepared and presented data to a number of diverse groups with varying levels of technical expertise
  - Responsible systems engineer for a subcontracted downconverter unit
  - Completed extensive modeling and performance evaluations utilizing SPW
  - Responsible for partitioning work and setting realistic short-term milestones in order to accomplish complex tasks
  - Developed and maintained an extensive link budget

Research

Research Engineer, Center for Wireless Telecommunications, Virginia Tech, Blacksburg, VA
2001 - Present

- Resource for graduate students in the Center
- RF communications systems engineer for multiple projects involving diffuse scattering, mesh architecture LMDS systems, interdisciplinary wireless communication system deployments, satellite communications, CDMA, and broadband point-to-multipoint wireless communication systems
- Supported meetings for numerous Virginia cities and counties interested in wireless deployments,
  including Chase City, Staunton, Grundy, Martinsville, Warren County, Henry County, and Patrick County.
- Reviewed a paper for GLOBECOM '03

Research Assistant, Information and Telecommunication Technology Center, University of Kansas, Lawrence, KS
1996 - 1998

- Designed and implemented a radio propagation measurement system at 5.8 GHz

Undergraduate Research Assistant, Lehigh University, Bethlehem, PA
1995-1996

- Designed SPW models to test a spatial diversity combining scheme developed by a graduate student

Teaching

Instructor, Electrical and Computer Engineering Department, Virginia Tech, Blacksburg, VA
July-August 2003

- ECE 4634 Analog and Digital Communications
  - System level analysis and design for digital and analog communication systems including modulation, receiver design, link budgets, signal-to-noise ratio, and bit error rate

Instructor, Electrical and Computer Engineering Department, Virginia Tech, Blacksburg, VA
May-July 2002

- ECE 3614 Introduction to Communication Systems
  - Overview of methods and issues in analog and digital communications including modulation, signal analysis, noise analysis, bandpass signals, power spectral density, and random variables

- **PUBLICATIONS**

Rondeau, T.W., C.J. Rieser, T.M. Gallagher, and C.W. Bostian, "Online Modeling of Wireless Channels with Hidden Markov Models and Channel Impulse Responses for Cognitive Radios." (To appear, *International Microwave Symposium*, June, 2004)

Miniuk, M.T., T.M. Gallagher, and C.W. Bostian, "Transmission Characteristics of 28 GHz NLOS Paths," (To appear, *2004 IEEE AP-S International Symposium and USNC /URSI National Radio Science Meeting, June 2004).*

Bostian, C.W., S.F. Midkiff, T.M. Gallagher, C.J. Rieser, and T.W. Rondeau, "Rapidly Deployable Broadband Communications for Disaster Response." (To appear, *International Symposium on Advanced Radio Technologies*, March, 2004)

Dillard, C.L., T.M. Gallagher, C.W. Bostian, and D.G. Sweeney, "Rough surface scattering from exterior walls." (Accepted, IEEE Transactions on Antennas and Propagation)

RamaSarma, V., C.W. Bostian, and T.M. Gallagher, "A coverage area estimation model for interference-limited non-line-of-sight point-to-multipoint fixed broadband wireless access systems," *IASTED International Conference on Wireless and Optical Communications*, July, 2003.

Dillard, C.L., T.M. Gallagher, C.W. Bostian, and D.G. Sweeney. "28 GHz scattering by brick and limestone walls," *2003 IEEE Antennas and Propagation Society International Symposium*, Vol. 3, pp. 1024-1027, June, 2003.

Gallagher, T.M., M.T. Miniuk, "Methodology and preliminary findings towards the characterization and evaluation of non-line-of-sight paths for fixed broadband wireless communications for emergency and disaster response," *National Conference on Digital Government Research*, May, 2003.

Bostian, C.W., S.F. Midkiff, W.M. Kurgan, L.W. Carstensen, D.G. Sweeney, and T.M. Gallagher, "Broadband communications for disaster response," *Space Communications*, Vol. 18, no 3-4, pp. 167-177, 2002.

Eshler, T., S.F. Midkiff, and T.M. Gallagher, "Simulating an adaptive link protocol for fixed broadband wireless," *OPNETWORK*, August, 2002.

- **HONORS/AFFILIATIONS**

  Institute of Electrical and Electronics Engineers (IEEE)
  IEEE Communications Society
  IEEE Antennas and Propagation Society
  Bradley Fellowship, Virginia Tech
  Stroebel Graduate Scholarship, University of Kansas
  Graduated with Honors at both Lehigh University and the University of Kansas

- **CITIZENSHIP: U.S.**

- **A LITTLE BIT ABOUT ME**

  Non-technical Jobs

  - Karaoke DJ
  - Plant foreman in an industrial ceramics plant
  - Assistant manager of the electronics department in a department store

  Interests

  - Participating in my children's extracurricular activities
  - Wine making
  - College sports

  Reflections

  - My wife is my partner in all things.
  - Nothing makes me happier than watching our children laugh out loud.
  - At work, a day doesn't go by where I don't have a substantial interaction with at least one student. Developing those relationships is the single most satisfying part of my job.
  - I'm the luckiest person I know because of the previous statements.

References for Timothy M. Gallagher

Dr. Charles W. Bostian
Alumni Distinguished Professor
Clayton Ayre Professor of Electrical and Computer Engineering
Bradley Department of Electrical and Computer Engineering
464 Whittemore Hall
Virginia Polytechnic Institute and State University
Blacksburg, VA 24061
(540) 231-5096
bostian@vt.edu

Dr. George E. Morgan
SunTrust Professor of Finance
Director, Center for Wireless Telecommunications
457 Whittemore Hall
Virginia Polytechnic Institute and State University
Blacksburg, VA 24061
(540) 231-5096
gmorgan@vt.edu

Dr. Scott F. Midkiff
Bradley Department of Electrical and Computer Engineering
2040N Torgersen Hall
Virginia Polytechnic Institute and State University
Blacksburg, VA 24061
(540) 231-5190
midkiff@vt.edu

Dr. James A. Roberts
Interim Vice Provost for Research
President and COO, KU Center for Research, Inc.
201 Youngberg Hall
The University of Kansas
Lawrence, Kansas 66045-7563
(785) 864-7248
jroberts@ukans.edu